Title

AN EXPERIMENTAL AND THEORETICAL STUDY OF HEAT TRANSFER IN CONSTANT VOLUME AND COMPRESSION-EXPANSION SYSTEMS INCLUDING THE EFFECTS OF FLAME PROPAGATION

Author

Woodard, J.B.

Publication Date

1982-03-01

Lawrence Berkeley Laboratory
UNIVERSITY OF CALIFORNIA

ENERGY & ENVIRONMENT DIVISION

AN EXPERIMENTAL AND THEORETICAL STUDY OF HEAT TRANSFER IN CONSTANT VOLUME AND COMPRESSION-EXPANSION SYSTEMS INCLUDING THE EFFECTS OF FLAME PROPAGATION

Joan Brune Woodard
(Ph.D. thesis)

March 1982

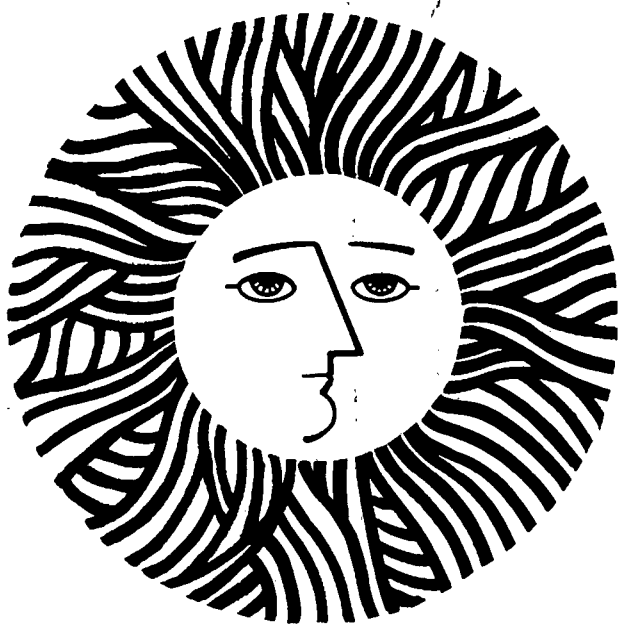

Prepared for the U.S. Department of Energy under Contract DE-AC03-76SF00098

DISCLAIMER

LBL-14097

AN EXPERIMENTAL AND THEORETICAL STUDY OF HEAT TRANSFER IN CONSTANT VOLUME AND COMPRESSION-EXPANSION SYSTEMS INCLUDING THE EFFECTS OF FLAME PROPAGATION

Joan Brune Woodard

Ph.D. Thesis

March 1982

Energy and Environment Division
Lawrence Berkeley Laboratory
University of California
Berkeley, CA 94720

This work was supported by the Assistant Secretary for Conservation and Renewable Energy, Office of Transportation Programs, Division of Transportation Energy Conservation of the U.S. Department of Energy under Contract DE-AC03-76SF00098; and Sandia National Laboratories, Livermore, CA.

AN EXPERIMENTAL AND THEORETICAL STUDY OF HEAT TRANSFER IN CONSTANT VOLUME AND COMPRESSION-EXPANSION SYSTEMS INCLUDING THE EFFECTS OF FLAME PROPAGATION

Ph.D. Joan Brune Woodard Mechanical Engineering Department

Sponsors: Sandia Laboratories Livermore
U.S. Department of Energy

Signature Chairman of Committee

ABSTRACT

The study of the heat transfer to the cylinder and piston surfaces in an internal combustion engine is of both practical and fundamental interest. Heat transfer processes are critical to the design and development of engines with respect to emissions, engine efifciency, and thermal stress in engine materials. In addition, experimental heat transfer data along with flame propagation results are needed to study and appraise analyses of the processes in engines. In this work, two studies of heat transfer phenomena are made. First an analysis of an observed reversal in the direction of the wall heat flux is presented. Then, an experimental study is reported in which simultaneous wall heat

flux, pressure, and flame propagation data are obtained. In particular, the interaction of the flame propagation and wall heat transfer is discussed.

In the first part of this study, an analytical solution for the reversal in direction of the wall heat flux during compression and expansion is derived. The results are in good agreement with experimental measurements. From the solution to the finite difference formulation of this problem, temperature profiles were calculated. From these temperature profiles and the analytical solution of the wall heat flux, a physical explanation for the heat transfer reversal is determined.

In the experimental portion of this work, simultaneous measurements of pressure, wall temperature, wall heat flux, and flame location and shape are obtained for combustion in constant volume, expansion, and compression-expansion systems. The experimental apparatus used in the study, simulates the compression-expansion strokes of an internal combustion engine while allowing full optical access to the combustion process with high-speed schlieren movies. The measurements showed that the wall temperature and heat flux rise rapidly when the flame passes. The flame speed, and correspondingly the time of the sharp rise in wall temperature and heat flux were found to vary considerably with equivalence ratio. For lean constant volume combustion, buoyancy was found to have a significant effect on the shape of the flame and on the corresponding wall temperature and heat flux variations.

ACKNOWLEDGEMENTS

The author wishes to thank Professors R. Greif and R. F. Sawyer for their valuable guidance during this research and for their friendship. The author would also like to express appreciation for the assistance and friendship of many others. Professor J. D. Dale of the University of Alberta provided guidance in the pressure instrumentation, and loaned the AVL pressure transducer to the author for the experimental work. Professor L. H. Grossman provided guidance in the final review of this work. K. Hom, H. E. Stewart, R. Jensen,and A. Shaw provided valuable assistance with the experimental system. A special thanks goes to the members of the Hesse Hall research group for their friendship which made the time spent on this work particularly enjoyable. D. Hirvo, G. Hubbard, and W. Pitz provided valuable assistance in the various phases of the experimental work. Sandia National Laboratories Livermore provided financial support for the author under their doctoral study program, and provided computational facilities, graphics support, and word processing support. Additional support for the research was provided by the Assistant Secretary for Conservation and Renewable Energy, Office of Transportation Programs, Division of Transportation Energy Conservation of the U.S. Department of Energy under Contract DE-AC03-76SF00098.

A most special thank you and sincere appreciation go to my parents, Mr. and Mrs. Harry H. Brune and my husband Jim. Without their support and love, this work would not have been possible.

TABLE OF CONTENTS

LIST OF FIGURES

NOMENCLATURE

A	Coefficient of polynomial of ϕ
c	Specific heat
$\frac{D}{Dt}$	Total derivative; $\frac{D}{Dt} = \frac{\partial}{\partial t} + u \frac{\partial}{\partial x}$
k	Conductivity
i	Square root of negative one
P	Pressure
q	Heat flux
T	Temperature
t	Time
u	Velocity
x	Direction normal to wall
z	Normalized transformed spatial coordinate
α	Thermal diffusivity
ϕ	Normalized temperature
Γ	Gamma function
γ	Ratio of specific heats
η	Integration variable
λ	Integration variable
ρ	Mass density
ψ	Transformed spatial coordinate
τ	Transformed time

CHAPTER 1

INTRODUCTION

1.1 Introduction

The development of a capability to predict the phenomena in an internal combustion engine has proven to be difficult. This entails the complexities of combustion and variable volume, thus encompassing variable pressure and temperature, chemical reactions, complex flow patterns, and high temperatures. This level of complexity which includes the interaction of these phenomena, is considerable, and suggests the need for basic experimental studies. Experimental heat transfer measurements in engines have been made for many years (e.g. Eichelberg, 1939). Most of these studies have concentrated on obtaining experimental data relative to the overall effects and performance of the system, although several recent studies have focused on specific phenomena.

The heat transfer to the cylinder walls and piston has received particular attention. Heat transfer data are used in assessing temperature and induced thermal stress distributions in the engine walls, which is useful for the design and development of internal combustion engines. The data are also important in studying the influence of thermal boundary layers on combustion processes near the chamber surface. In addition, heat transfer data are important for improving the modeling and simulation of internal combustion engine performance.

In this work, two studies of heat transfer phenomena are

presented. First an analysis of an observed directional reversal in heat transfer is discussed. Then an experimental study of wall heat transfer, flame propagation and their interaction is presented.

1.2 Wall Heat Transfer During Compression and Expansion in the Absence of Combustion

The complexity of the phenomena in an internal combustion engine has led investigators to study particular aspects of the problem including the heat transfer during compression and expansion in the absence of combustion. Early work in this area presented temperature variations with time at points below the inner surface of the cylinder wall (Eichelberg, 1939). From this information, heat transfer rates were calculated including the heat transfer to the cooling liquid. These same experimental measurements were reexamined by Annand (1963) who found some defects in the existing empirical relations and proposed another formulation. Annand also briefly reviewed some of the analytical work on this problem that has been presented (Oguri, 1960) and found that even though the predicted variations of heat transfer rates agreed with experimental observations, the assumptions to some extent seemed arbitrary. Annand and Ma (1970) measured the instantaneous heat transfer rates at five different locations on the cylinder head of a small compression-ignition engine. The heat flux magnitudes and variations during the cycle were found to vary greatly with location. Analyses of the phenomena increased in complexity, for example, by including the effects of turbulence in the work by Gosman and Watkins (1976). This particular work predicted heat transfer magnitudes that were lower than experimental engine data, but followed similar trends. The higher values of the engine heat flux data are

attributable to higher turbulence levels caused by flow through the valves. An experimental and theoretical study of the heat transfer during piston compression was presented by Nikanjam (1977). This study developed an analytical prediction of the heat transfer variation during compression, and found good agreement with experimental data. Keck (1981) presented an analysis of the thermal boundary layer in a gas subject to time dependent pressure. In his work, both heat transfer rates and displacement thickness were calculated.

One important result of the experimental studies of these phenomena is an observed directional reversal in the wall heat transfer during compression and expansion. This has been observed in measurements of instantaneous heat fluxes in a diesel engine (Le Feuvre, et al., 1969) and in measurements in a spark ignition engine (Alkidas, 1979). The heat transfer which initially is in the direction from the gas to the walls, is observed to change so that the gas is now heated by the walls. This occurs even though the free stream or bulk gas temperature is greater than the wall temperature. This reversal of the heat transfer was also measured by Dao (1972) who did some computational work using a finite difference formulation. Annand and Pinfold (1980) presented even more detailed data on this phenomena.

In Chapter 2 an analytical solution for the heat transfer reversal during compression and expansion is obtained. Heat transfer rates are predicted which are compared to experimental measurements. A finite difference formulation is used to predict the variation in temperature profiles. From the analytical solution and the temperature profiles, a physical explanation of the phenomena is then developed.

1.3 Experimental Study of Wall Heat Transfer, Flame Propagation, and Their Interaction

The interaction of a flame with a cold wall has been studied in an attempt to understand internal combustion engines as well as other systems. Mathematical models have been proposed for various aspects of the phenomena. Kurkov and Mirsky (1969) presented an analysis of laminar flame extinction at a parallel cold wall assuming a one-dimensional process and using one-step chemical kinetics. Hock, Peters, and Adomeit (1981) obtained a solution using two-step chemical kinetics for the one-dimensional problem and found significant differences from the results using one-step kinetics. Carrier, Fendell, and Feldman (1980) present an analysis of a flame passing a perpendicular wall. Heperkan (1980) performed both an experimental and theoretical study of wall heat transfer for combustion in a shock tube. Unfortunately, the experimental data that would be useful to appraise most of these analytical models and solutions are often incomplete and inappropriate as Ferguson and Keck (1977) point out.

Experimental data in fired internal combustion engines are available. Overbye, et al. (1961) obtained wall heat flux data in spark ignition engines including a study of the effect of deposits on the combustion chamber wall. Yoshida, Harigaya, and Miyazaki (1980) obtained heat flux measurements to the piston of a pre-chamber type diesel engine. The effect of the inlet jet flow was studied. Alkidas and Cole (1981) studied the transient heat flux and heat rejection to the coolant in a divided chamber diesel engine. Much of the data from engines include many of the complexities relating to overall engine

operation. It is therefore difficult to utilize these data to study the specific, localized phenomena; e.g. flame wall interactions, etc. Some data are available for the one-dimensional propagation of a flame in a constant volume chamber (Isshiki and Nishiwaki, 1974), and for the steady state problem of a flame on a burner (Yamazaki and Ikai, 1971). However, there is a pressing need for more data as pointed out by Ferguson and Keck (1977), and Alkidas and Myers (1981); in particular, simultaneous data on flame propagation and flame wall interaction for the same conditions are needed.

In this study simultaneous data on flame propagation, pressure, and wall heat flux are obtained. In particular the dependence of the wall heat flux on the propagation of the flame including location and shape is analyzed. Combustion near the lean limit is studied and compared with stoichiometric results. The experimental apparatus used in this work is described in Chapter 3. In Chapter 4 the determination of the wall heat flux from the surface temperature measurements is described. The experimental measurements are presented in Chapter 5, and the heat flux results are presented and discussed in Chapter 6. The work is then summarized in Chapter 7.

CHAPTER 2

UNSTEADY HEAT TRANSFER DURING COMPRESSION AND EXPANSION IN THE ABSENCE OF COMBUSTION

2.1 Introduction

Experimental results for the wall heat flux in reciprocating internal combustion engines reveal the complexity of the physical processes that occur in these systems. One important result is an observed directional reversal in the wall heat transfer (Le Feuvre, et al., 1969 and Alkidas, 1979) in unfired engines. That is, the heat transfer which initially is in the direction from the gas to the walls, changes to the direction from the walls to the gas. This occurs even though the free stream or bulk temperature of the gas is greater than the wall temperature. Thus the application of Newton's law of cooling $q = h(T_\infty - T_{wall})$ is not useful since a negative heat transfer coefficient, h, would arise. This reversal of the heat transfer was also observed by Dao, (1972) who did some computational work predicting the reverse in heat transfer using a finite difference formulation. Annand and Pinfold (1980) obtained data on this phenomena.

In this work an analytical solution to this problem is developed. This solution agrees well with experimental data and with the finite difference formulation of the problem. This analytical solution is especially useful and provides the unsteady wall heat flux solely as a function of the instantaneous volume of the cylinder. A theory of the physical mechanism is proposed and temperature profiles are obtained which provide supporting evidence for this theory.

2.2 Analysis

The determination of the heat flux at the wall is based on the solution of the conduction equation in the solid and the conservation equations of continuity, momentum and energy in the gas. The two solutions are joined by requiring the temperature and the heat flux to be continuous at the interface. It is assumed that the gradients in the gas are restricted to a small boundary layer and that outside this region the gas is compressed isentropically. The gas and solid are thermally semi-infinite with only one spatial dimension of interest, the dimension perpendicular to the plane wall boundary. The temperature rise in the gas is large such that it can be assumed that mechanical contributions to the energy and momentum balances can be neglected. The viscous stress and body force terms are also neglected. At the temperature of interest, the gas, air, does not emit or absorb radiant energy.

On the solid side of the interface, the conduction equation is

$$\frac{\partial T}{\partial t} = \alpha_s \frac{\partial^2 T}{\partial x^2} \qquad (2.2\text{-}1)$$

where $\alpha_s = k_s/\rho_s c_s$. The initial and boundary conditions are:

$$T(x,0) = T_i \qquad (2.2\text{-}2a)$$

$$T(0,t) = T_w(t) \qquad (2.2\text{-}2b)$$

$$T(\infty,t) = T_i \qquad (2.2\text{-}2c)$$

The solution to this problem which is given in Carslaw and Jaeger (1978), obviously requires the knowledge of $T_w(t)$ and T_i. Since the wall temperature variation $T_w(t)$ is not known, the gas side problem must be considered. In detail, continuity of temperature and heat flux at the interface between the gas and the solid, is assumed. This will provide the necessary condition to completely specify the problem.

The equations in the gas are:

$$\frac{\partial \rho}{\partial t} + \frac{\partial}{\partial x}(\rho u) = 0 \qquad (2.2\text{-}3)$$

$$\rho \frac{\partial u}{\partial t} + \rho u \frac{\partial u}{\partial x} = -\frac{\partial P}{\partial x} \qquad (2.2\text{-}4)$$

$$\rho c_p \frac{DT}{Dt} = \frac{DP}{Dt} + \frac{\partial}{\partial x}\left(k \frac{\partial T}{\partial x}\right) \qquad (2.2\text{-}5)$$

Note that the velocity, u, is in the direction perpendicular to the wall. The initial and boundary conditions are:

$$T = T_i \qquad \text{at } t = 0 \qquad (2.2\text{-}6a)$$

$$T = T_w(t) \qquad \text{at } x = 0 \qquad (2.2\text{-}6b)$$

$$T = T_\infty(t) \qquad \text{at } x \to \infty \qquad (2.2\text{-}6c)$$

An order of magnitude analysis is presented in Appendix A and shows that the energy and momentum equations can be simplified with the pressure being only a function of time, that is, $P = P_\infty(t)$. The conservation equations to be solved are therefore given by:

$$\frac{\partial \rho}{\partial t} + \frac{\partial}{\partial x}(\rho u) = 0 \qquad (2.2\text{-}7)$$

$$\rho c_p \frac{DT}{Dt} = \frac{dP_\infty}{dt} + \frac{\partial}{\partial x}\left(k \frac{\partial T}{\partial x}\right) \qquad (2.2\text{-}8)$$

A method similar to that used by Isshiki and Nishiwaki (1974) is used to obtain the gas heat flux at the wall. The Eulerian coordinates x, t are transformed to the Lagrangian coordinates ψ, t according to:

$$\frac{\partial \psi}{\partial x} = \frac{\rho}{\rho_i}, \quad \frac{\partial \psi}{\partial t} = -\frac{\rho u}{\rho_i} \qquad (2.2\text{-}9)$$

These transformations satisfy the equation of continuity, Equation (2.2-7). Applying the transformation gives

$$\frac{\partial}{\partial t}\Big|_x = \frac{\partial}{\partial \psi}\Big|_t \frac{\partial \psi}{\partial t}\Big|_x + \frac{\partial}{\partial t}\Big|_\psi \frac{\partial t}{\partial t}\Big|_x = \frac{\partial}{\partial t}\Big|_\psi - \frac{\rho u}{\rho_i} \frac{\partial}{\partial \psi}\Big|_t \qquad (2.2\text{-}10)$$

$$\frac{\partial}{\partial x}\Big|_t = \frac{\partial}{\partial \psi}\Big|_x \frac{\partial \psi}{\partial x}\Big|_t + \frac{\partial}{\partial t}\Big|_\psi \frac{\partial x}{\partial t}\Big|_t = \frac{\rho}{\rho_i} \frac{\partial}{\partial \psi} \qquad (2.2\text{-}11)$$

so that the energy equation in ψ, t coordinates becomes:

$$\rho c_p \frac{\partial T}{\partial t} = \frac{dP_\infty}{dt} + \frac{\rho}{\rho_i} \frac{\partial}{\partial \psi}\left(k \frac{\rho}{\rho_i} \frac{\partial T}{\partial \psi}\right) \qquad (2.2\text{-}12)$$

To proceed further it is convenient (but not necessary) to assume a linear variation of the thermal conductivity of an ideal gas. This gives:

$$k \frac{\rho}{\rho_i} = k_i \frac{T}{T_i} \frac{\rho}{\rho_i} = k_i \frac{P}{P_i} = k_i \frac{P_\infty}{P_i} \tag{2.2-13}$$

which yields:

$$\rho c_p \frac{\partial T}{\partial t} = \frac{dP_\infty}{dt} + \frac{\rho}{\rho_i} k_i \frac{P_\infty}{P_i} \frac{\partial^2 T}{\partial \psi^2} \tag{2.2-14}$$

Transforming the time according to:

$$d\tau = \frac{P_\infty}{P_i} dt \tag{2.2-15}$$

so that:

$$\frac{\partial}{\partial t} = \frac{\partial}{\partial \tau} \frac{d\tau}{dt} = \frac{P_\infty}{P_i} \frac{\partial}{\partial \tau} \tag{2.2-16}$$

yields:

$$\frac{\partial T}{\partial \tau} = \frac{\gamma-1}{\gamma} \frac{T}{P_\infty} \frac{dP_\infty}{d\tau} + \alpha_i \frac{\partial^2 T}{\partial \psi^2} \tag{2.2-17}$$

Outside the thermal boundary layer the compression is isentropic as shown in Nikanjam (1977), and for constant specific heats:

$$\frac{P_\infty}{P_i} = \frac{T_\infty}{T_i}^{\gamma/(\gamma-1)} \tag{2.2-18}$$

Thus

$$\frac{\partial T}{\partial \tau} = \frac{T}{T_\infty} \frac{dT_\infty}{d\tau} + \alpha_i \frac{\partial^2 T}{\partial \psi^2} \qquad (2.2\text{-}19)$$

If we now let $\phi = \frac{T}{T_\infty} - 1$ we obtain the diffusion equation

$$\frac{\partial \phi}{\partial \tau} = \alpha_i \frac{\partial^2 \phi}{\partial \psi^2} \qquad (2.2\text{-}20)$$

subject to the following initial and boundary conditions:

$$\phi\ (\psi,0) = 0 \qquad (2.2\text{-}21a)$$

$$\phi\ (0,\tau) = \frac{T_w}{T_\infty} - 1 \qquad (2.2\text{-}21b)$$

$$\phi\ (\infty,\tau) = 0 \qquad (2.2\text{-}21c)$$

Two alternative methods of obtaining the wall heat flux in this problem are available and used here. One is a numerical solution using the finite difference technique. From this method, temperature profiles as well as heat flux are obtainable. This method is described in Appendix C.

The second method is an analytical solution*. The wall heat flux is given by:

*In addition to the analytical solution developed here, it is also possible to obtain the wall heat flux using the Duhamel integral (Carslaw and Jaeger, 1978).

$$q_{w,g} = -k \left.\frac{\partial T}{\partial x}\right|_{x=0} = -k \frac{\rho}{\rho_i} \left.\frac{\partial T}{\partial \psi}\right|_{\psi=0} = -k \frac{\rho}{\rho_i} T_\infty \left.\frac{\partial \phi}{\partial \psi}\right|_{\psi=0} \quad (2.2\text{-}22)$$

Substituting Equations (2.2-13) and (2.2-18) into this relation yields:

$$q_{w,g} = -k_w \left(\frac{T_\infty}{T_i}\right)^{(\gamma/\gamma-1)} \frac{T_i}{T_w} T_\infty \left.\frac{\partial \phi}{\partial \psi}\right|_{\psi=0} \quad (2.2\text{-}23)$$

A solution may be readily obtained for a polynomial variation of ϕ_w, i.e., for:

$$\phi_w = \frac{T_w}{T_\infty} - 1 = A_0 + A_1\tau + A_2\tau^2 + A_3\tau^3 + A_4\tau^4 \quad (2.2\text{-}24)$$

(Note that variations in both T_w and T_∞ may be incorporated in this polynomial). In detail, for:

$$\frac{\partial \phi_m}{\partial \tau} = \alpha_i \frac{\partial^2 \phi_m}{\partial \psi^2} \quad (2.2\text{-}25)$$

$$\phi_m (\psi, 0) = 0 \quad (2.2\text{-}26a)$$

$$\phi_m (0, \tau) = A_m \tau^m \quad (2.2\text{-}26b)$$

$$\phi_m (\infty, \tau) = 0 \quad (2.2\text{-}26c)$$

the solution, for any positive integer m is:

$$\phi_m = A_n \Gamma (n + 1) (4\tau)^n i^{2n} \operatorname{erfc} (\psi/2\sqrt{\alpha_i \tau}) \quad (2.2\text{-}27)$$

where $n = \frac{m}{2}$.

Since the partial differential equation and the boundary conditions are linear, solutions may be superposed. Therefore, for the fourth order polynomial of Equation (2.2-24), we obtain the following temperature distribution:

$$\phi(\psi,\tau) = A_0 \operatorname{erfc} z + A_1\, \Gamma(2)\, (4\tau)\, i^2 \operatorname{erfc} z + A_2\, \Gamma(3)\, (4\tau)^2\, i^4 \operatorname{erfc} z$$

$$+ A_3\, \Gamma(4)\, (4\tau)^3\, i^6 \operatorname{erfc} z + A_4\, \Gamma(5)\, (4\tau)^4\, i^8 \operatorname{erfc} z \qquad (2.2\text{-}28)$$

where $z \equiv \dfrac{\psi}{2\sqrt{\alpha_i \tau}}$. For the heat flux we have:

$$\frac{\partial \phi}{\partial \psi} = \frac{\partial \phi}{\partial z}\,\frac{\partial z}{\partial \psi} = \frac{1}{2\sqrt{\alpha_i \tau}}\,\frac{\partial \phi}{\partial z} = \frac{1}{2\sqrt{\alpha_i \tau}}\left[-\frac{2 A_0}{\sqrt{\pi}} e^{-z^2}\right.$$

$$- 4 A_1\, \tau\, i \operatorname{erfc} z - 32 A_2\, \tau^2\, i^3 \operatorname{erfc} z - 384 A_3\, \tau^3\, i^5 \operatorname{erfc} z$$

$$\left. - 6144 A_4\, \tau^4\, i^7 \operatorname{erfc} z\right] \qquad (2.2\text{-}29)$$

The wall heat flux is therefore given by:

$$q_{w,g} = -k \left.\frac{\partial T}{\partial x}\right|_{x=0} = k_w \left(\frac{T_\infty}{T_i}\right)^{(\gamma/\gamma-1)} \frac{T_\infty}{\sqrt{\alpha_i}} \left[0.564 A_0\, \tau^{-1/2}\right.$$

$$+ 1.128 A_1\, \tau^{1/2} + 1.504 A_2\, \tau^{3/2} + 1.805 A_3\, \tau^{5/2}$$

$$\left. + 2.06 A_4\, \tau^{7/2}\right] \qquad (2.2\text{-}30)$$

Since the variation in T_∞ is so much greater than that in T_w, it is permissible to assume that T_w is a constant as follows:

$$\phi_w(\tau) = \frac{T_w(\tau)}{T_\infty(\tau)} - 1 \approx \frac{T_w}{T_\infty(\tau)} - 1 \qquad (2.2\text{-}31)$$

The wall heat flux therefore is given by:

$$q_{w,g} = \sqrt{k_i \rho_i c_{pi}} \left(\frac{T_\infty}{T_i}\right)^{(\gamma/\gamma-1)} T_\infty \left\{0.564\, A_0\, \tau^{-1/2} + 1.128\, A_1\, \tau^{1/2} + 1.504\, A_2\, \tau^{3/2} + 1.805\, A_3\, \tau^{5/2} + 2.06\, A_4\, \tau^{7/2}\right\} \qquad (2.2\text{-}32)$$

Thus the wall heat flux is given solely in terms of engine parameters. That is, from rod length, crank radius etc. the piston displacement may be calculated (see Appendix D). From this the pressure, bulk gas temperature $T_\infty(\tau)$, and the coefficients A_0, A_1, A_2, etc. are readily obtained. A description of the program to calculate the wall heat flux and a sample calculation are given in Appendix B.

For the comparison of this analytical solution with experimental data, lower as well as higher order polynomials for ϕ_w were also considered. For higher order polynomials additional terms are necessary. The solution for the sixth order polynomial is:

$$\phi(\psi,\tau) = A_0 \operatorname{erfc} z + A_1\, \Gamma(2)\, (4\tau)\, i^2\operatorname{erfc} z + A_2\, \Gamma(3)\, (4\tau)^2\, i^4 \operatorname{erfc} z$$

$$+ A_3\, \Gamma(4)\, (4\tau)^3\, i^6 \operatorname{erfc} z + A_4\, \Gamma(5)\, (4\tau)^4\, i^8 \operatorname{erfc} z$$

$$+ A_5\, \Gamma(6)\, (4\tau)^5\, i^{10} \operatorname{erfc} z + A_6\, \Gamma(7)\, (4\tau)^6\, i^{12} \operatorname{erfc} z \qquad (2.2\text{-}33)$$

where $z \equiv \dfrac{\psi}{2\sqrt{\alpha_i \tau}}$

The expression for the wall heat flux is given by:

$$q_{w,g} = \sqrt{k_i \rho_i c_{pi}} \left(\frac{T_\infty}{T_i}\right)^{(\gamma/\gamma-1)} T_\infty \left\{0.564\, A_0\, \tau^{-1/2}\right.$$

$$+ 1.128\, A_1\, \tau^{1/2} + 1.504\, A_2\, \tau^{3/2} + 1.805\, A_3\, \tau^{5/2} + 2.06\, A_4\, \tau^{7/2}$$

$$\left. + 2.292\, A_5\, \tau^{9/2} + 2.50\, A_6\, \tau^{11/2}\right\} \qquad (2.2\text{-}34)$$

2.3 Results and Discussion

The analytical solution for the unsteady wall heat flux, $q_{w,g}$, was obtained from the boundary layer equations in the gas using the approximation that $T_w(\tau)/T_\infty(\tau) \approx T_w/T_\infty(\tau)$. This is a very good approximation because the free stream gas temperature, T_∞, undergoes a large change in contrast to the surface temperature, T_w, which only experiences a small change. A comparison of these results with the experimental data of Dao (1972) is shown in Figure 2.3-1. The agreement is seen to be very good. Note that the experimental data shows some irregularity at the beginning and at the end of the cycle. This is due, in part, to the fact that these data are from a recompression cycle that occurs between two cycles with the normal opening and closing of valves, etc.

The results from the analytical solution for the heat flux $q_{w,g}$, shown in Figure 2.3-1, are based on the fourth order polynomial function for $(T_w/T_\infty) - 1$, as given in Equation 2.2-32. A third order polynomial was found to be inadequate, while the results from the fifth and sixth order polynomials (cf. Equation 2.2-34) were virtually identical to the fourth order polynomial.

A determination of the wall heat flux employing a numerical finite difference method was also carried out. This consisted of a numerical calculation in the gas and in the solid subject to the requirement that the unknown temperature and heat flux be equal at the gas-solid interface. The details are presented in Appendix C. A comparison of the

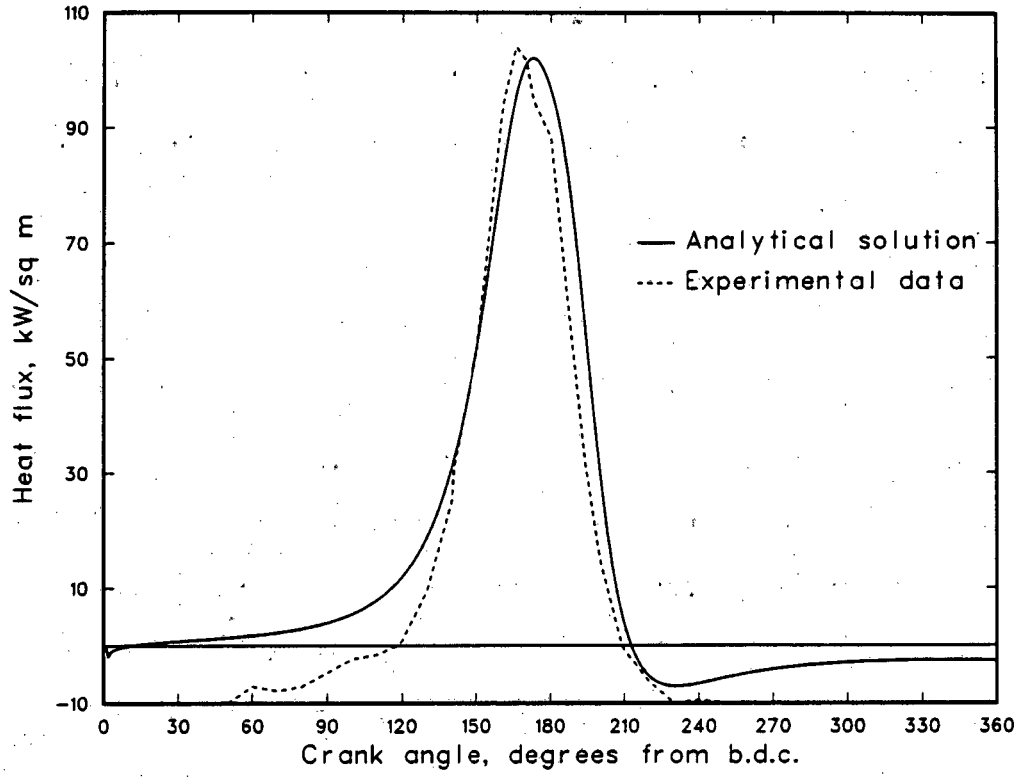

Figure 2.3-1: Unsteady wall heat flux analytical solution compared to experimental data from Dao (1972).

result from the analytical solution, $q_{w,g}$, with that from the finite difference calculation is shown in Figure 2.3-2. Good agreement is found.

An investigation of the effect on the finite difference results of using smaller increments in time and space was made. The results were found to be virtually identical with the present calculations which used a time increment of one crank angle degree ($\Delta t = 2.17 \times 10^{-4}$ sec) and spatial increments of $\Delta x = 7.67 \times 10^{-5}$ m in the solid. Because of the nature of the transformations used on the gas side equations and the stability constraints of the problem, the spatial increment in the gas varies with time. (See Appendix C).

In Figure 2.3-1 it is seen that the wall heat flux decreases rapidly after the top-dead-center position (180 degrees) is reached and indeed turns negative. Thus, there is a transfer of energy from the wall to the gas even though the free stream gas temperature, T_∞, is always greater than (or equal to) the wall temperature, T_w. This phenomenon can be explained by referring to the calculated temperature profiles shown in Figure 2.3-3. Only the gas temperature profile is shown but recall that the results did require a simultaneous calculation of conduction in the wall and convection in the gas with a matching of the temperature and the heat flux at the interface. During the compression and expansion process, the free stream gas temperature, T_∞, undergoes large changes which is in contrast to the very small changes in the temperature of the surface of the cylinder, T_w. This is clearly shown in Figure 2.3-3.

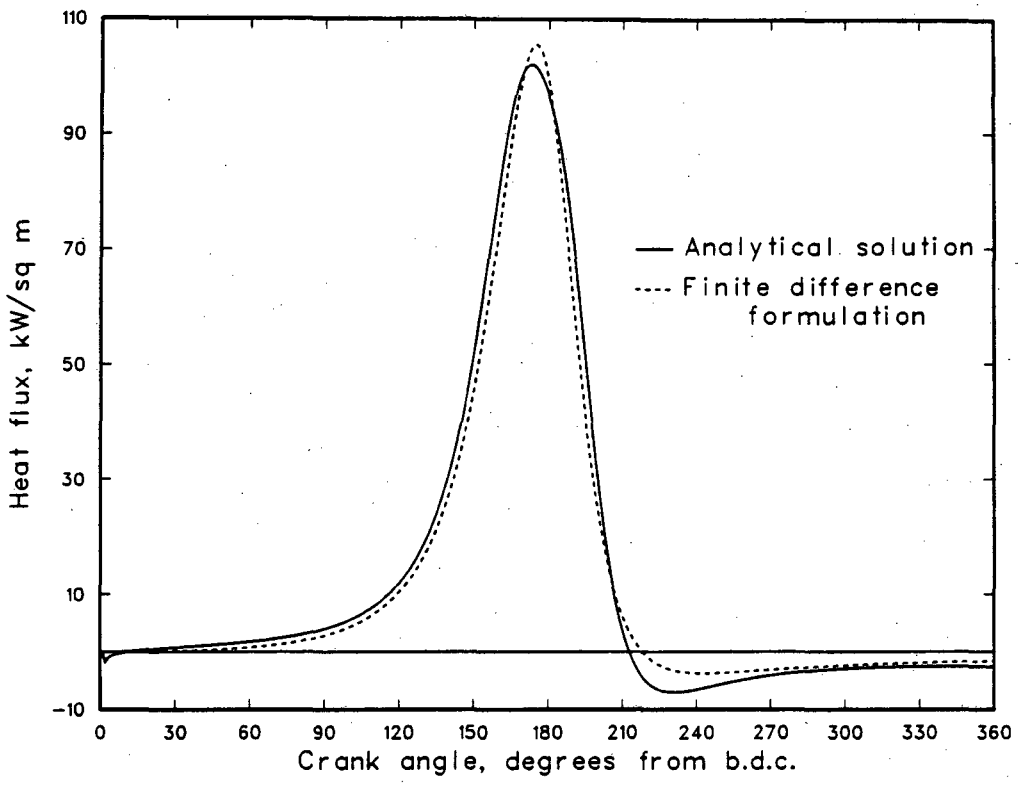

Figure 2.3-2: Comparison of unsteady wall heat flux analytical solution and finite difference solution.

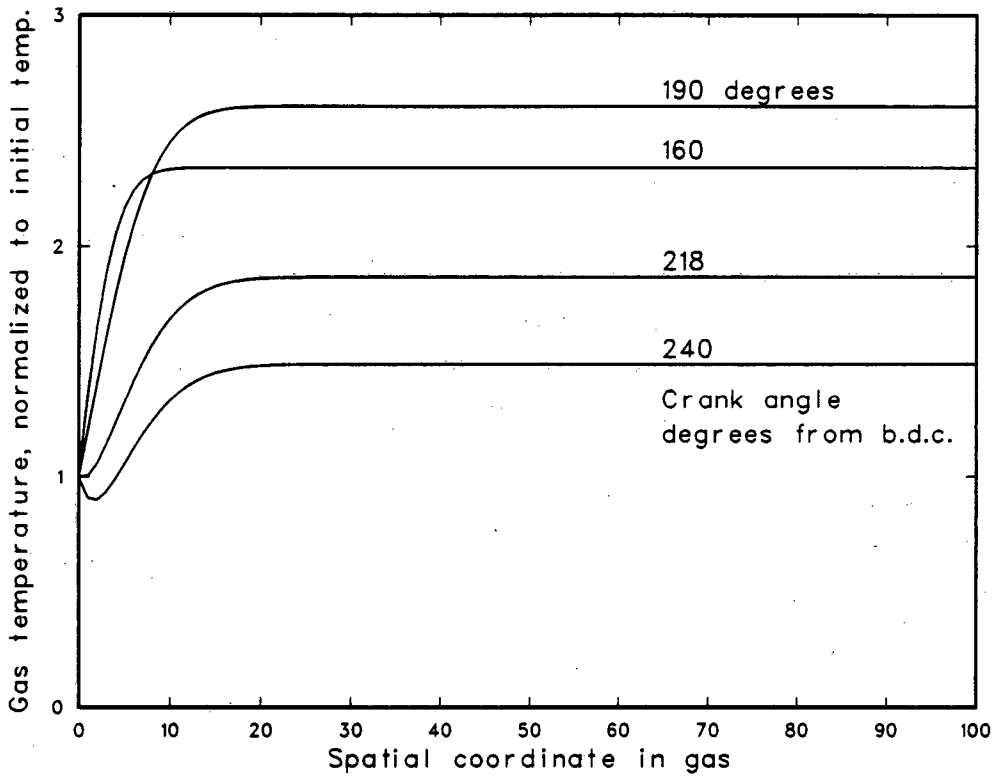

Figure 2.3-3: Temperature profiles in the gas for various crank angles; results from finite difference solution.

Again, referring to Figure 2.3-3 the curve labeled "160 degrees" exhibits the anticipated temperature profile of a compressed gas with a monotonic decrease from the hot free stream gas, T_∞, to the cold wall, T_w. At 190 degrees the compression has been completed and the expansion has begun (cf. Figure 2.3-2 for the heat flux). As the expansion continues, the gas temperature decreases substantially while the wall temperature changes slightly. (It is emphasized that the wall temperature is not assumed constant here; rather, the calculations yield very little change for T_w.) Note that for the 218 degree case the temperature gradient at the wall is almost zero even though the free stream temperature is considerably greater than the surface temperature. As the expansion continues the gas temperature decreases further with (still) little change in the wall temperature. As shown in the related analysis in Appendix H, this results from the large value of the parameter $k\rho c$ for cast iron in comparison to the small value for air. Note that the large value of the heat capacity ρc of the cast iron keeps the temperature change small and the large value of the thermal conductivity minimizes the temperature gradient.

For the 240 degree case, the temperature profile is no longer monotonic, but exhibits a minimum (zero heat flux), as is shown in Figure 2.3-3. It is seen that the expansion has cooled in the gas in the region near the surface to a value less than the wall temperature. Thus, the cold wall transfers energy to the colder adjoining gas even though the free stream value, T_∞, is much greater than the wall value, T_w.

CHAPTER 3

EXPERIMENTAL SYSTEM FOR THE STUDY OF HEAT TRANSFER AND FLAME PROPAGATION

3.1 Introduction

Experiments were performed in a combustion system to study heat transfer, flame propagation, and their interaction. To study these phenomena, data for the wall temperature variation, chamber pressure variation, and flame location are needed. The wall temperature variation was obtained using a thin film resistance thermometer, the pressure measurement made using a piezioelectric transducer, and the flame location obtained from high speed schlieren movies. The thin film resistance thermometer was chosen for its fast response time (~1 microsecond); similarly the piezioelectric pressure transducer was used for its fast response characteristics. Photographic detection of the flame front location was chosen in order to detect the shape of the flame front as well as location.

The data on temporal wall temperature variation provide sufficient information to determine the unsteady wall heat flux. The methodology is discussed in Chapter 4. The pressure data provide information needed for modeling of the heat transfer phenomena. The photographic records of the flame front location are used in explaining the observed variations in heat transfer, and are needed for modeling purposes. In addition, the pressure data and flame front location data provide sufficient information to calculate the flame speed with respect to the unburnt gases. This calculation is described and results are reported by Woodard, et al. (1981).

3.2 System Description

The experimental system used in this study provides for the simultaneous acquisition of pressure measurements, wall temperature measurements, and schlieren movies. The system consists of the compression - expansion apparatus (CE-1) which creates the environment for the combustion event, the instrumentation for the measurement of the desired quantities, and the computer system for conversion and storage of the data. The system is shown in Figure 3.2-1. The apparatus and instrumentation are described in the next sections.

The control of the event starts with the schlieren camera, Hycam, which sends a trigger to the control panel when the camera has attained the desired film speed. The control panel then simultaneously triggers the computer system for acquisition of the measurements, the CE-1 driver section if needed, and the ignition source.

3.3 Experimental Apparatus

The compression expansion apparatus (CE-1) (Oppenheim, 1976) was designed to simulate, as closely as possible, the environment inside the cylinder of an internal combustion engine while allowing full optical access to the combustion event. The CE-1 consists of three parts: the test section, the driver section, and the snubber section. The test section consists of a horizontally mounted duct of square cross section (3.8 cm x 3.8 cm). The duct is enclosed on the two vertical sides with optical quality borosilicate glass windows. The horizontal sides have two access ports each, in which are located the pressure transducer and the temperature gauge, as well as the inlet and outlet valves. On one endwall of the duct is a moveable aluminum

Figure 3.2-1: Experimental system and instrumentation.

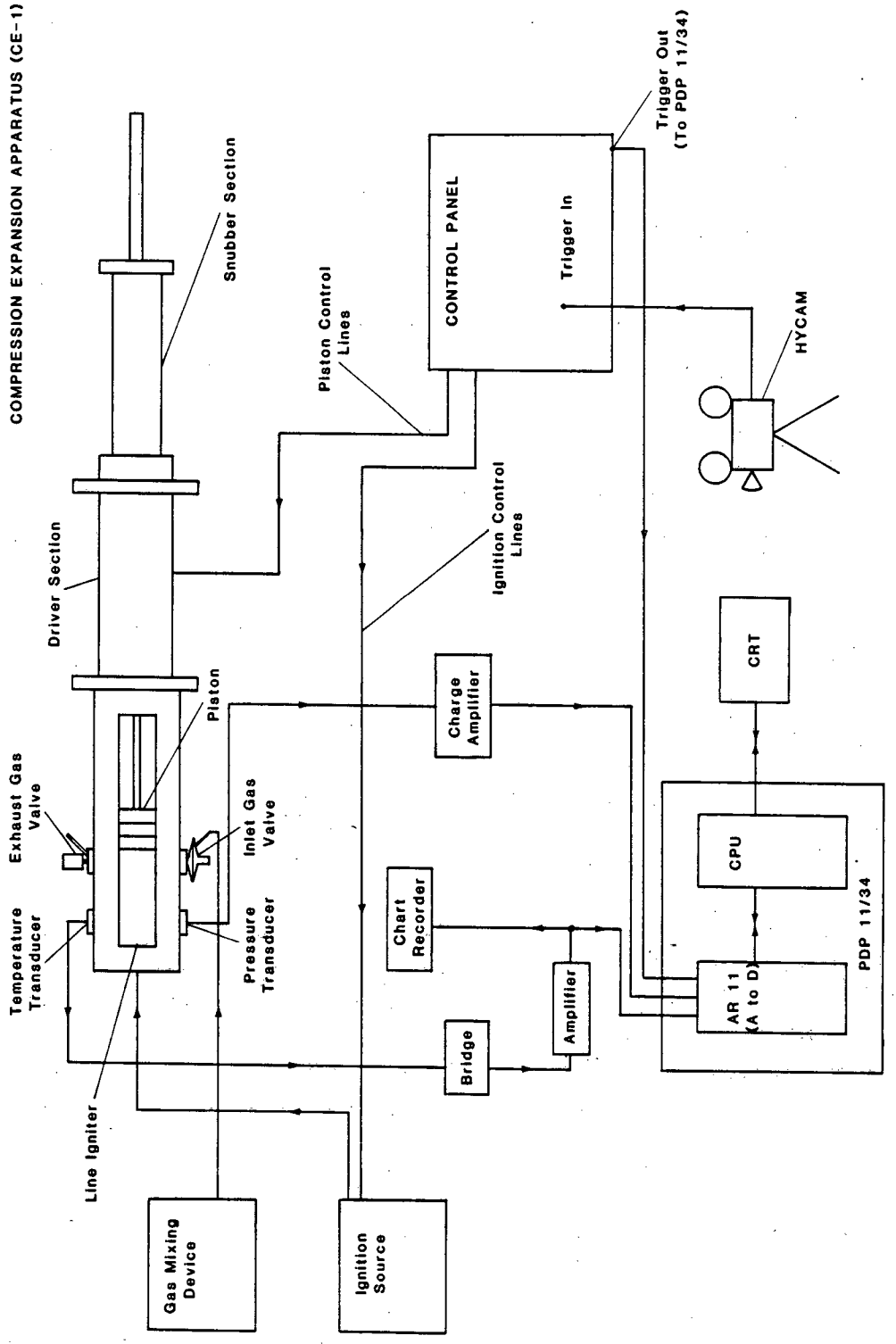

piston. On the opposite endwall is the igniter. The igniter is a line ignition system consisting of a horizontal row of fifteen 0.0508 cm spark gaps formed by brass electrodes, filed to a knife edge. The line of spark gaps runs from window to window at the midpoint of the endwall. The ignition system and its location were designed to obtain, as closely as possible, flame uniformity in the direction perpendicular to the windows. The igniter was driven by a high voltage discharge system operated at 46 kV with an ignition energy of approximately 265 mJ. The timing of the igniter is variable and is controlled at the system control panel.

The CE-1 piston can be operated in four modes: (1) constant volume, (2) ignition expansion, (3) compression ignition, and (4) compression ignition expansion. The movement of the piston required for the last three modes is accomplished by the driver section. The piston in the test section is connected to a piston in the driver section. Force on the driver piston by means of compressed air moves both pistons. The flow of compressed air from a reservoir at 725 kPa is controlled by solenoid valves. The response time and variability of the valves negated the systematic execution of experiments. The timing of ignition relative to the fully compressed position of the piston (top dead center, t.d.c.) was found to be variable. Therefore, limited experimental work was conducted for these modes of operation.

The trajectory of the test piston is controlled by the snubber section. In the snubber section a piston is attached to the same rod as the driver and test section pistons. The snubber piston moves through an enclosure of varying diameter. Flowing around the snubber piston is a light oil, SAE 10, which creates varying hydraulic forces

on the piston. These forces control the piston trajectory. Because of the inertia of the three pistons and connecting rods, the piston velocity is slightly lower than desired in the initial part of the event. However, the agreement with the approximately sine wave variation for an engine piston position is still very good (Smith, 1977).

3.4 Wall Temperature Instrumentation

The wall temperature gauge shown in Figure 3.4-1 consists of a thin platinum film deposited on a glass ceramic base, Macor, which is manufactured by Corning Glass Works (Corning, 1978). The film acts as a resistance which is part of a Wheatstone bridge circuit. The platinum film resistance varies with changes in the film temperature, i.e., with the wall temperature. The wall temperature gauge was located in the upper access port nearest the line igniter as seen in Figure 3.2-1, except in those experimental cases where noted otherwise. The response characteristic of the thin film gauge and the bridge circuit is of the order of one microsecond. For calibration purposes and initial temperature measurement, a copper - constantan thermocouple is mounted on the surface. The relationship between the platinum film resistance and the surface temperature is determined by heating the gauge in an oven. The bridge output and thermocouple temperature determine the calibration. The gauge calibration was found to be linear to within 1% over the temperature range of interest.

3.5 Pressure Instrumentation

The pressure in the test section during combustion was measured with a piezioelectric transducer manufactured by AVL, model 12 QP300 CVK. The transducer was located in the lower access port nearest

Figure 3.4-1: Wall temperature gauge.

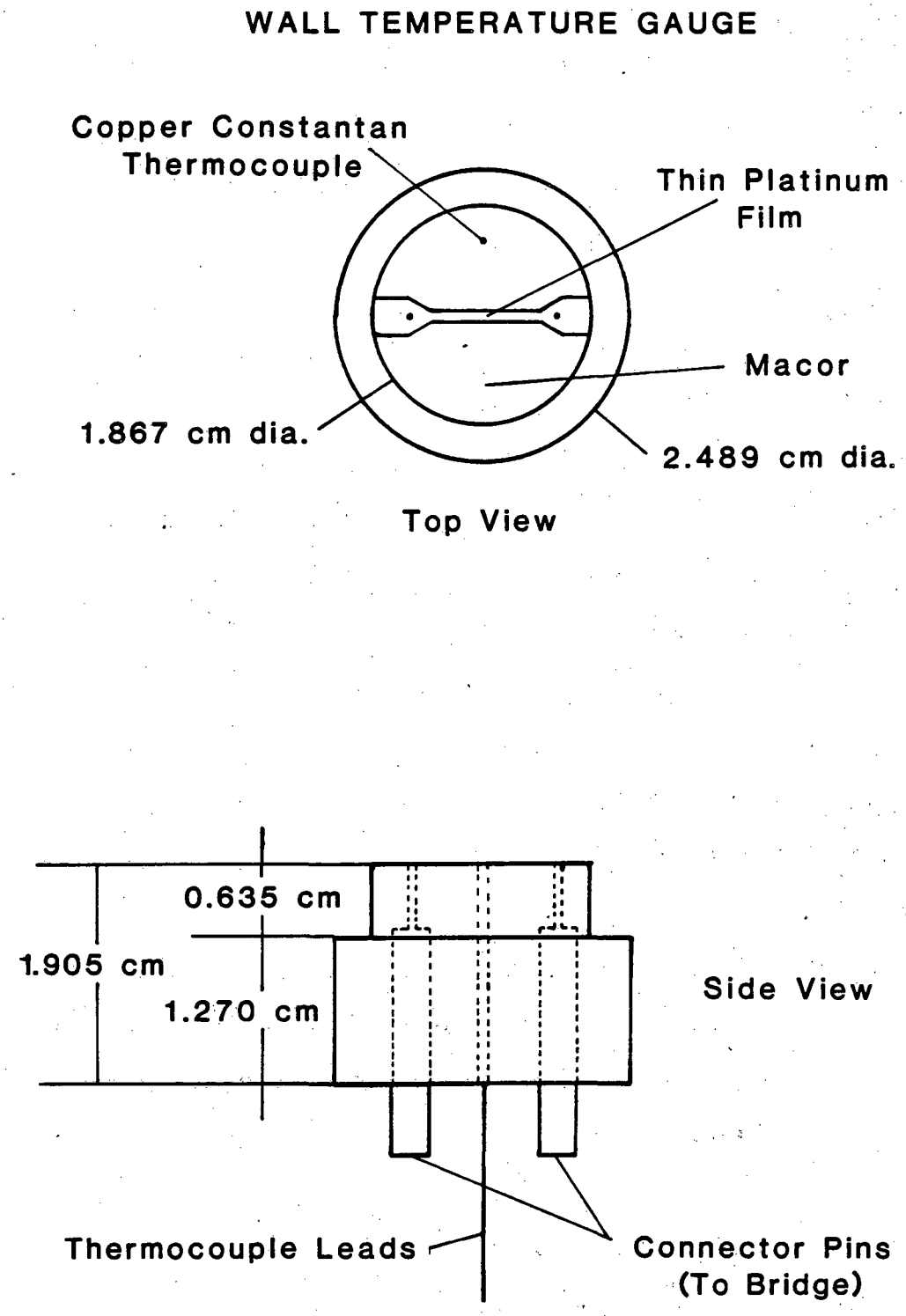

the line igniter. The calibration of the transducer signal was dynamically verified in a shock tube. The shock tube tests showed a rise time for the transducer of approximately ten microseconds, which is more than sufficient for the combustion events being investigated.

3.6 Schlieren Movie Equipment

To determine the flame location and flame shape during the combustion events, high speed schlieren movies were taken simultaneously with the pressure and wall temperature data. The schlieren equipment is shown in Figure 3.6-1. The camera is a Hycam model 41-0004 operated at approximately 5400 frames per second. The light source is a Oriel Xenon lamp collimated through a 2.0 mm hole. Parallel light is provided from the light source through the test section, and to the camera by use of two sperical mirrors each with a focal length of 3.94 meters. Between the spherical mirror and camera is a vertical knife edge schlieren stop. The movies were recorded on Kodak Tri-X Reversal film.

3.7 Gas Mixing Apparatus

The test section was filled with a premixed fuel/air mixture by use of a flow-through purging system. The fuel/air mixture is introduced through the inlet valve. The mixture displaces the burnt product gases which then flow out the outlet valve. The mixture flows into the test section for a sufficiently long time to allow a complete purge. The equivalence ratio of the combustible mixture is controlled by flow rotometers. The gas mixing apparatus was calibrated using a Hewlett Packard Model 5750 Gas Chromatograph with a thermal conductivity detector and a flame ionization detector. The results

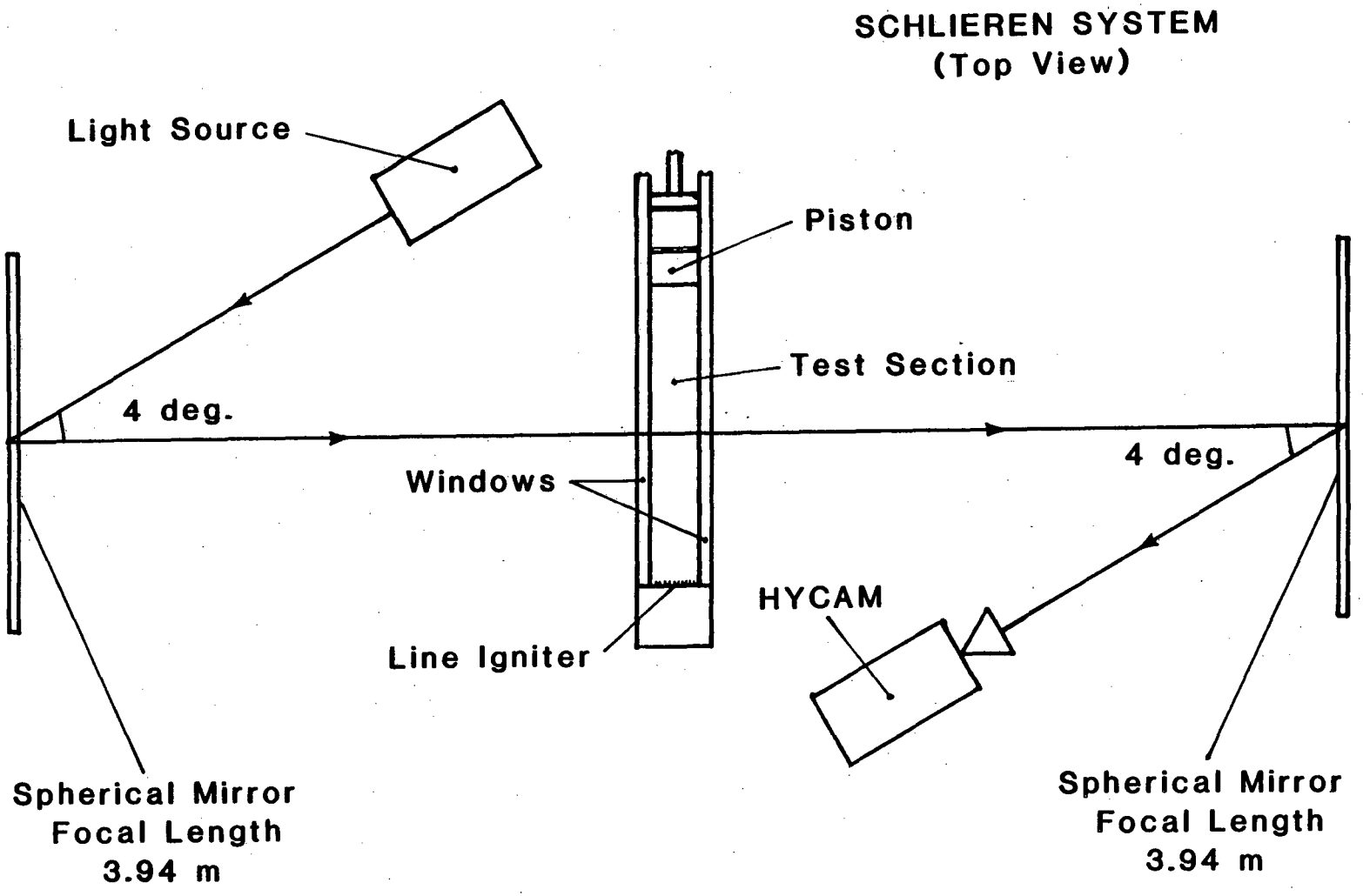

Figure 3.6-1: Schematic of schlieren system.

were directly analyzed on an Autolab System IV integrator. Both the calibration and the repeatability of the mixing device were assessed using the gas chromatograph, and the error in the delivered equivalence ratio was found to be approximately 1%.

3.8 Data Acquisition

The pressure and wall temperature data were sampled by a PDP 11/34 minicomputer using an AR-11 analog to digital converter. The software written for the data acquisition permits samples to be taken from both the pressure and wall temperature signals every 200 microseconds. This system provides much greater resolution of the data both in magnitude and temporal variation, as compared to the previous methods which used analog oscilloscopes.

The use of the minicomputer introduced the possibility of damage to the computer from ground loops and current surges. To prevent such damage the instrumentaton was connected to the power outlet through a 15 amp isolation transformer. The use of the transformer however, added a low level noise to the sampled data. The noise being a very low level, was easy to remove as described in Appendix F.

CHAPTER 4

DETERMINATION OF WALL HEAT FLUX

4.1 Assumptions

The wall heat flux is determined from the transient wall temperature measurements. The time duration of the experiments is sufficiently small and the Macor temperature gauge of sufficient thickness that the temperature gauge can be considered thermally infinite; that is, the Fourier number ($= \alpha t/S^2$) is found to be 0.0009 which is much less than one. The one dimensional heat conduction equation is:

$$\frac{\partial T}{\partial t} = \alpha \frac{\partial^2 T}{\partial x^2} \qquad (4.1\text{-}1)$$

where x is the direction perpendicular to the wall surface, and the thermal diffusivity, $\alpha = k/\rho c$. The initial and boundary conditions are:

$$T(x,0) = T_i \qquad (4\text{-}1.2a)$$

$$T(0,t) = T_w(t) \qquad (4\text{-}1.2b)$$

$$T(\infty,t) = T_i \qquad (4\text{-}1.2c)$$

4.2 Solution

The solution for this problem with variable wall temperature, $T_w(t)$, can be found using the solution for constant wall temperature and the Duhamel integral theorem as in Carslaw and Jaeger (1978). The solution for constant wall temperature, T_w, is given by :

$$(T(x,t) - T_i) = (T_w - T_i)\left(1 - \frac{2}{\sqrt{\pi}} \int_0^{\frac{x}{2\sqrt{\alpha t}}} e^{-\eta^2}\right) d\eta$$

$$= (T_w - T_i)\left(1 - \text{erf}\ \frac{x}{2\sqrt{\alpha t}}\right) \equiv F(x,t) \qquad (4.2\text{-}1)$$

Using the Duhamel integral theorem, the solution for the transient wall temperature problem can then be written as:

$$(T(x,t) - T_i) = \int_0^t (T_w(\lambda) - T_i) \frac{\partial}{\partial t} F(x,t-\lambda)d\lambda$$

or

$$(T(x,t) - T_i) = (T_w(0) - T_i)\left(1-\text{erf}\left(\frac{x}{2\sqrt{\alpha t}}\right)\right) +$$

$$\int_0^t \left(1-\text{erf}\left(\frac{x}{2\sqrt{\alpha(t-\lambda)}}\right)\right) \frac{dT_w(\lambda)}{d\lambda}\, d\lambda \qquad (4.2\text{-}2)$$

The wall heat flux is given by:

$$q_w = -k \left.\frac{\partial T}{\partial x}\right|_{x=0} = \sqrt{\frac{k\rho c}{\pi}} \int_0^t \frac{1}{\sqrt{(t-\lambda)}} \frac{dT_w(\lambda)}{d\lambda}\, d\lambda \qquad (4.2\text{-}3)$$

By integrating by parts, the following convenient result for numerical calculation is obtained:

$$q_w(t) = \sqrt{\frac{k\rho c}{\pi}} \left[\frac{T_w(t)-T_i}{\sqrt{t}} + \frac{1}{2} \int_0^t \frac{T_w(t)-T_w(\lambda)}{(t-\lambda)^{3/2}} \right] d\lambda \qquad (4.2\text{-}4)$$

The values for the properties of the gauge material, Macor, are:

$$k = 1.676 \text{ W/m K}$$

$$\rho = 2520.02 \text{ kg/m}^3$$

$$c = 460.55 \text{ J/kg K}$$

The properties are approximately constant for the temperature range considered.

Thus the wall heat flux depends only on the wall temperature variation and the properties k, ρ, and c. With Equation (2.2-4), these property values, and the experimental measurements, a numerical calculation of the wall heat flux can be made. The methodology for this calculation and a description of the computer program is given in Appendix G.

CHAPTER 5

EXPERIMENTAL MEASUREMENTS

5.1 Introduction

The interaction of a flame with a cold wall involves a complex interplay of fluid mechanics, heat transfer, thermodynamics and chemical processes. The importance of the problem, e.g. for efficiency and emissions considerations, dictates the need to achieve an understanding of the phenomena (Ferguson and Keck, 1977). Mathematical models, and related analytical and numerical results, have been presented for various aspects of the phenomena. These works have addressed both the one-dimensional problem of a flame impinging on a parallel wall, e.g. Kurkov and Mursky (1969) who used one step chemical kinetics and Hocks, Peters, and Adomeit (1981) who used two step kinetics, and the two dimensional case of a flame passing a perpendicular wall, e.g. Carrier, Fendell, and Feldman (1980). Unfortunately, experimental data on the interaction of a flame with a cold wall are limited as has been pointed out by Ferguson and Keck (1977). Isshiki and Nishiwaki (1974) present some temperature and pressure data for one-dimensional flame propagation in constant volume chambers. However, much of the available data are from engines as in Alkidas and Myers (1981) or for the problem of a steady state flame on a burner (Yamazaki and Ikai, 1971). Ferguson and Keck (1977) and Alkidas and Myers (1981) both indicate a need for data on flame propagation and flame-wall interaction (i.e. flame quenching) for the same conditions. In this study, simultaneous data on flame propagation and wall heat transfer during the combustion of gaseous mixtures are

obtained.

The experimental apparatus described in Chapter 3 was used in this study. This apparatus was operated in three distinct modes with independent parameters of equivalence ratio and wall temperature gauge location. Table 5.1-1 summarizes the combinations of factors investigated. Note that repeatability was tested for only the constant volume mode.

Table 5.1-1

Mode of Operation	Equivalence Ratio	Temperature Gauge Location	Repeatability
Constant Volume	X	X	X
Expansion	X		
Compression-Expansion	X		

The constant volume mode of operation was used primarily because of a problem with repeatable ignition timing as discussed in Chapter 3. To study the effect of equivalence ratio for each mode of operation, simultaneous pressure and wall temperature data, and schlieren movies were obtained. Data were obtained for equivalence ratios varying from 1.1 to 0.6 in increments of 0.1, except where noted. For temperature gauge location and repeatability tests, only pressure and wall temperature data were obtained. The conditions for each experimental run are listed in Table 5.1-2. The combustible mixture was methane and air which was ignited with a constant ignition energy of 265 mJ for all cases. This energy level was necessary to ignite the lean mixtures. The pressure and wall temperature data were sampled every 200 μs with

TABLE 5.1-2: Experimental Conditions

Fuel/Oxidizer:	Gaseous Premixed Methane/Air
Ignition Energy:	265 mJ
Data Sampling Rate:	200 μs
Initial Pressure:	Atmospheric
Initial Temperature:	Ambient
Film:	Kodak Tri-X Reversal
Schlieren Stop:	Vertical Knife Edge
Camera Speed:	5400 frames per second

with the initial values at ambient conditions. The schlieren effect for the high speed movies was created by a vertical knife edge stop. The images were recorded on Tri-X Reversal film at a speed of 5400 frames per second.

In this chapter a sample of the experimental measurements are presented with an emphasis on the extremes of the variations. The remainder of the experimental data are presented in Appendix I. The actual experimental measurements, which include the low level noise introduced by the isolation transformer, are presented here. The heat flux results as well as a detailed discussion are presented in Chapter 6.

5.2 Constant Volume Measurements

The temporal variation of pressure for constant volume combustion at an equivalence ratio of 1.0 is presented in Figure 5.2-1. The pressure rises to a maximum with a change in slope occurring at approximately 20 ms. The maximum value of pressure occurs at approximately 60 ms which corresponds fairly well with the conclusion of the combustion event. In Figure 5.2-2 the pressure variation for an equivalence ratio of 0.6 is shown. Here the change in the slope of the pressure variation occurs slightly later, at approximately 70 ms. For this case, the combustion event is much longer in duration, taking approximately 320 ms to complete.

From the schlieren movies taken simultaneously with the pressure and temperature data, the location and shape of the flame front during the combustion event were obtained. These data, for an equivalence ratio of 1.0, are shown in Figure 5.2-3. Initially the flame front is elongated with a correspondingly large surface area. As the flame

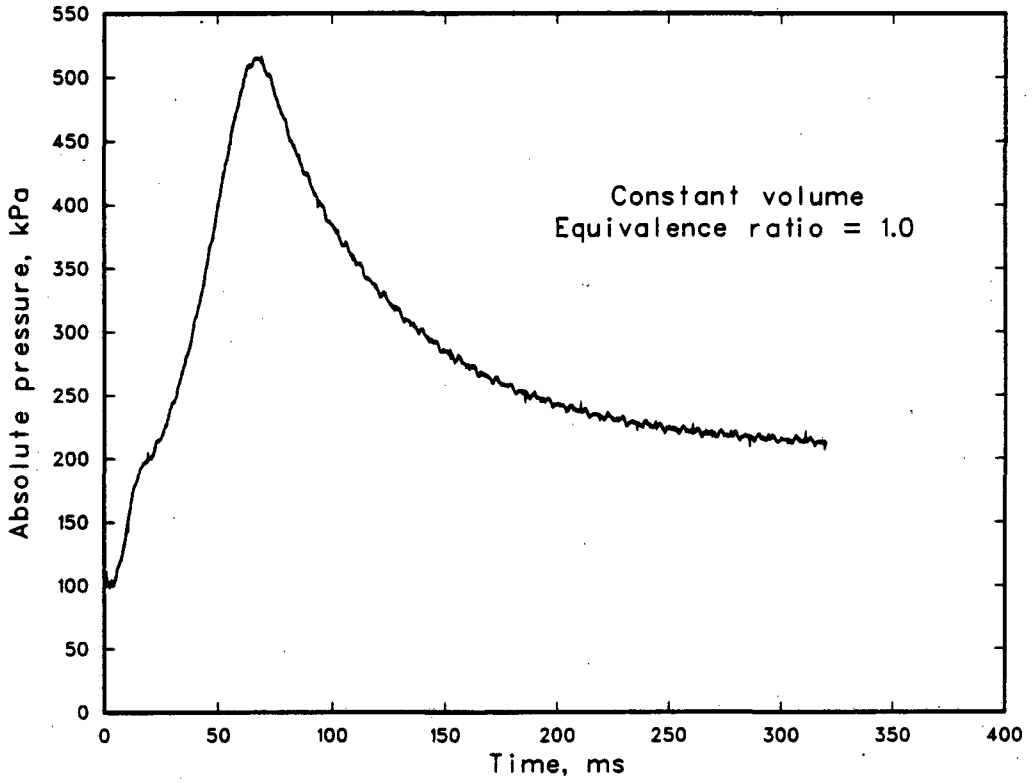

Figure 5.2-1: Absolute pressure variation with time; constant volume combustion; equivalence ratio 1.0.

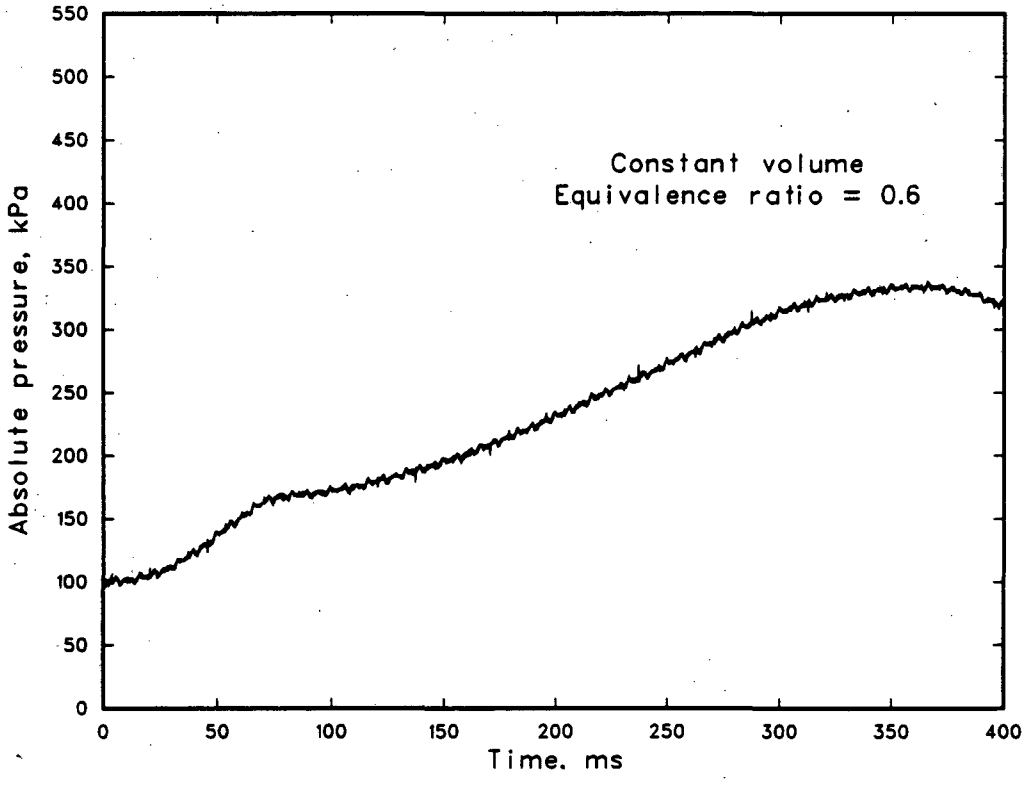

Figure 5.2-2: Absolute pressure variation with time; constant volume combustion; equivalence ratio 0.6.

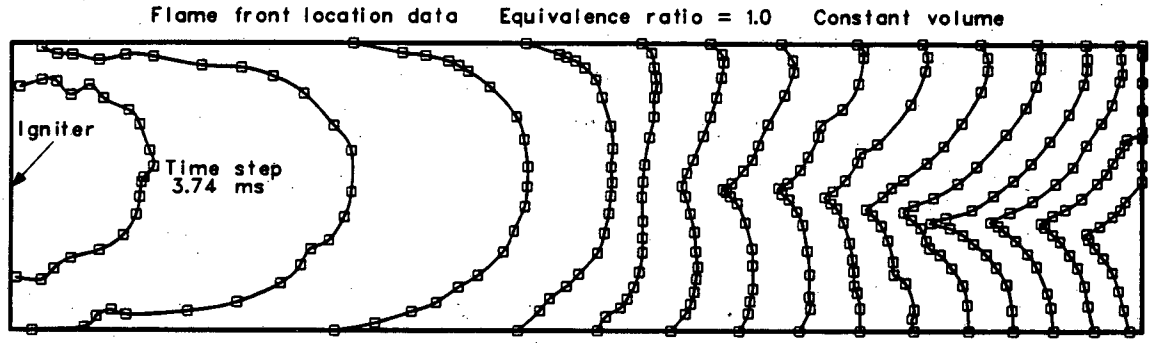

Figure 5.2-3: Flame front location from schlieren movies for time steps of 3.74 ms starting at ignition; total elapsed time to last location shown in 56.1 ms; constant volume combustion; equivalence ratio 1.0.

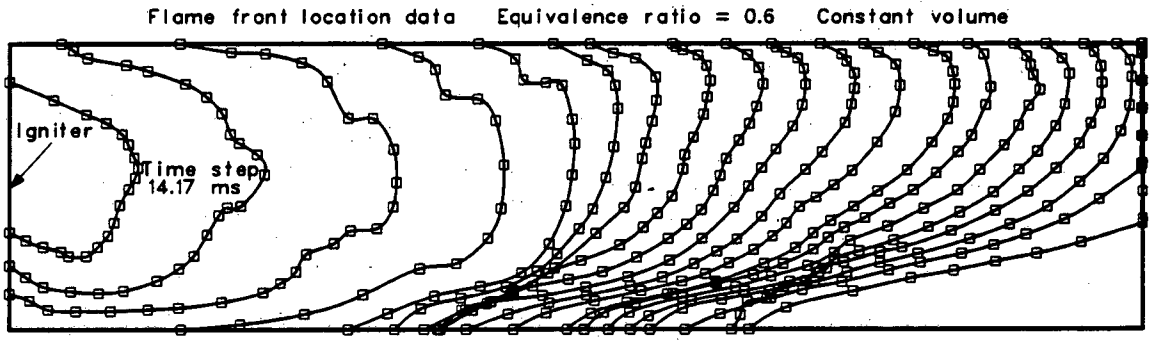

Figure 5.2-4: Flame front location from schlieren movies for time steps of 14.17 ms starting at ignition; total elapsed time to last location shown is 283.4 ms; equivalence ratio 0.6; constant volume combustion.

comes in contact with the side walls, the surface area of the flame decreases substantially and the flame assumes a more vertical, planar shape. The time when the flame changes to the vertical shape attached to the side walls, corresponds to the change in slope in the pressure variations. This indicates that this phenomena is related to the quenching of the large flame surface area on the side walls. It is important to emphasize that this correspondence was found for all equivalence ratios studied, i.e. from 0.6 to 1.1. As the flame progresses down the chamber, an instability arises near the centerline. Also noticeable is an effect due to buoyancy which causes the upper portion of the flame to appear to progress more rapidly. The burnt gases behind the flame are at a much higher temperature than the unburnt gases in front of the flame, and tend to rise due to buoyancy. The flame thus assumes a more horizontal profile which is clearly seen in Figure 5.2-4 for the case of an equivalence ratio of 0.6. The combustion event for this case is much longer allowing the buoyant forces to produce a much greater effect.

The simultaneous wall temperature variation for an equivalence ratio of 1.0 is presented in Figure 5.2-5. These data were obtained from a gauge located in the instrumentation port on the top surface near the igniter (see Figure 3.2-1). The flame passes the gauge very early in the combustion event, and this is accompanied by a steep temperature rise as seen in Figure 5.2-5. This is followed by a more gradual increase to a maximum value which occurs at the conclusion of the combustion event. It is emphasized that the time when the steep temperature rise begins; namely, at 10 ms, corresponds well with the time the flame passes in the vicinity of the gauge (cf. Figure 5.2-3).

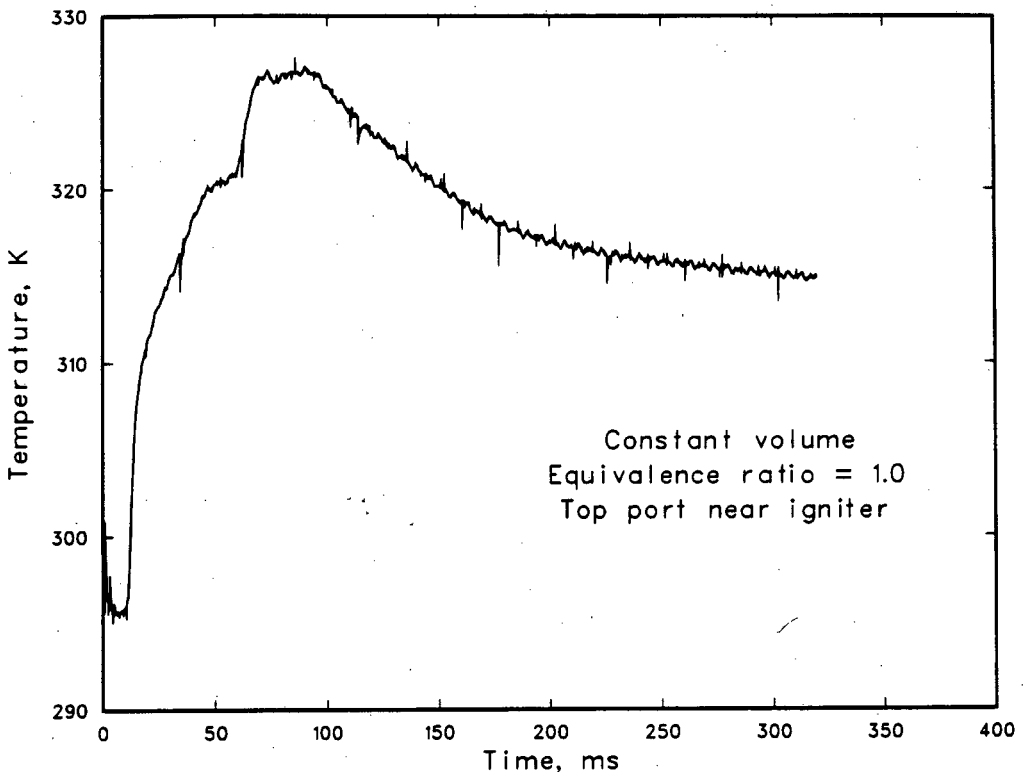

Figure 5.2-5: Wall temperature variation near igniter with time; constant volume combustion; equivalence ratio 1.0; without voltage follower.

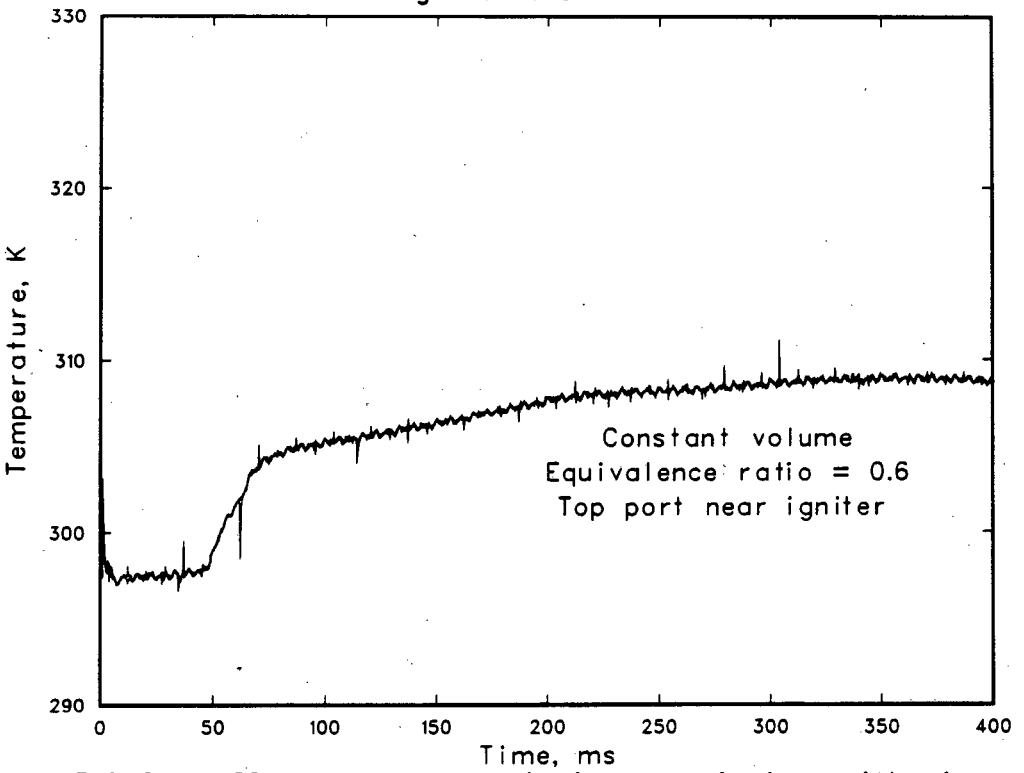

Figure 5.2-6: Wall temperature variation near igniter with time; constant volume combustion; equivalence ratio 0.6; without voltage follower.

The same general results are also found for an equivalence ratio of 0.6. Here the flame is much slower so the rise in temperature as the flame passes, occurs much later, at approximately 50 ms (cf. Figures 5.2-4 and 5.2-6). These temperature measurements were made without a voltage follower which resulted in an impedance imbalance in the data acquisition system. A discussion of this error is included in Section 5.4.

5.3 Effect of Gauge Location on Wall Temperature Variation

Wall temperature variations were also obtained for temperature gauges located in the upper and lower instrumentation ports far from the igniter. The flame passes these locations much later in the combustion event. With the gauge located in the port in the top surface, the results in Figure 5.3-1 and 5.3-2 were obtained for equivalence ratios of 1.0 and 0.6, respectively. As previously discussed, for both equivalence ratios, the rise in temperature due to the flame passage occurs much later than that for a gauge near the igniter. Results for the gauge located in the lower port far from the igniter, are presented in Figure 5.3-3 and 5.3-4 for equivalence ratios of 1.1 and 0.6 respectively. The time of the temperature rise for the near stoichiometric cases (Figure 5.3-1 and 5.3-3) do not differ substantially for the upper and lower ports. However, for the lean case, the effect of buoyancy observed in the high speed schlieren movies, has a significant effect on the temperature variation (Figures 5.3-2 and 5.3-4). The rapid temperature rise for the upper port occurs at 225 ms which is much shorter than the 425 ms that was observed for the lower port.

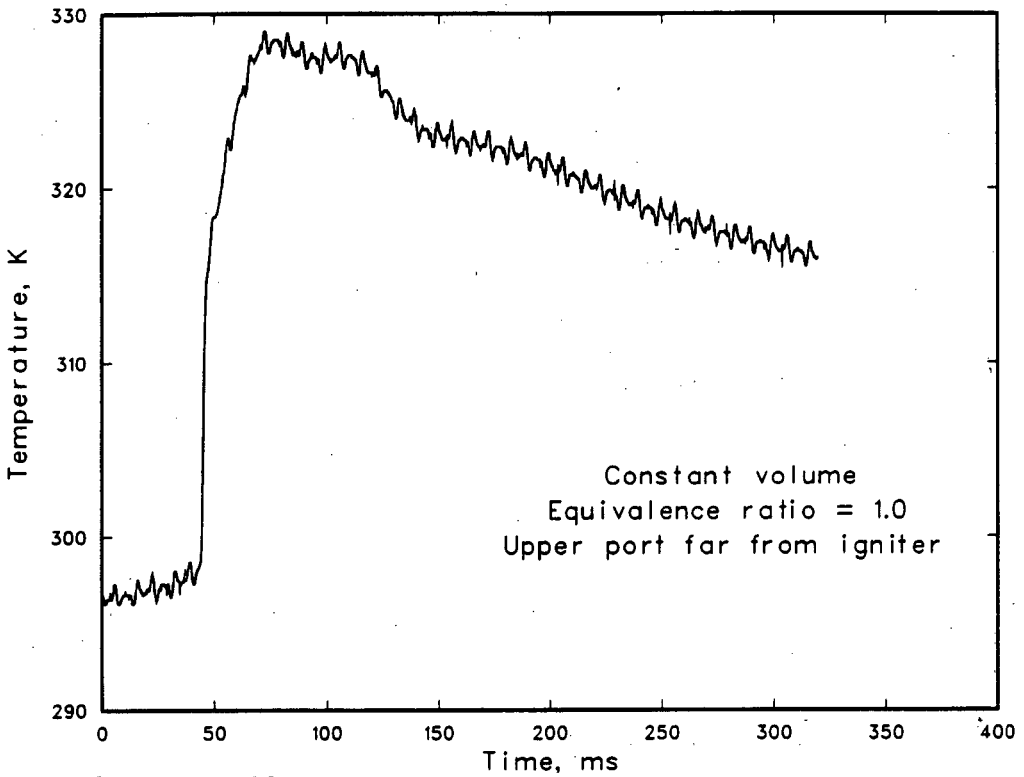

Figure 5.3-1: Wall temperature variation with time at upper port far from igniter; constant volume combustion; equivalence ratio 1.0.

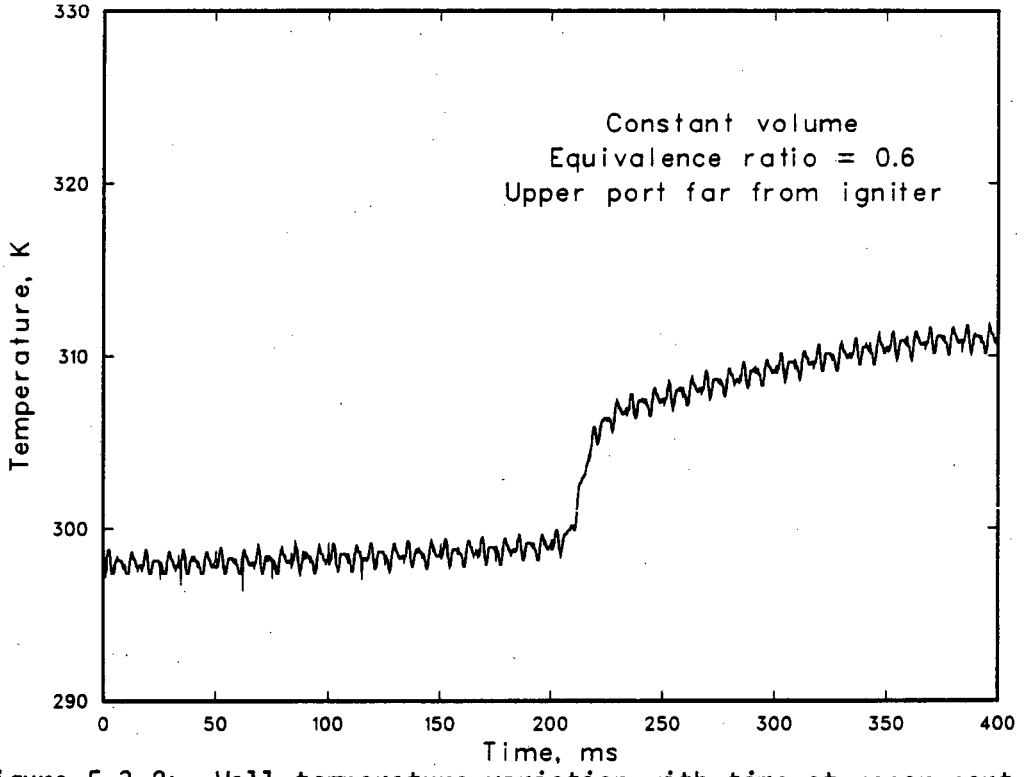

Figure 5.3-2: Wall temperature variation with time at upper port far from igniter; constant volume combustion; equivalence ratio 0.6.

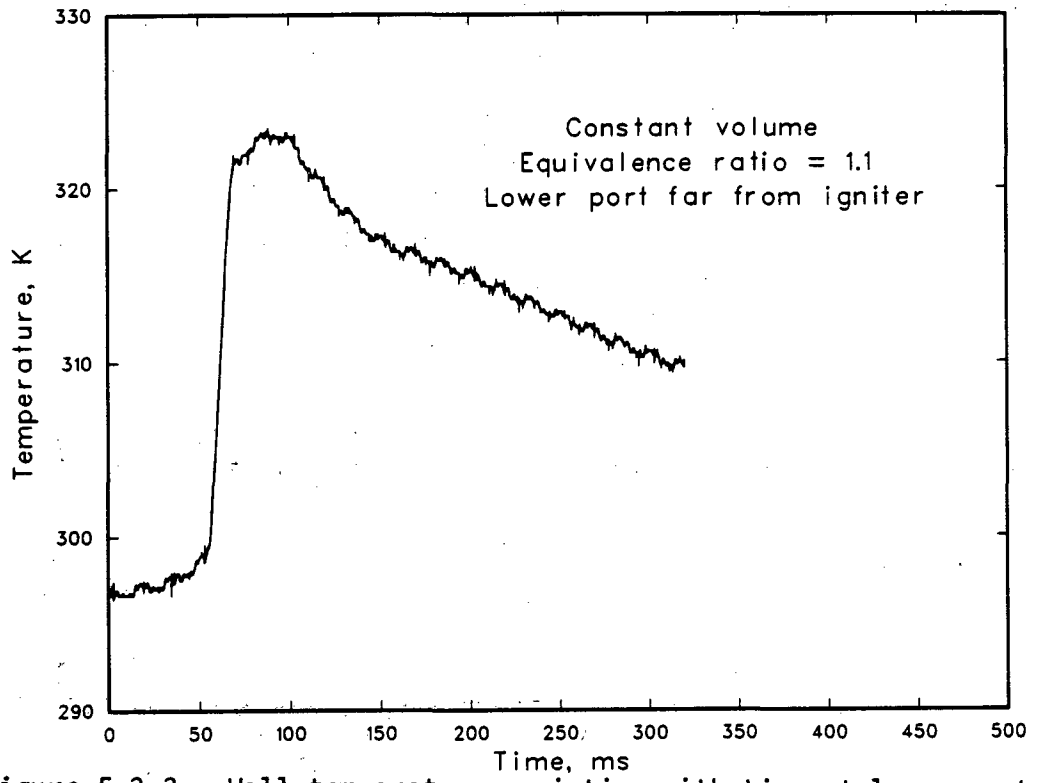

Figure 5.3-3: Wall temperature variation with time at lower port far from igniter; constant volume combustion; equivalence ratio 1.1.

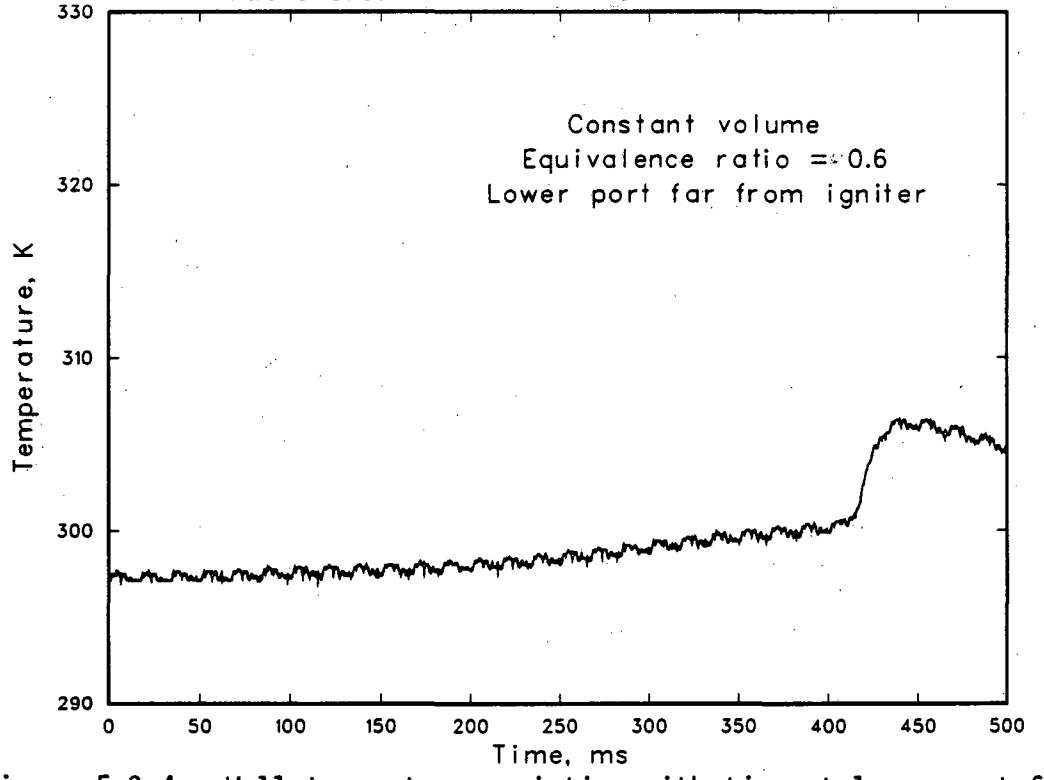

Figure 5.3-4: Wall temprature variation with time at lower port far from igniter; constant volume combustion; equivalence ratio 0.6.

5.4 Assessment of Repeatability and Error

To assess the repeatability of the experiment, several tests for identical experimental conditions were made. In Figure 5.4-1, the repeatability of the wall temperature variation for an equivalence ratio of 1.0 is presented. During combustion, the run to run variation in the temperature variation is of the order of 10 percent. The general shapes of the curves are similar as is the time of the initial temperature rise. The effect of this run to run variation on the wall heat flux is discussed in Chapter 6.

During the initial stages of this experimental study, a mismatch in the impedance in the wall temperature data acquisition system was found. This was corrected by the inclusion of a voltage following circuit. The measurements taken without the voltage follower, however, include an error. To assess the magnitude of this error, measurements for identical conditions without the voltage follower were made (see Figure 5.4-2). By comparing Figure 5.4-1 and 5.4-2, it is seen that the shape of the temperature variation is not affected, but the measured changes in temperature without the voltage follower, are approximately 10 to 15 percent lower than the temperature changes with the follower. The effect of the impedance imbalance on heat flux is discussed in Chapter 6.

5.5 Expansion and Compression-Expansion Measurements

Tests were also carried out in this study for variable volume conditions. For the expansion mode of operation, equivalence ratios from 1.1 to 0.7 were considered. The pressure variation for combustion during expansion for an equivalence ratio of 1.0 is presented in Figure 5.5-1. The pressure is constant for the first 30 ms until the

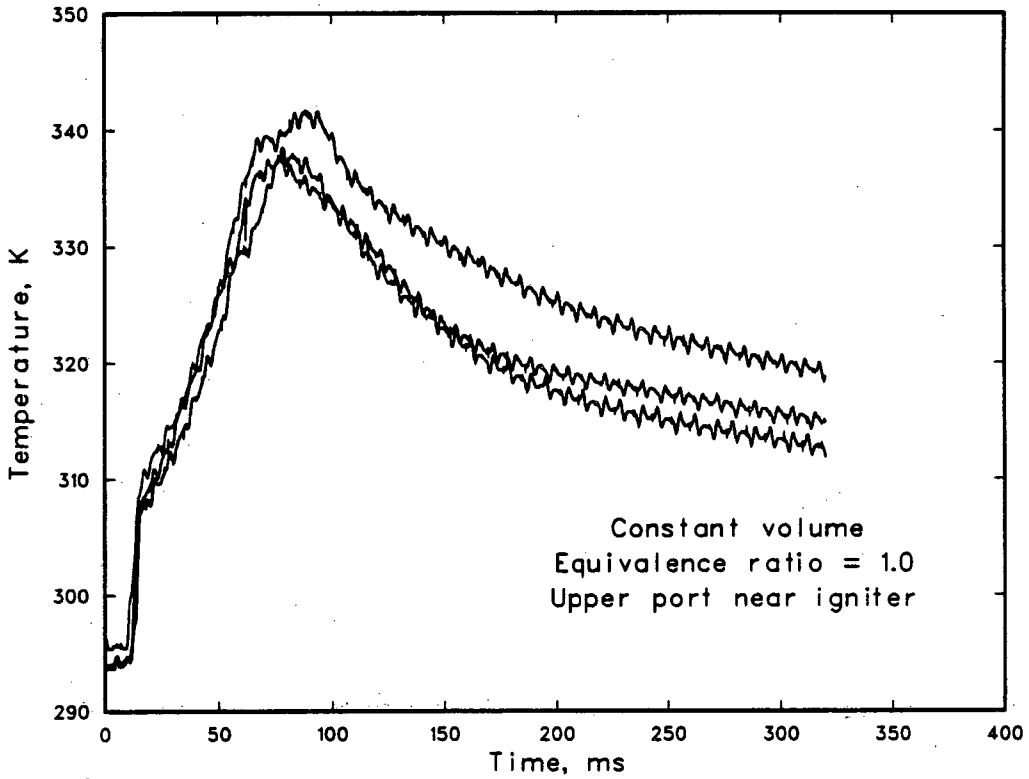

Figure 5.4-1: Repeatability of wall temperature variation with time; three measurements for identical conditions.

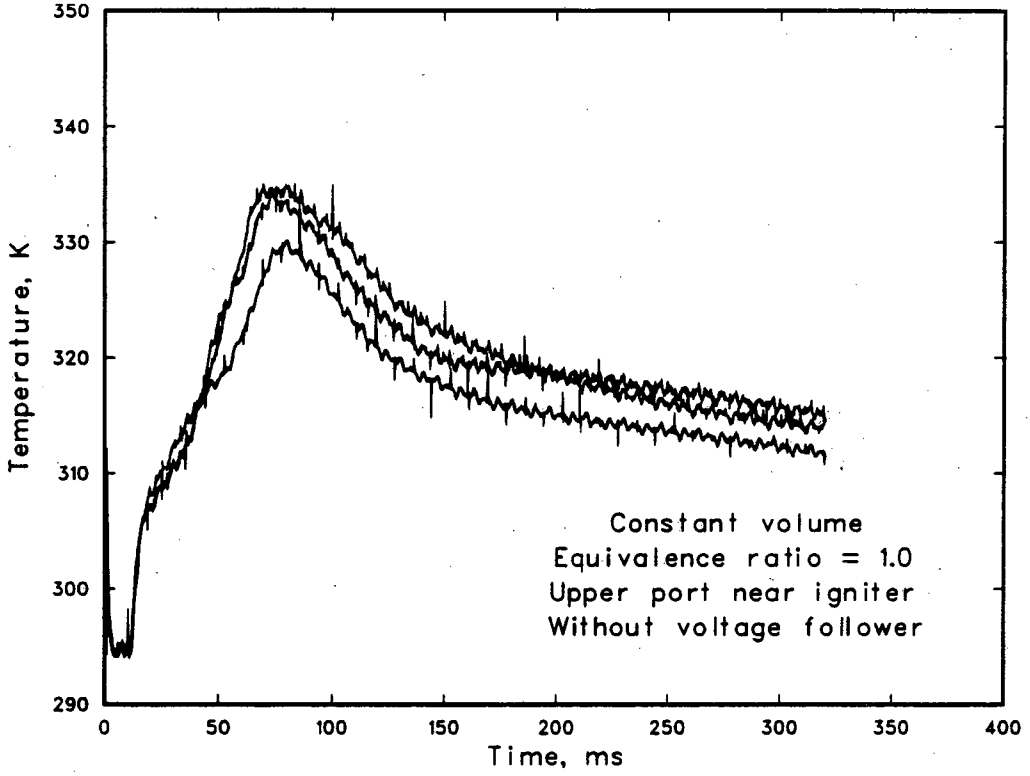

Figure 5.4-2: Repeatability of wall temperature variation with time, without voltage follower; three measurements for identical conditions.

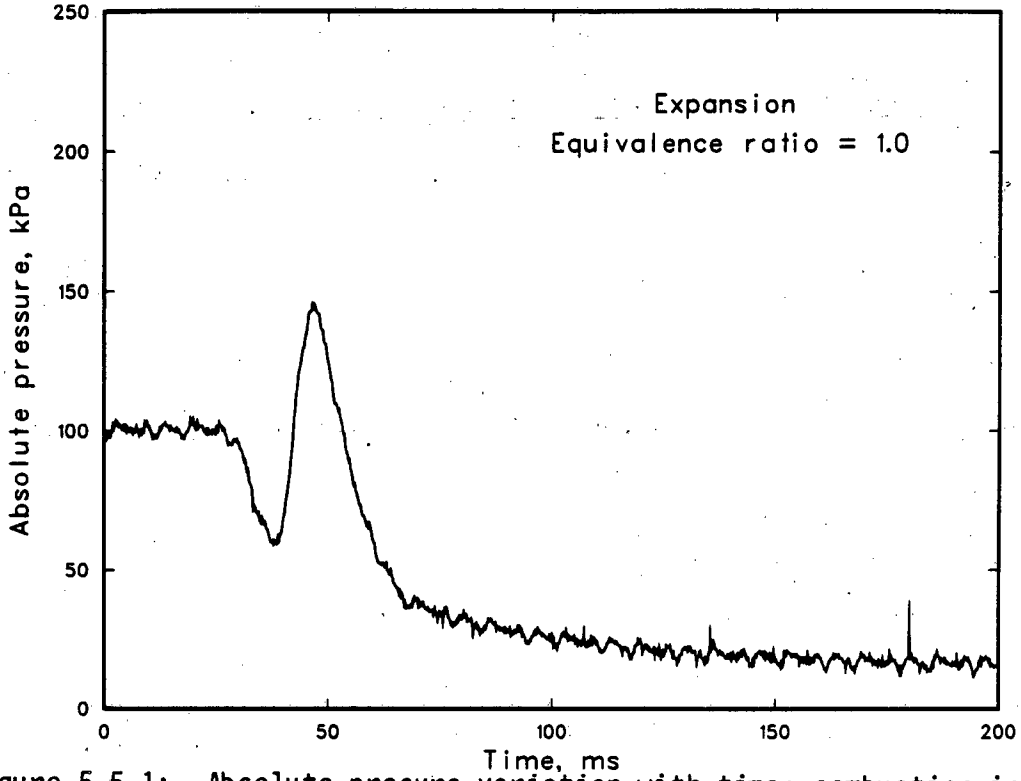

Figure 5.5-1: Absolute presure variation with time; combustion in an expanding volume; equivalence ratio 1.0; ignition takes place at t = 35 ms.

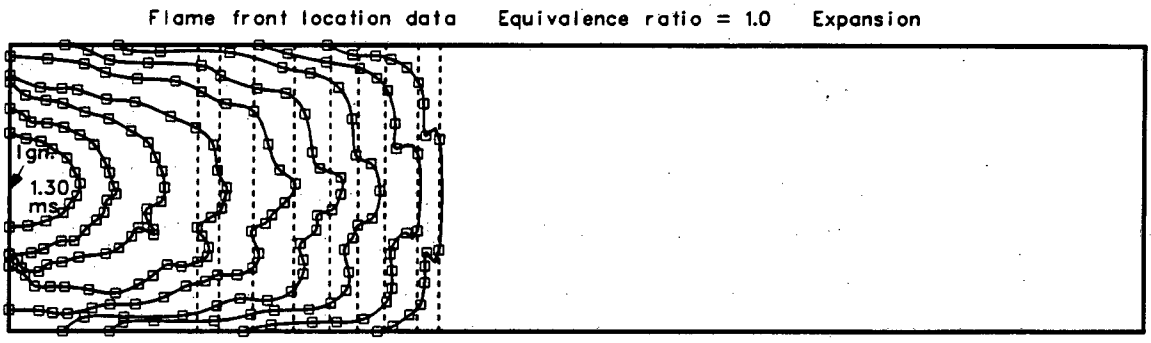

Figure 5.5-2: Flame front location and piston face location from schlieren movies for time steps of 1.30 ms starting from ignition (i.e. ignition is t = 0 ms); total elapsed time to last location shown is 11.7 ms; combustion in an expanding volume; equivalence ratio 1.0.

apparatus driver section initiates the piston motion. The volume starts to expand accompanied by a decrease in pressure. Ignition takes place at approximately 35 ms, approximately 5 ms after the expansion has begun. As the combustion process develops, the pressure rises to a maximum value at about 50 ms. Further expansion and cooling then causes a pressure decrease. The flame front location and piston face location from the schlieren movies taken simultaneously with these data, are presented in Figure 5.5-2. Corresponding to each flame front is a dotted line representing the piston face as it moves away from the igniter endwall. The wall temperature variation at the port near the igniter is shown in Figure 5.5-3. The sharp spike at approximately 35 ms denotes the time of ignition. The temperature rises sharply to a peak at approximately 50 ms and then decreases as the gas expands and cools.

Tests were also carried out for combustion in a compression-expansion mode for equivalence ratios ranging from 1.0 to 0.7. The pressure variation for this mode is shown in Figure 5.5-4 for an equivalence ratio of unity. The first spiked peak in pressure corresponds to a piston rebound at the fully compressed postion. This is caused by the relatively slow solenoid valves in the driver section of the experimental appratus. This is then followed by an increase in pressure resulting from the combustion of the compressed gas. The subsequent expansion and cooling yields the observed decrease in pressure. The wall temperature variation during compression-combustion-expansion is presented in Figure 5.5-5. The temperature first rises gradually as a result of the compression. Ignition is marked by the sharp spike. Combustion then yields a rapid rise in wall

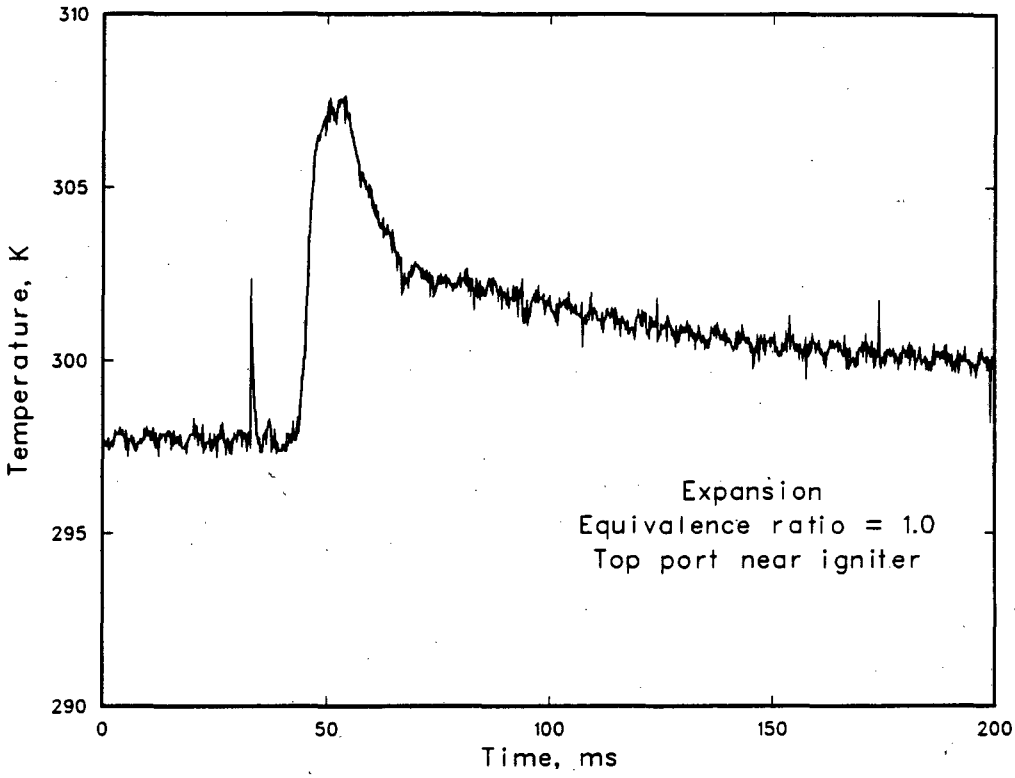

Figure 5.5-3: Wall temperature variation with time; combustion in expanding volume; equivalence ratio 1.0; without voltage follower.

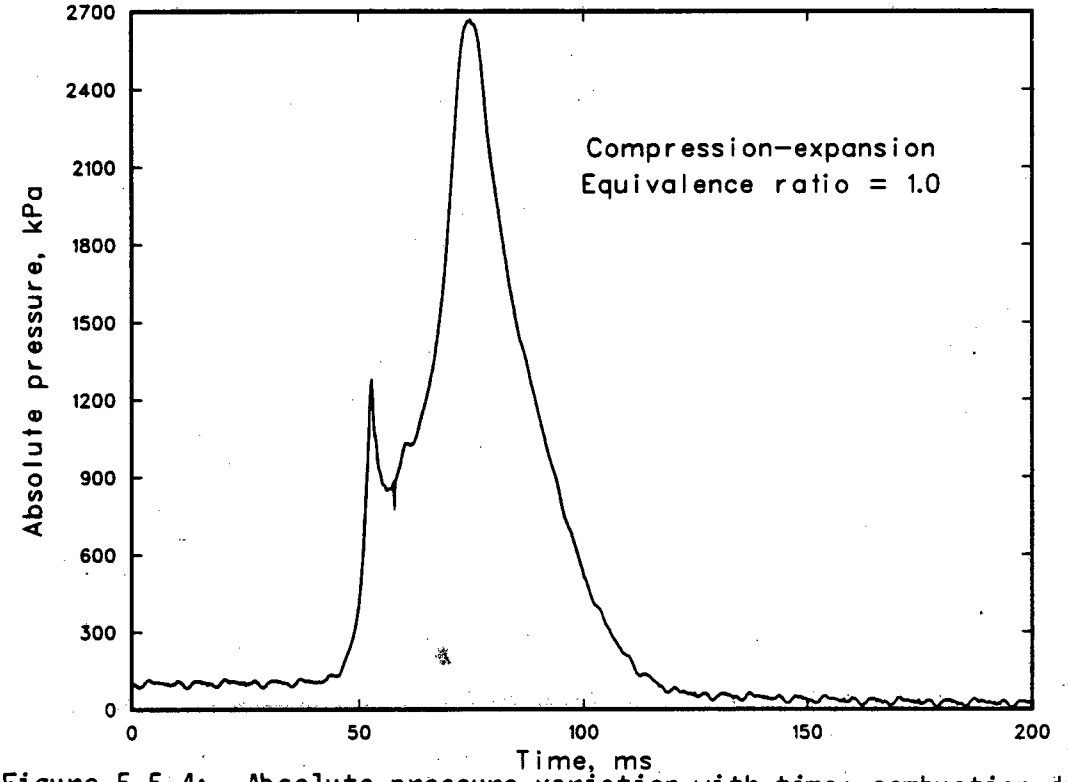

Figure 5.5-4: Absolute pressure variation with time; combustion during compression-expansion; equivalence ratio 1.0.

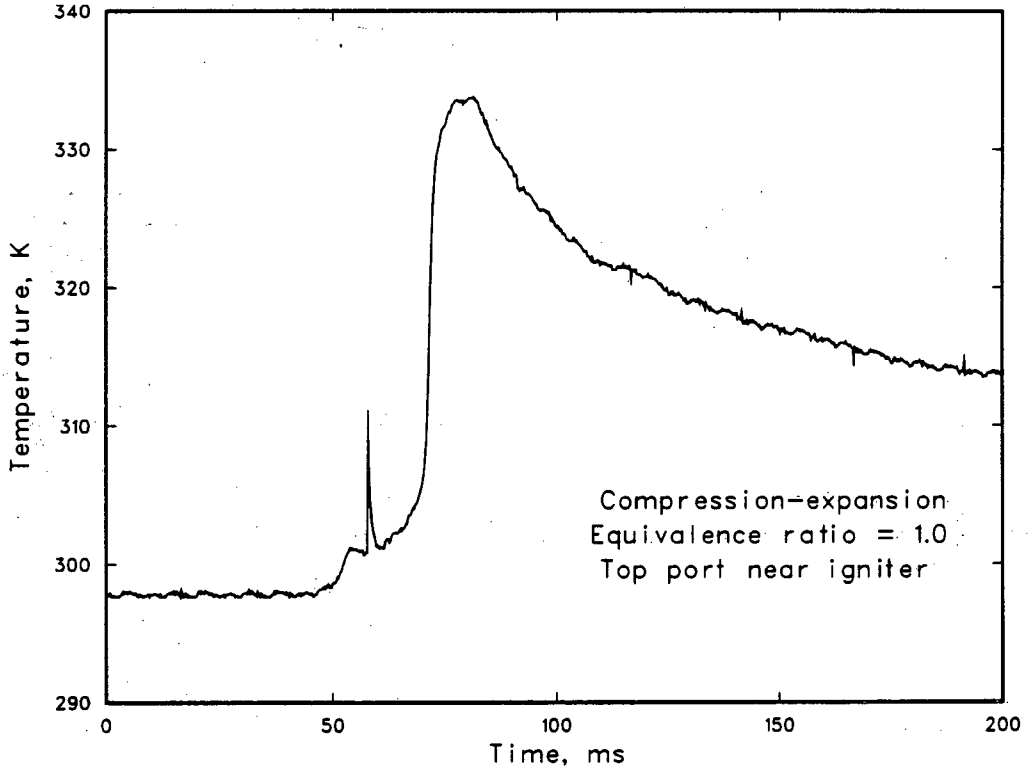

Figure 5.5-5: Wall temperature variation with time; combustion during compression-expansion; equivalence ratio 1.0; without voltage follower.

temperature to its maximum, which is then followed by a temperature decrease resulting from the expansion and cooling.

CHAPTER 6

RESULTS AND DISCUSSION

6.1 Introduction

The variations of wall heat flux with respect to time were obtained from each set of experimental data. The theoretical methods presented in Chapter 4 were applied to each set of wall temperature data presented in Chapter 5 and Appendix I.

The wall heat flux variations are useful in understanding the interaction of a flame with a cold wall. In addition, these results along with flame propagation data adds particular insight into the integral phenomena. The wall heat flux variations are important in studying the mathematical models and the analytical and numerical results which have been obtained by various authors (see Chapter 1 and 5 for a more detailed discussion). Using experimental measurements of pressure, and flame shape and location, many of these models yield the species concentrations and the temperature gradients (and thus the wall heat flux). The experimental wall heat flux variations may therefore be used in evaluating the applicability of these models and the assumptions used.

In this chapter, the heat flux results for the cases presented in Chapter 5 are discussed. The remaining results are presented in Appendix I.

6.2 Constant Volume Measurements

The temporal variation of the wall heat flux for constant volume combustion at an equivalence ratio of 1.0 is presented in Figure 6.2-1. These results are for the upper port near the igniter. At this

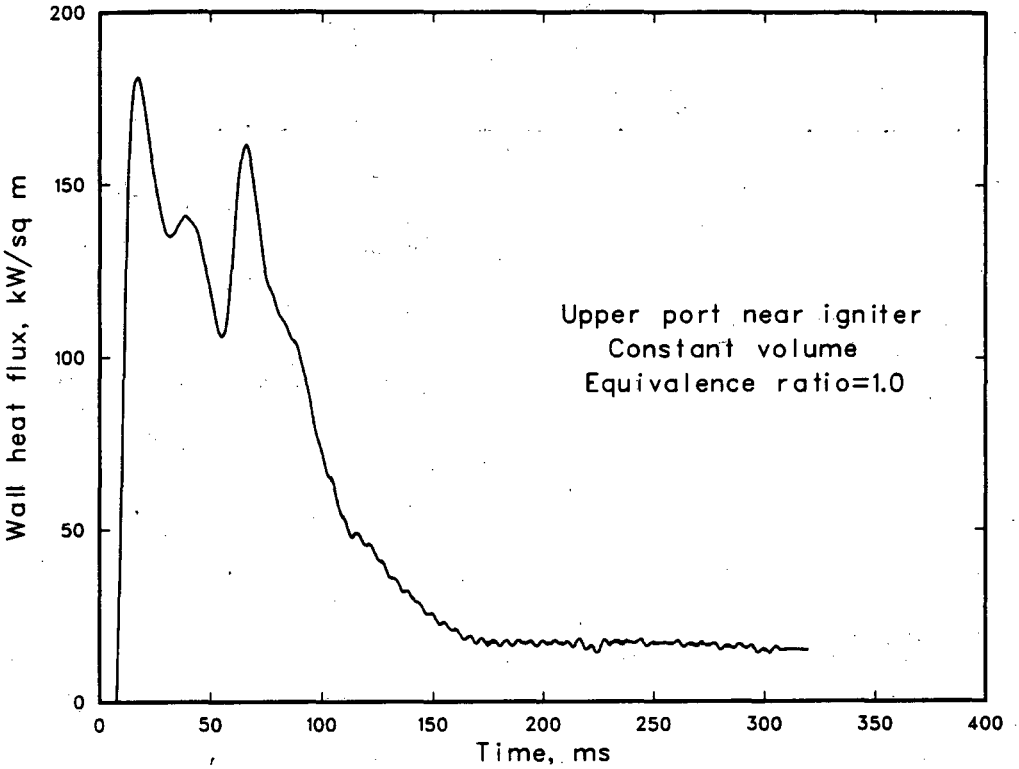

Figure 6.2-1: Wall heat flux variation with time near igniter; constant volume combustion; equivalence ratio 1.0; without voltage follower.

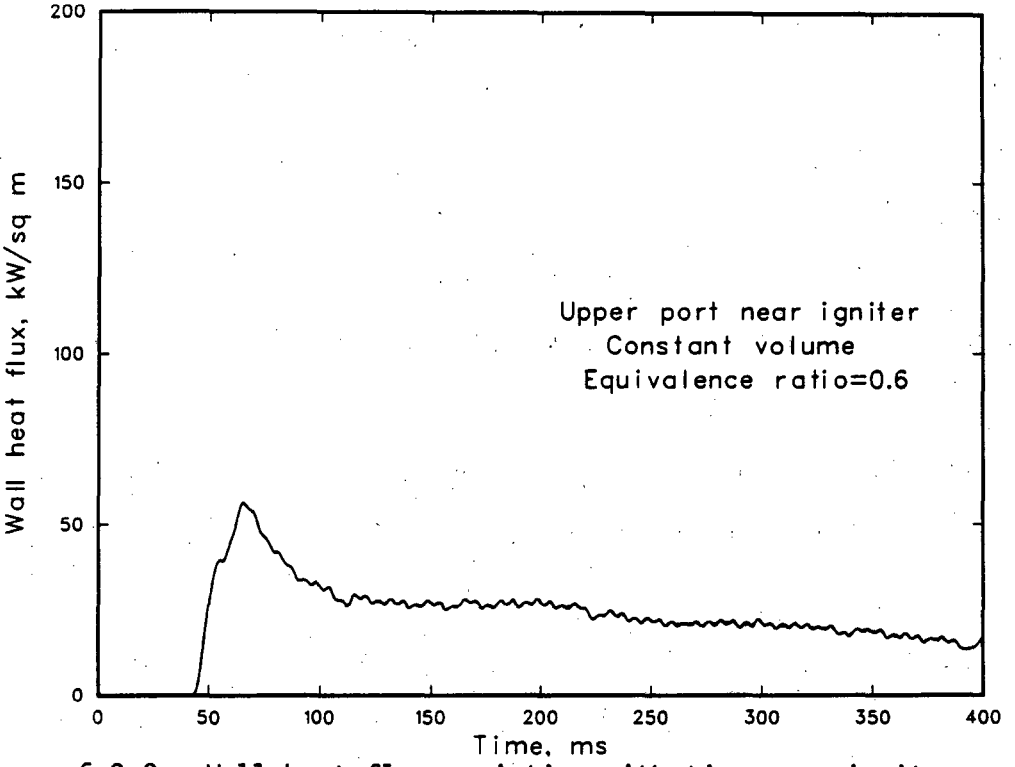

Figure 6.2-2: Wall heat flux variation with time near igniter; constant volume combustion; equivalence ratio 0.6; without voltage follower.

location the flame, which is approximately prependicular to the wall here, passes early during the combustion event causing initially a sharp rise in the heat flux to a maximum. The heat flux decreases briefly and then rises to a second major peak occurring at the conclusion of the combustion event. During the second rise in the heat flux, the relatively hot burnt gases behind the flame experience additional compression due to continued combustion. In general, two prominent maximum values were found in the heat flux variations for most of the equivalence ratios studied. A less pronounced third peak has also been observed infrequently. This third peak appeared only for a few equivalence ratios and was not repeatable for identical experimental conditions.

These same general results are also found for an equivalence ratio of 0.6 as presented in Figure 6.2-2. The heat flux shows a steep rise to a maximum value at approximately 60 ms. This is much later than the stoichiometric case because of the much lower flame speed. These results were calculated from temperature measurements made without a voltage follower, as discussed in Chapter 5. A discussion of this effect is included in Section 6.4.

6.3 Effect of Temperature Gauge Location

From the wall temperature measurements obtained for gauges located in the upper and lower instrumentation ports far from the igniter, heat flux variations were calculated. At these locations the flame passes at a much later time during the combustion event. For the upper port far from the igniter, the heat flux variations presented in Figure 6.3-1 and 6.3-2 were obtained for equivalence ratios of 1.0 and 0.6, respectively. During the period before the flame passes the gauge

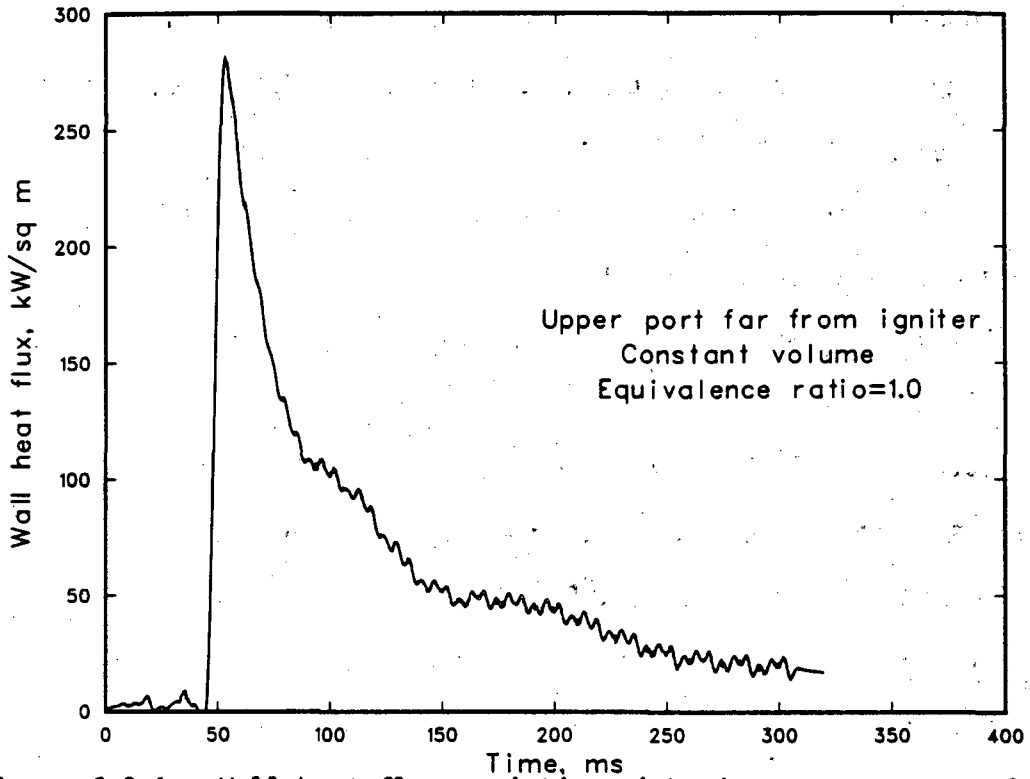

Figure 6.3-1: Wall heat flux variation with time at upper port far from igniter; constant volume combustion; equivalence ratio 1.0.

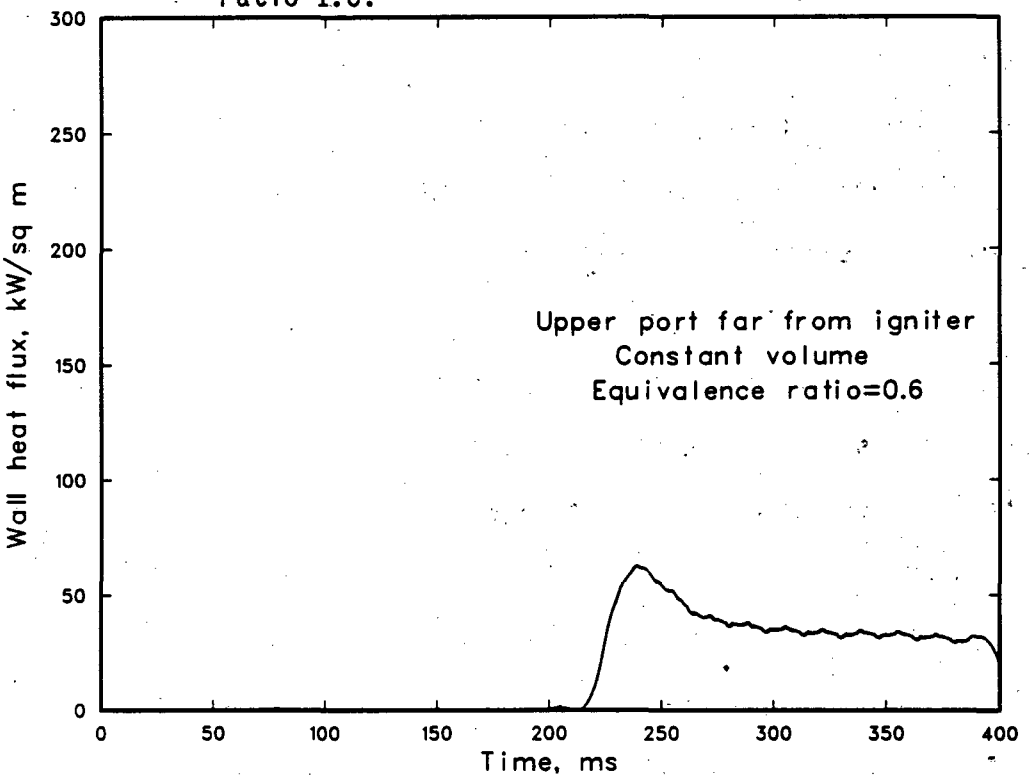

Figure 6.3-2: Wall heat flux variation with time at upper port far from igniter; constant volume combustion; equivalence ratio 0.6.

(i.e. before 45 ms for an equivalence ratio of 1.0 and before 225 ms for an equivalence ratio of 0.6), the relatively cool unburnt gases near the gauge are being compressed by the combustion. This compression of the unburnt gases causes a slight increase in pressure, temperature, and heat flux. Then, as the flame passes the gauge the heat flux rises sharply. For all the equivalence ratios studied, only one maximum value in the heat flux variations was observed. For this gauge location the subsequent compression of the burnt gases after the flame passes the gauge has a much smaller effect than for the case of the gauge near the igniter (cf. Figure 6.2-1).

With the gauge located in the lower port far from the igniter, the results shown in Figures 6.3-3 and 6.3-4 were obtained for equivalence ratios of 1.1 and 0.6. For the near stoichiometric case, Figure 6.3-3, the heat flux variation does not differ significantly from the case of the gauge in the upper port far from the igniter (Figure 6.3-1). The compression of the unburnt gases first causes a slight rise in heat flux until approximately 50 ms. The flame then passes the gauge causing a very sharp rise to the maximum value at the conclusion of the combustion. For both of these near stoichiometric cases, i.e. at both the upper and lower ports, the flame is approximately perpendicular to the wall as its passes the gauge. This is in contrast to the results for the lean condition. For an equivalence ratio of 0.6, the heat flux variation at the lower port far from the igniter (Figure 6.3-4) differs markedly from that at the upper port far from the igniter (Figure 6.3-2). Recall that for the lean cases the flame shape approaches a more horizontal profile near the conclusion of the combustion event due to the effect of buoyancy (see Figure 5.2-4). Thus the flame does not

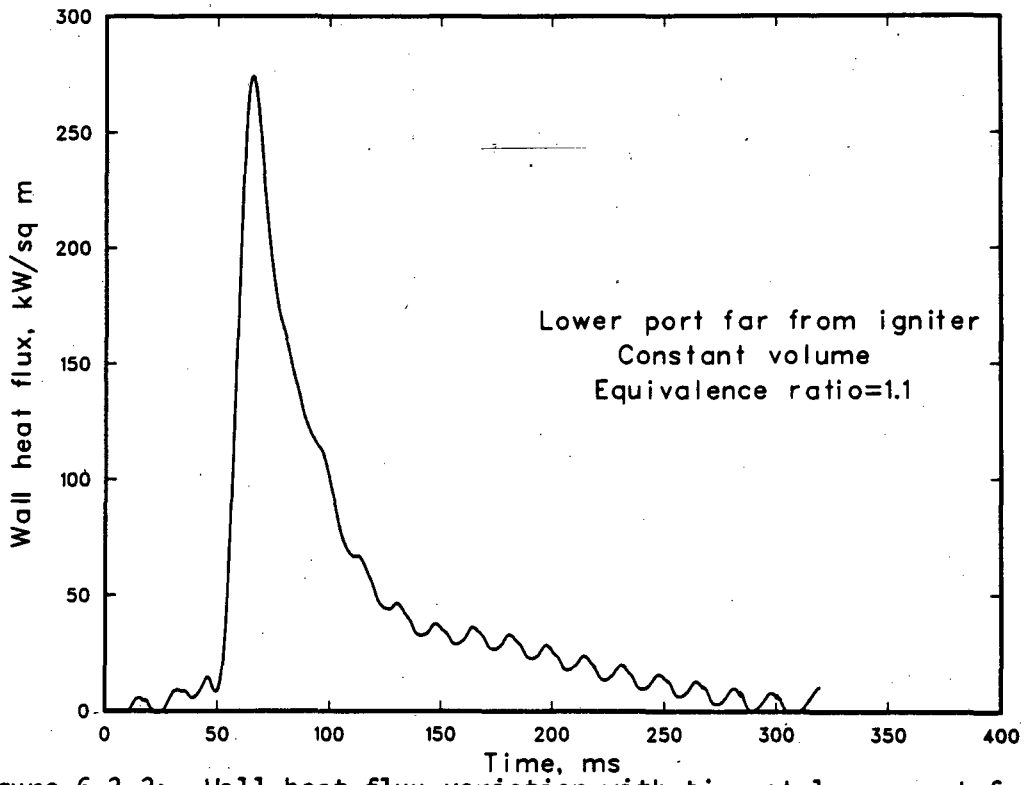

Figure 6.3-3: Wall heat flux variation with time at lower port far from igniter; constant volume combustion; equivalence ratio 1.1.

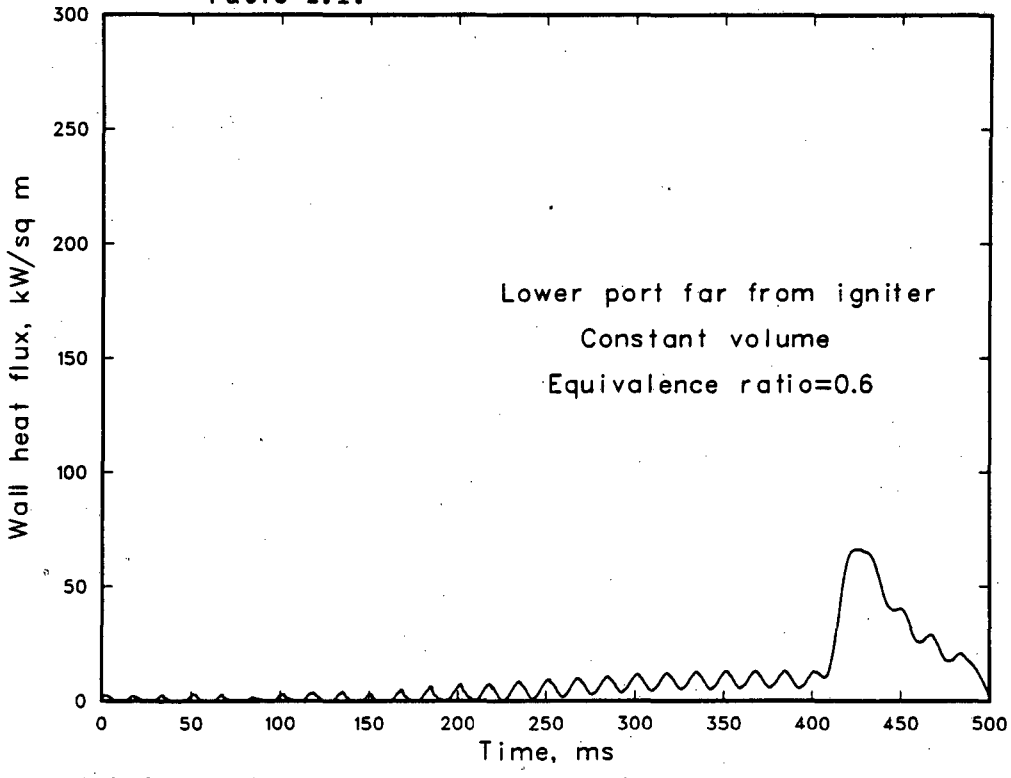

Figure 6.3-4: Wall heat flux variation with time at lower port far from igniter; constant volume combustion; equivalence ratio 0.6.

pass the lower port far from the igniter until some time after it has passed the upper port. For the lower port the steep rise in heat flux occurs at 420 ms while the corresponding time at the upper port is 220 ms. Also, the flame shape data obtained from the schlieren movies shows that at the lower port far from the igniter, for the lean case the flame is approximately parallel to the horizontal wall as it approaches the end of the chamber. This is in contrast to all the other cases where the flame remains perpendicular to the wall as it traverses the chamber.

6.4 Assessment of Repeatability and Error

In Figure 6.4-1, the repeatability of the wall heat flux variation for an equivalence ratio of 1.0 is presented. The run to run variation in the heat flux during the first steep rise and the maximum value is very small. During the second rise to a maximum, significant variations of the order of 15 percent are found. Note that the less pronounced third peak is not repeatable, occurring during approximately half the measurements.

As discussed in Chapter 5, during the initial stages of these measurements, a mismatch in the impedance in the wall temperature data acquisition system was found. The measurements taken during this time without the voltage follower, include this error. To determine this error in the heat flux, results for identical conditions without the voltage follower were obtained and are presented in Figure 6.4-2. The same general run to run variability observed in the measurements with the voltage follower is also found here. A comparison of these results with those in Figure 6.4-1 show that the heat flux results without the follower are approximately 15 to 20 percent lower than the results with

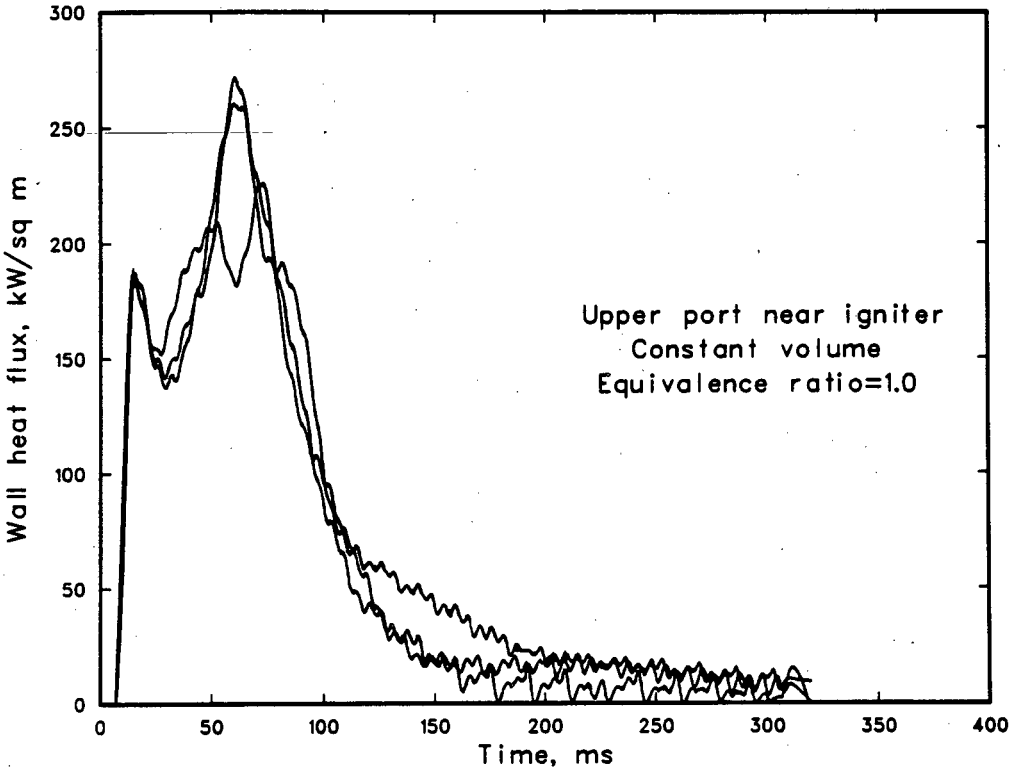

Figure 6.4-1: Repeatability of wall heat flux variation with time; three measurements for identical conditions.

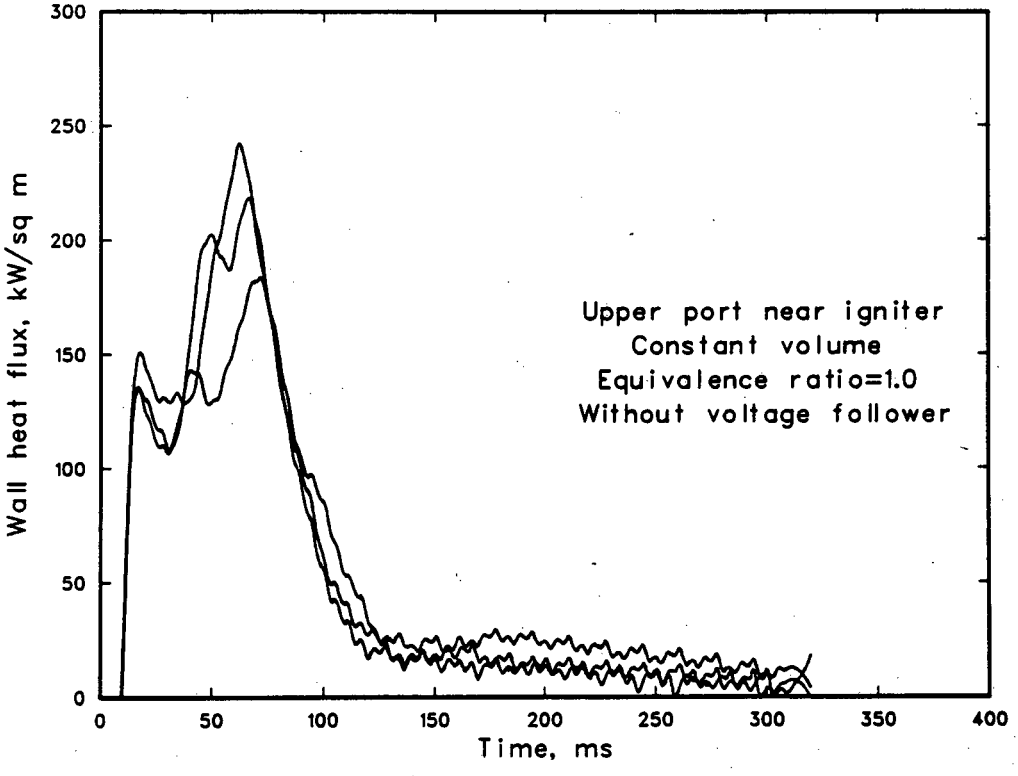

Figure 6.4-2: Repeatability of wall heat flux variation with time, without voltage follower; three measurements for identical.

the follower.

6.5 Expansion and Compression-Expansion Results

Wall heat flux variations were also obtained from the experimental data for variable volume conditions. The wall heat flux variation for combustion during expansion with an equivalence ratio of 1.0 is presented in Figure 6.5-1. During the first 40 ms the expansion is occurring with no significant effect on the heat flux. The gas is then ignited, and the passage of the flame near the gauge results in a rapid increase in the heat flux. As the combustion process concludes, further expansion and cooling causes a rapid decrease in the heat flux. Note that the expansion case yields a lower maximum value than the constant volume case.

Tests were also carried out for a compression-combustion-expansion sequence. Results for the heat flux for an equivalence ratio of 1.0 are presented in Figure 6.5-2. The compression results in a small rise in the heat flux at approximately 50 ms. The piston rebound discussed in Chapter 5 then causes the heat flux to decrease. This phenomena is related to the analysis in Chapter 2. Combustion has started, however, and when the flame passes the gauge, the heat flux rises rapidly to a maximum as in the previous cases. The combustion process concludes as the expansion continues with a sharp decrease in the heat flux. Note that the combustion of the compressed gases yields a much higher heat flux than that observed for combustion of gases at atmospheric pressure in a constant volume.

6.6 Summary

For constant volume combustion with the temperature gauge located near the igniter, the wall heat flux rises rapidly as the flame passes

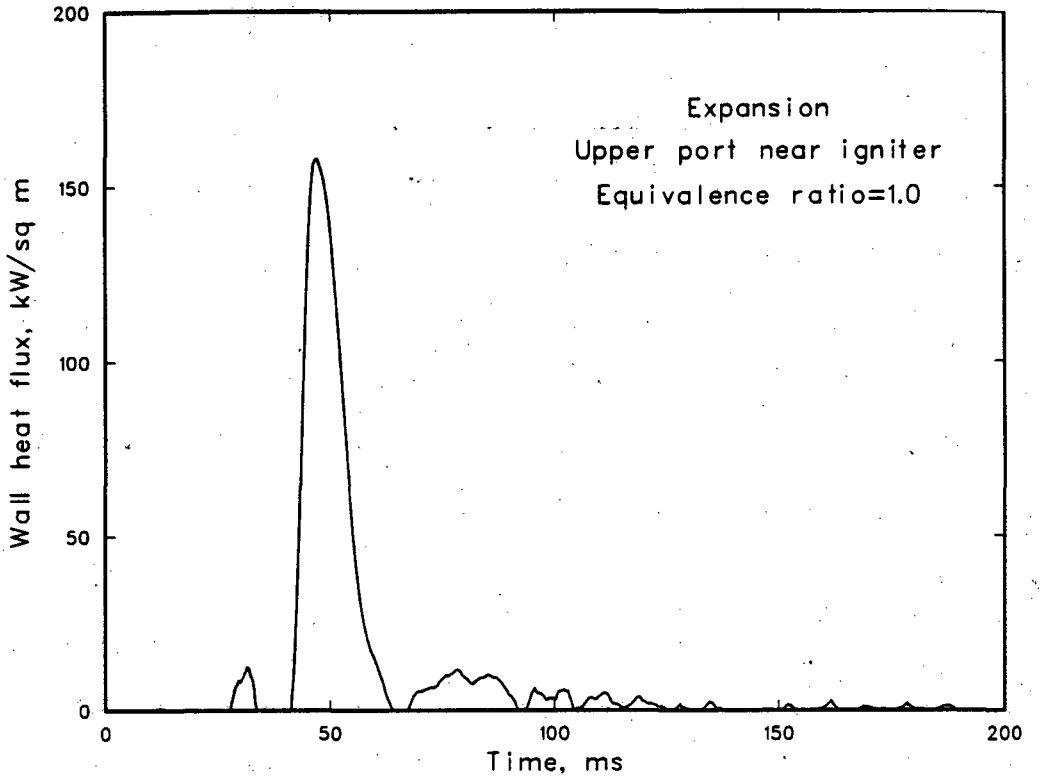

Figure 6.5-1: Wall heat flux variation with time; combustion in an expanding volume; equivalence ratio 1.0; without voltage follower.

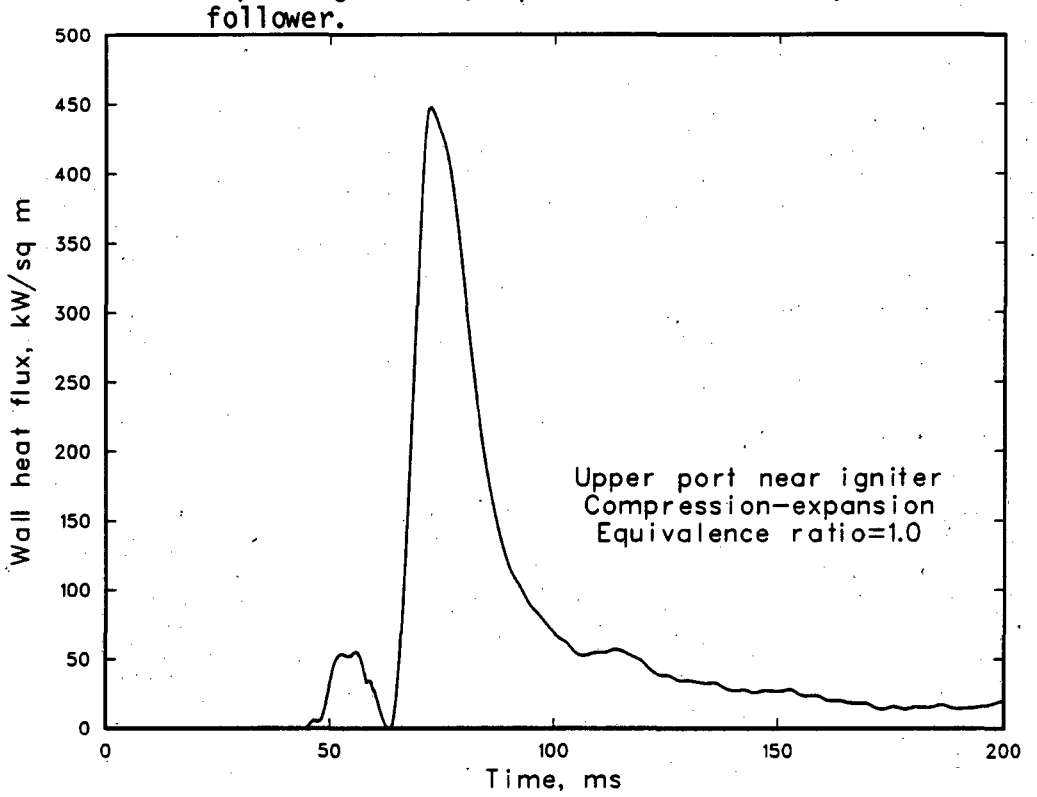

Figure 6.5-2: Wall heat flux variation with time; combustion during compression-expansion; equivalence ratio 1.0; without voltage follower.

this location. The relatively hot burnt gases then continue to compress the colder gases until combustion is completed. A second maximum value observed in the heat flux coincides with the peak pressure as seen in Figure 6.6-1.

The variations in pressure and heat flux with equivalence ratio observed in this study agree well with previous observations by Alkidas and Myers, 1981. In their work in engines, the measured peak pressures were approximately four times higher than the measurements here for constant volume combustion, and the peak pressure was observed to be highest near stoichiometric conditions. Their peak wall heat flux measurements in engines were approximately six times higher than the constant volume combustion measurements presented here, and again the peak heat flux was observed to reach a maximum near stoichiometric conditions. The variation in peak pressure with equivalence ratio for constant volume combustion is shown in Figure 6.6-2. The pressure peaks approximately at stoichiometric conditions. For the same constant volume condition, the variation with equivalence ratio of the peak heat flux near the igniter is shown in Figure 6.6-3. Both the first and second peaks in the heat flux reach a maximum near stoichiometric conditions.

From the results obtained at the upper port far from the igniter, the variation of the peak heat flux with equivalence ratio is similar to that obtained near the igniter (see Figure 6.6-4).

An overall comparison of the constant volume heat flux variation with time for all three gauge locations and two equivalence ratios is shown in Figure 6.6-5. This comparison summarizes the effect of flame propagation on the wall heat flux. First, comparing the results for an

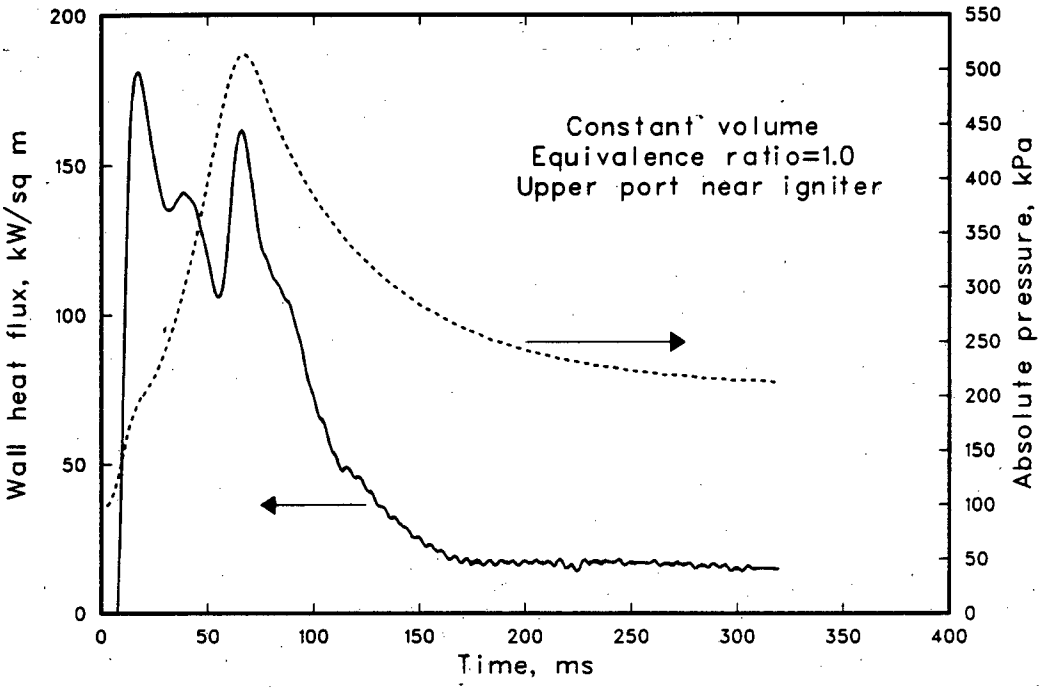

Figure 6.6-1: Comparison of the variation with time of wall heat flux and pressure; constant volume combustion; equivalence ratio 1.0.

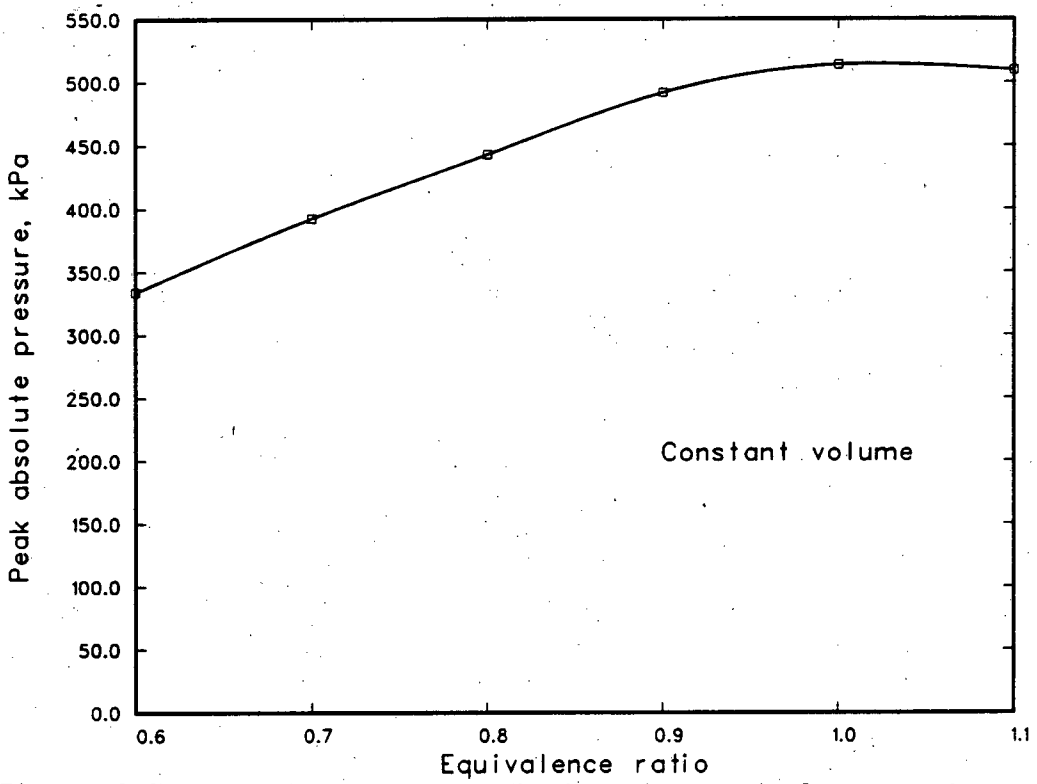

Figure 6.6-2: Peak pressure variation with equivalence ratio; constant volume combustion.

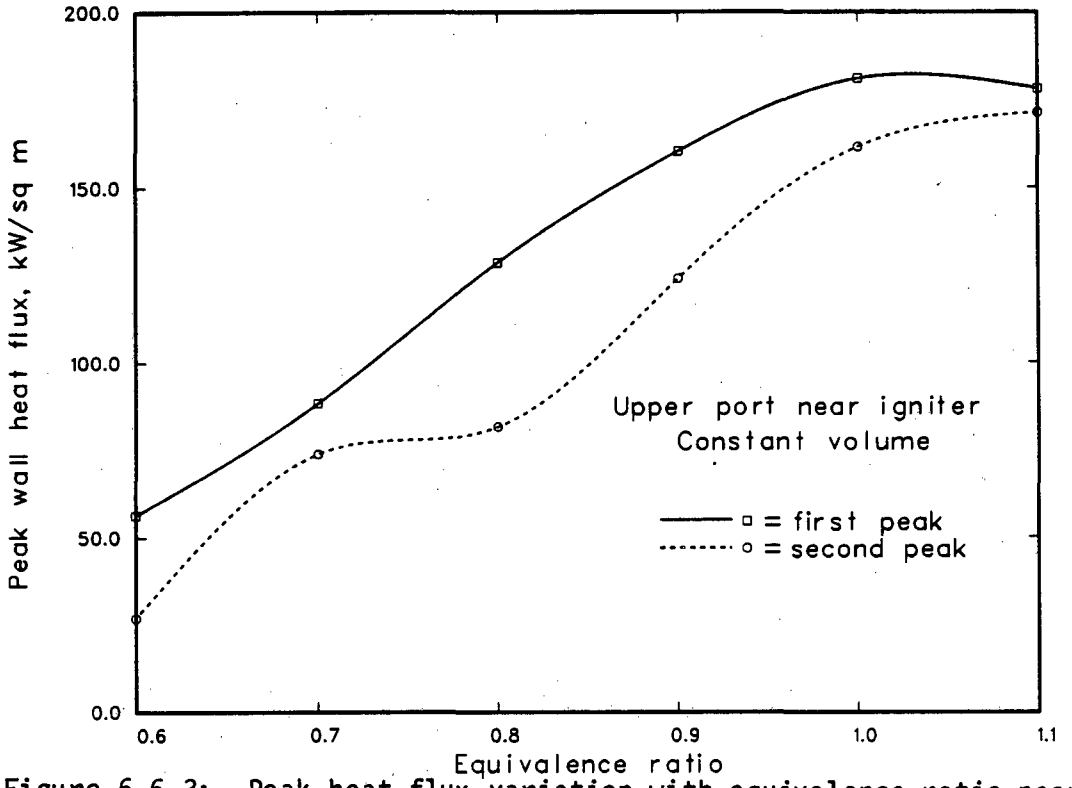

Figure 6.6-3: Peak heat flux variation with equivalence ratio near igniter; constant volume combustion.

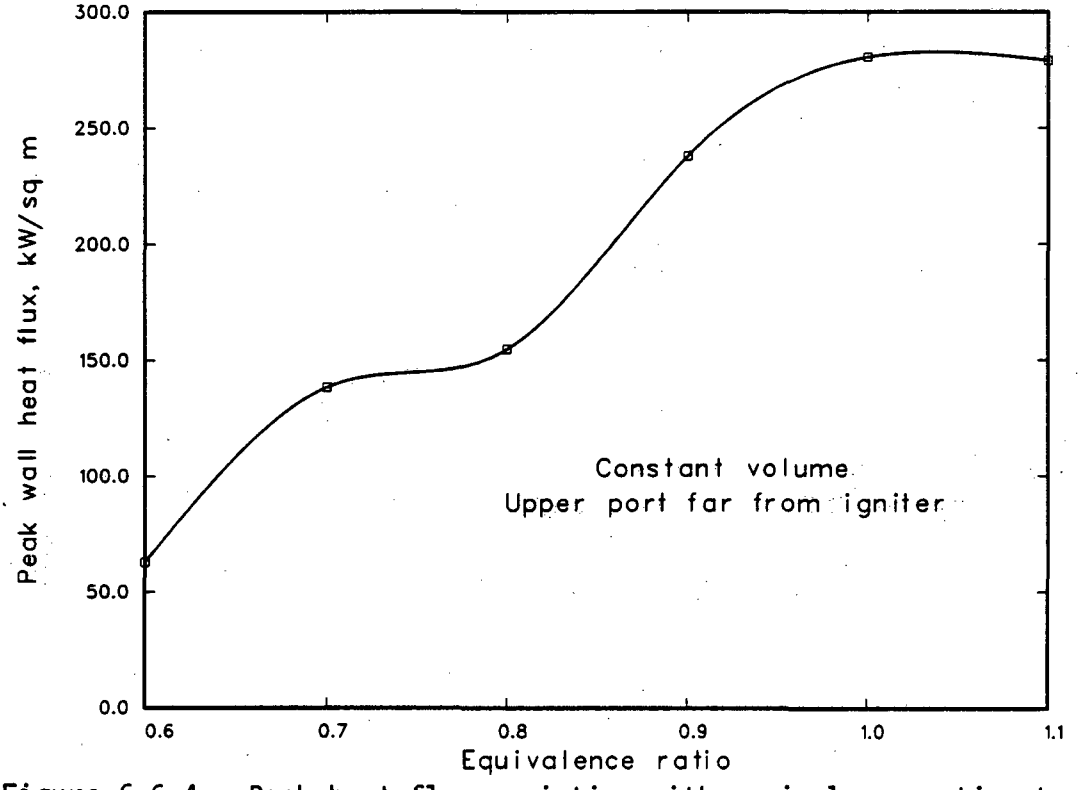

Figure 6.6-4: Peak heat flux variation with equivalence ratio at upper port far from igniter; constant volume combustion.

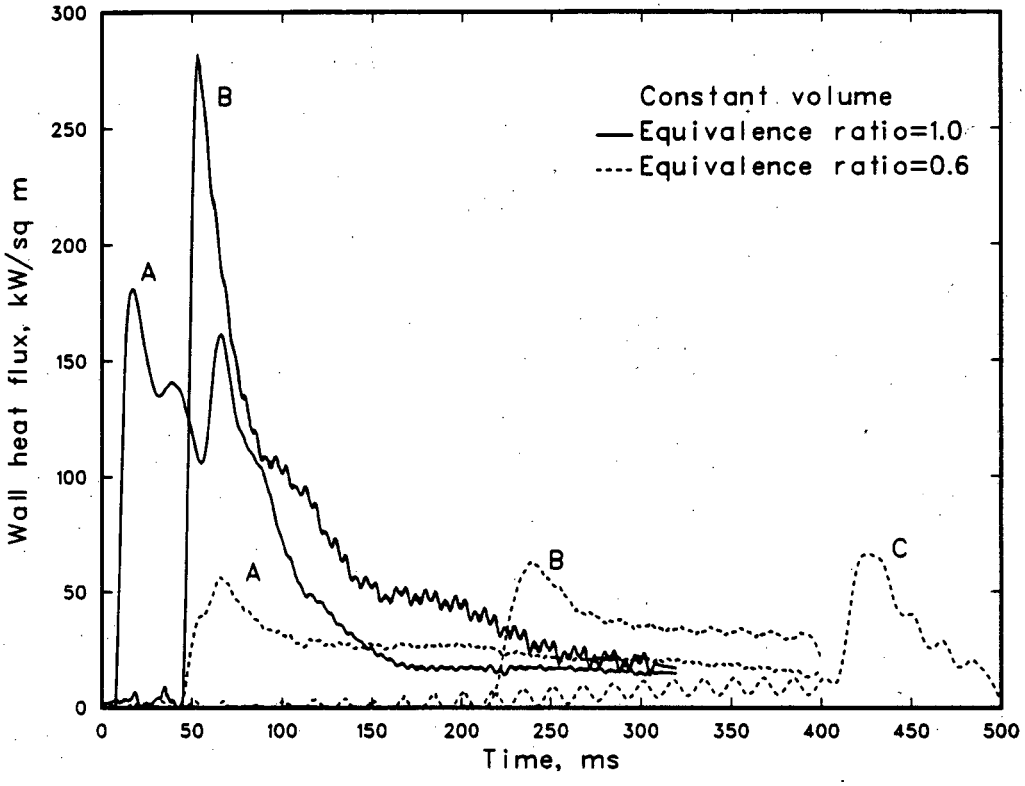

Figure 6.6-5: Wall heat flux variation with time; constant volume combustion; equivalence ratio 1.0 and 0.6 ; A - upper port near igniter, B - upper port far from igniter, C - lower port far from igniter.

equivalence ratio of 1.0, the results for the port near the igniter, labeled A in the figure, show an increase in heat flux as the flame passes at approximately 10 ms. For the upper port far from the igniter, labeled B, the corresponding rise due to the passage of the flame occurs much later at approximately 45 ms. For the lower port far from the igniter, the results, not shown here, are similar to those obtained at the upper port. For an equivalence ratio of 0.6 there is a strong variation of the heat flux with respect to location. Near the igniter, the dotted curve labeled A exhibits an increase in the heat flux from the passing flame at approximately 50 ms. At the upper port far from the igniter, labeled B, the corresponding increase occurs at approximately 225 ms. The flame for the lean case is much slower than in the stoichiometric case. Finally, for the lower instrumentation port far from the igniter, the shape of the flame is altered due to buoyancy. With a lean mixture, the flame has a more horizontal profile due to buoyant forces. Thus the rise in heat flux at the lower port due to the flame occurs much later, at approximately 420 ms.

CHAPTER 7

CONCLUSIONS AND RECOMMENDATIONS

7.1 Unsteady Heat Transfer During Compression and Expansion in the Absence of Combustion

An analytical solution for the directional reversal in wall heat flux during compression and expansion in the absence of combustion was derived. The results are in good agreement with experimental measurements. From the solution to the finite difference formulation to this problem, temperature profiles were calculated. From these temperature profiles and the analytical solution, a physical explanation for the heat transfer reversal was determined.

7.2 Experimental Results for Wall Heat Flux and Flame Propagation and Their Interaction

Experimental measurements of pressure, wall temperature, heat flux, and flame location and shape were obtained for combustion in constant volume, expansion, and compression-expansion systems. From these measurements, an understanding of the interaction of flame propagation and wall heat flux has been obtained. In addition, this study has provided a complete set of experimental data which are especially useful in appraising analytical and numerical models of the interaction of a flame with a wall.

Specifically, the rapid increase in the wall temperature and the heat flux due to flame passage was presented. The flame speed and, correspondingly, the time of the sharp rise in wall temperature and heat flux were found to vary considerably with equivalence ratio. For lean constant volume combustion, buoyancy was found to have a

significant effect on the shape of the flame and on the wall temperature and heat flux variations.

REFERENCES

Annand, W. J. D. (1963). "Heat Transfer in the Cylinders of Reciprocating Internal Combustion Engines." Proceedings of Institution of Mechanical Engineers, Vol. 177, No. 36, 973-990.

Annand, W. J. D., and Ma, T. H. (1970). "Instantaneous Heat Transfer Rates to the Cylinder Head Surface of a Small Compression-Ignition Engine." Proceedings of Institution of Mechanical Engineers, Vol. 185, 976-987.

Annand, W. J. D., and Pinfold, D. (1980). "Heat Transfer in the Cylinder of a Motored Reciprocating Engine." SAE Paper No. 800457.

Alkidas, A. C. (1979). "Heat Transfer Characteristics of a Spark-Ignition Engine." ASME Paper 79-HT-76 presented at the Joint ASME/AIChE 18th National Heat Transfer Conference, San Diego, CA, August 6-8.

Alkidas, A. C. and Cole, R. M. (1981). "The Distribution of Heat Rejection from a Single-Cylinder Divided-Chamber Diesel Engine." SAE Paper No. 810959.

Alkidas, A. C. and Myers, J. P. (1981). "Transient Heat Flux Measurements in the Combustion Chamber of a Spark-Ignition Engine." ASME Paper 81-WA/HT-1 presented at the Winter Annual Meeting.

Carrier, G. F., Fendell, F. E., and Feldman, P. S. (1980). "Interaction of a Planar Laminar Premixed Flame with a Perpendicular Wall." SAE Paper No. 800285.

Carslaw, H. S., and Jaeger, J. C. (1978). Conduction of Heat in Solids, Oxford University Press, Oxford.

Corning (1978). "Macor Machinable Glass Ceramic Technical Bulletin." Corning, New York.

Dao, K. (1972). "Heat Transfer with Cyclic Pressure Variations (in Piston Engines)." Ph.D. Thesis, Department of Mechanical Engineering, University of Wisconsin.

Eichelberg, I. G. (1939). "Some New Investigations on Old Combustion Engine Problems - I.", Engineering, Vol. 148.

Ferguson, C. R., and Keck, J. C. (1977). "On Laminar Flame Quenching and Its Application to Spark Ignition Engines." Combustion and Flame 28: 197-205.

Gosman, A. D., and Watkins, A. P. (1976). "Calculations of Turbulent Heat Transfer in a Closed Piston/Cylinder System." Preliminary version courtesy of authors.

Haskell, K. H., and Vandevender, W. H. (1980). "Brief Instructions for Using the Sandia Mathematical Subroutine Library." SAND79-2382.

Heperkan, H. (1980). "An Experimental and Theoretical Study of Heat Transfer With Combustion." Ph.D. Thesis, Department of Mechanical Engineering, University of California, Berkeley, California.

Hocks, W., Peters, N., and Adomeit, G. (1981). "Flame Quenching in Front of a Cold Wall Under Two-Step Kinetics." Combustion and Flame 41: 157-170.

Isshiki, N. and Nishiwaki, N. (1974). "Basic Study of Inside Convective Heat Transfer of Internal Combustion Engines." Proceedings of the Fifth International Heat Transfer Conference, Tokyo, September 3-7.

Keck, J. C. (1981). "Thermal Boundary Layer in a Gas Subject to a Time Dependent Pressure." Letters in Heat and Mass Transfer, Vol. 8, 313-319.

Kurkov, A. P. and Mirsky, W. (1969). "An Analysis of the Mechanics of Flame Extinction By a Cold Wall." Twelfth Symposium (International) on Combustion, The Combustion Institute, Pittsburgh, Pennsylvania.

Le Feuvre, T., Myers, P. S., and Uyehara, O. A. (1969). "Experimental Instantaneous Heat Fluxes in a Diesel Engine and Their Correlation." SAE Paper No. 690464.

McNair, H. M. and Bonelli, E. J. (1968). Basic Gas Chromatography. Consolidated Printers, Berkeley, California.

Nikanjam, M. (1977). "An Experimental and Theoretical Study of Unsteady Heat Transfer During Piston Compression." Ph.D. Thesis, Department of Mechanical Engienering, University of California, Berkeley, California.

Oguri, T. (1960). "Theory of Heat Transfer in the Working Gases of Internal Combustion Engines." Bulletin of Japan Society of Mechanical Engineers, Vol. 3 (11) 370-377.

Oppenheim, A. K., Cheng, R. K., Teichman, K., Smith O. I., Sawyer, R. F., Hom, K., Stewart, H. E. (1976). "A Cinematographic Study of Combustion in an Enclosure Fitted with a Reciprocating Piston." Presented at the Conference on Stratified Charge Engines, London, November 23-24.

Overbye, V. D., Bennethum, J. E., Uyehara, O. A., and Myers, P. S. (1961). "Unsteady Heat Transfer in Engines." SAE Volume 69.

Smith, O. I. (1977). "Lean Limit Combustion in an Expanding Chamber", Ph.D. Thesis, Department of Mechanical Engineering, University of California, Berkeley, California.

Woodard, J. B., Hirvo, D. H., Grief, R., and Sawyer, R. F. (1981). "Wall Heat Transfer and Flame Propagation in a Constant Volume Duct." Presented at the Western States Section/The Combustion Institute Fall Meeting, Tempe, Arizona, October 19-20.

Yamazaki, S. and Ikai, S. (1971). "Experimental Study on the Flame Near a Cold Wall." Transactions of Japan Society of Mechanical Engineers, No. 296. Vol. 37, 772.

Yamazaki, S., and Ikai, S., (1971). "Study on Laminar One-Dimensional Premixed Flame with Heat Loss." Transactions of Japan Society of Mechanical Engineers, No. 293, Vol. 37, 121.

Yoshida, M., Harigaya, Y., and Miyazaki, T. (1981). "Relation Between Gas Flow Pattern and Heat Flux on Piston Crown Surface." J.S.A.E. Review, March.

Appendix A

Uniform Pressure Assumption

From the analysis and assumptions in Chapter 2, the conservation equations in the gas are:

$$\frac{\partial \rho}{\partial t} + \frac{\partial}{\partial x}(\rho u) = 0 \qquad \text{(A-1)}$$

$$\rho \frac{\partial u}{\partial t} + \rho u \frac{\partial u}{\partial x} = - \frac{\partial P}{\partial x} \qquad \text{(A-2)}$$

$$\rho c_p \frac{DT}{Dt} = \frac{DP}{Dt} + \frac{\partial}{\partial x}\left(k \frac{\partial T}{\partial x}\right) \qquad \text{(A-3)}$$

An order of magnitude analysis of the terms in these equations is now considered. From experimental data on wall heat transfer in engines (Alkidas, 1979 and Dao, 1972) the maximum rate of heat transfer at the gas wall interface is typically:

$$\left(k \frac{\partial T}{\partial x}\right)_{x=0,\ max} = 1000 \ \ kW/m^2 \qquad \text{(A-4)}$$

The heat transfer far from the interface is zero, so the typical order of magnitude is taken to be 500 kW/m^2. The typical rise time to this heat flux value is $\tau = 4.2 \times 10^{-3}$ sec. The gas temperature far from the wall rises from 25°C to 500°C. An average value of the conductivity of air in the range of interest is 44×10^{6} kW/m°C, so the temperature gradient is of the order of: 1.1×10^{7}°C/m. Since the variation in the gas temperature from the interface to a distance far from the interface is of the same order as T_∞, $(T_\infty - T_W \approx T_\infty)$, we can calculate a typical length scale as:

$$X = \frac{T_\infty}{\frac{\partial T}{\partial X}} = \frac{500}{500/44x10^{-6}} = 44x10^{-6}m \qquad (A-5)$$

From this result the order of magnitude of the velocity is obtained:

$$U = 0\left(\frac{X}{\tau}\right) = \frac{44x10^{-6}m}{4.17x10^{-3}sec} = 1.1x10^{-2}m/sec \qquad (A-6)$$

With this information the magnitude of the terms in the energy balance can be compared. First consider the energy transport by convection:

$$\rho c_p\, u\, \frac{\partial T}{\partial x} = 0\left(\rho c_p\, U\, \frac{T_\infty}{X}\right) \qquad (A-7)$$

With values of .64 kg/m^3 and 1.04 kJ/kg°C for density and specific heat, the energy transport is of order $8x10^4$ kW/m^2. The ratio of energy transport by conduction to that by convection is:

$$\frac{\frac{\partial}{\partial x}\left(k\, \frac{\partial T}{\partial x}\right)}{\rho c_p\, u\, \frac{\partial T}{\partial x}} = 0\left(\frac{k\, \frac{T_\infty}{X^2}}{\rho c_p\, U\, \frac{T_\infty}{X}}\right) = 0\left(\frac{k}{\rho c_p \tau}\right) = 1.6x10^{-2} \qquad (A-8)$$

Thus, the dominant energy transport is by convection. The pressure spatial gradient and pressure rate of change will be compared to this.

To evaluate the ratio of spatial pressure gradients to energy transport by convection, it is necessary to assume that the terms in the momentum equation, $\frac{\partial P}{\partial x}$, $\rho u \frac{\partial u}{\partial x}$, $\rho \frac{\partial u}{\partial t}$, are of the same order. Then the ratio can be calculated:

$$\frac{u\ \frac{\partial P}{\partial x}}{\rho c_p\, u\ \frac{\partial T}{\partial x}} = \frac{u\ (\rho u\ \frac{\partial u}{\partial x})}{\rho c_p\, u\ \frac{\partial T}{\partial x}} = \frac{\rho\ U^3/X}{\rho c_p\, U\ \frac{\partial T}{\partial x}} = 2.1\times10^{-7} \qquad \text{(A-9)}$$

For calculation of the ratio of pressure rate of change to energy transport by convection, the pressure rise is of the order of 40 bars. The ratio then is:

$$\frac{\frac{\partial P}{\partial t}}{\rho c_p\, u\ \frac{\partial T}{\partial x}} = \frac{\frac{P}{\tau}}{\rho c_p\, U\ \frac{\partial T}{\partial x}} = 6.0 \qquad \text{(A-10)}$$

From Equations (A-9) and (A-10) it is seen that $u\ \frac{\partial P}{\partial x} << \frac{\partial P}{\partial t}$ and the pressure can be taken as a function of time. The momentum equation becomes simply $P = P_\infty(t)$. The final governing equations are:

$$\frac{\partial \rho}{\partial t} + \frac{\partial}{\partial x}\ (\rho u) = 0 \qquad \text{(A-11)}$$

$$\rho c_p\ \frac{dP}{\partial t} = \frac{DT_\infty}{dt} + \frac{\partial}{\partial x}\ (k\ \frac{\partial T}{\partial x}\ ) \qquad \text{(A-12)}$$

Appendix B

Analytical Solution of Diffusion Equation

The analytical solution for the wall heat flux reduces to:

$$q_{w,g} = \sqrt{k_i \rho_i c_{pi}} \left(\frac{T_\infty}{T_i}\right)^{\gamma/\gamma-1} T_\infty \left\{ 0.564\, A_0\, \tau^{-1/2} \right. \tag{B-1}$$

$$\left. + 1.128\, A_1\, \tau^{1/2} + 1.504\, A_2\, \tau^{3/2} + 1.805\, A_3\, \tau^{5/2} + 2.06\, A_4\, \tau^{7/2} \right\}$$

The calculation of this heat flux first involves the determination of the transformed time, $\tau(t)$. This function is defined as:

$$\tau = \int_0^t \frac{P_\infty}{P_i}\, dt \tag{B-2}$$

The pressure data, $P_\infty(t)$, is calculated from the experimental engine geometry using the isentropic relation PV^γ = constant. (See Appendix D). The integrand of the equation (B-2) can be represented as a series of straight line segments of the form:

$$\left(\frac{P_\infty}{P_i}\right)_{n,n+1} = A_{n,n+1} + B_{n,n+1}\, t \tag{B-3}$$

where $A_{n,n+1}$ and $B_{n,n+1}$ are calculated from:

$$\frac{\left(\frac{P_\infty}{P_i} - \frac{P_\infty}{P_i}\right)_n}{t - t_n} = \frac{\left(\frac{P_\infty}{P_i}\right)_{n+1} - \left(\frac{P_\infty}{P_i}\right)_n}{t_{n+1} - t_n} \tag{B-4}$$

so:

$$\frac{P_\infty}{P_i} = \underbrace{\left(\frac{P_\infty}{P_i}\right)_n - \frac{\left(\frac{P_\infty}{P_i}\right)_{n+1} - \left(\frac{P_\infty}{P_i}\right)_n}{t_{n+1} - t_n} t_n}_{A_{n,n+1}} + \underbrace{\frac{\left(\frac{P_\infty}{P_i}\right)_{n+1} - \left(\frac{P_\infty}{P_i}\right)_n}{t_{n+1} - t_n}}_{B_{n,n+1}} t \qquad \text{(B-5)}$$

(See Figure B-1). The integrand of Equation (B-2) can then be written:

$$\tau = \sum_{n=1}^{359} \int_{t_n}^{t_{n+1}} \left(A_{n,n+1} + B_{n,n+1}\ t\right) dt$$

$$\tau = \sum_{n=1}^{359} \left[A_{n,n+1}\left(t_{n+1} - t_n\right) + B_{n,n+1}\left(\frac{t_{n+1}^2}{2} - \frac{t_n^2}{2}\right)\right] \qquad \text{(B-6)}$$

The next step is the determination of the coefficients A_0, A_1, etc. of the polynomial curve fit to the function $\phi = \frac{T_w}{T_\infty(t)} - 1$. Using the isentropic relation, this can be written:

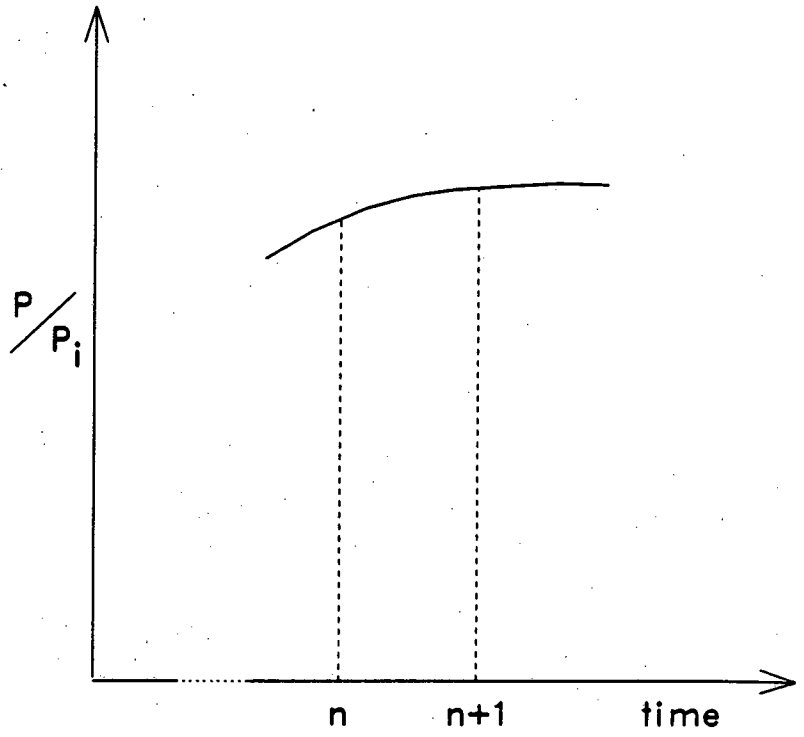

Figure B-1: Representation of pressure data as a series of straight line segments.

$$\phi_w = \frac{T_w}{T_i \left(\frac{P}{P_i}\right)^{(\gamma-1)/\gamma}} - 1.0 \qquad \text{(B-7)}$$

From the pressure data calculated as in Appendix D, the function ϕ_w can then be evaluated for each value of τ. A polynomial of desired order is then fit to $\phi_w(\tau)$ using the mathematical library routine TJMAR (Haskell and Vandevender, 1980) yielding values for the coefficients A_0, A_1, etc. With these coefficients and values for τ and T_∞, the heat flux can be calculated from Equation (B-1).

A listing of the computer program is shown in Figure B-2.

Figure B-2: Computer program to calculate the analytical solution for unsteady wall heat flux.

```
      PROGRAM QDUGAS(INPUT,OUTPUT,TAPE6=OUTPUT,TAPE7=INPUT,
     1TAPE8,PRESS,TAPE2=PRESS,TWTFD,TAPE4=TWTFD,TAUD,TAPE5=TAUD,
     1QGD,TAPE3=QGD)
C       THIS PROGRAM CALCULATES THE WALL HEAT TRANSFER BASED ON GAS
C       SIDE ANALYSIS,A POLYNOMIAL CURVE FIT, AND CLOSED FORM SOLUTION
C       OF THE DUHAMEL INTEGRATION OF THE TRANSFORMED CONSERVATION
C       EQUATIONS
      DIMENSION COEF(7),TWTF(2000),TAU(2000)
      REWIND 2
      CALL POLYFIT(COEF,TWTF,TAU)
      CALL QGAS(COEF,TWTF,TAU)
      STOP
      END
      SUBROUTINE POLYFIT(C,TWTF,TAU)
      DIMENSION P(2000),C(7),TWTF(2000),TAU(2000),A(2000),B(2000),T(2000
     1)
      DIMENSION WORK(65),LIN(16),XIN(9),IB(1)
C
C       THIS ROUTINE DOES A FIFTH ORDER POLYNOMIAL FIT TO
C       TW/TINF-1.  TW IS ASSUMED TO BE CONSTANT, EQUAL TO TINITIAL
C       AND TINF IS CALCULATED, USING ISENTROPIC RELATIONS, FROM
C       NORMALIZED PRESSURE DATA.  LEAST SQUARES FIT IS
C       CALCULATED USING A SANDIA MATH LIBRARY ROUTINE
C       CALLED TJMAR1.
      EXTERNAL FUNCT
      N=360
      GAMMA=1.38
      READ(2,10)(P(I),I=1,N)
   10 FORMAT(10(1X,F6.3))
      DO 20 I=1,N
      TWTF(I)=(1.0/(P(I)**((GAMMA-1.0)/GAMMA)))-1.0
   20 CONTINUE
      WRITE(4,30) (TWTF(I),I=1,N)
   30 FORMAT(4(1X,F15.9))
      T(1)=60./(614.*360.)
      A(1)=1.0
      B(1)=(P(1)-1.0)/(T(1)-0.0)
      DO 40 I=2,N
      IM=I-1
      T(I)=60./(614.*360.)*FLOAT(I)
      A(I)=P(IM)-((P(I)-P(IM))/(T(I)-T(IM)))*T(IM)
      B(I)=((P(I)-P(IM))/(T(I)-T(IM)))
   40 CONTINUE
      TAU(1)=A(1)*T(1)+B(1)/2.0*(T(1)**2.0)
      DO 50 I=2,N
      IM=I-1
      TAU(I)=TAU(IM)+A(I)*(T(I)-T(IM))+
     1B(I)/2.0*(T(I)**2.0-T(IM)**2.0)
   50 CONTINUE
      WRITE(5,60) (TAU(I),I=1,N)
   60 FORMAT(4(1X,F15.9))
      LIN(1)=5
      LIN(2)=N
      LIN(3)=0
      LIN(4)=0
      LIN(5)=1
      LIN(6)=2
      LIN(7)=3
      LIN(8)=5
      LIN(9)=0
      LIN(10)=2
      LIN(11)=0
```

Figure B-2: continued

```
      LIN(15)=5
      LIN(16)=-1
      XIN(1)=-100.
      XIN(2)=100.
      XIN(3)=-1.
      XIN(4)=-1.
      XIN(5)=-1.
      XIN(6)=-1.
      XIN(7)=-1.
      XIN(8)=-1.
      XIN(9)=-1.
      IB(1)=0
      DO 70 I=1,7
      C(I)=1.
   70 CONTINUE
      CALL TJMAR1(C,LIN,XIN,WORK,TAU,TWTF,IB,FUNCT,DERIV)
      WRITE(6,80)(WORK(I),I=1,6)
   80 FORMAT(6(1X,F15.9))
   90 FORMAT(1X,F20.10)
      WRITE (6,90)(C(I),I=1,7)
      RETURN
      END
      SUBROUTINE FUNCT(I,XDATA,Y,B,F,RES,PRNT)
      DIMENSION XDATA(2000),Y(1),B(7),PRNT(7)
      F=B(1)+B(2)*XDATA(I)
     1       +B(3)*(XDATA(I)**2.0)
     2       +B(4)*(XDATA(I)**3.0)
     3       +B(5)*(XDATA(I)**4.0)
      RES=Y(I)-F
      RETURN
      END
      SUBROUTINE OGAS(B,TWTF,TAU)
C      THIS ROUTINE CALCULATES WALL HEAT TRANSFER FROM GAS SIDE
C      ANALYSIS USING THE POLYNOMIAL CURVE FIT TO TW/TINF-1.
      DIMENSION OG(2000),T(2000),B(7),TAU(2000),TWTF(2000)
      N=360
      DENSG=1.4721
      CONDUG=.0214
      SPECHG=1005.25
      TINIT=243.78
      CONS=((DENSG*CONDUG*SPECHG)**.5)*TINIT
      GAMMA=1.38
      EXPON=(GAMMA/(GAMMA-1.0))+1.0
      B(1)=.564*B(1)
      B(2)=1.128*B(2)
      B(3)=1.504*B(3)
      B(4)=1.805*B(4)
      B(5)=2.06*B(5)
      DO 50 I=1,N
      T(I)=60./(614.*360.)*FLOAT(I)
   50 CONTINUE
      DO 60 I=1,N
      TRATIO=1./(TWTF(I)+1.)
      OG(I)=B(1)*(TAU(I)**(-.5))
     1       +B(2)*(TAU(I)**.5)
     1       +B(3)*(TAU(I)**1.5)
     2       +B(4)*(TAU(I)**2.5)
     3       +B(5)*(TAU(I)**3.5)
      OG(I)=OG(I)*(TRATIO**EXPON)*CONS
      OG(I)=(-1.)*OG(I)
      WRITE(3,70) OG(I)
   70 FORMAT(1X,F20.5)
   60 CONTINUE
```

Figure B-2: continued

```
      D1=T(I)/1000.
      D2=TAU(I)/1000.
      D3=QG(I)/1000.
      WRITE(6,90) I,D1,D2,D3
   90 FORMAT(1X,I5,2(F15.9,5X),F12.3)
   80 CONTINUE
      RETURN
      END
```

Appendix C

Finite Difference Formulation of Diffusion Equation

The finite difference formulation for wall heat flux requires that both the conduction equation in the solid and the transformed equation in the gas be put in finite difference form.

For the solid:

$$\frac{\partial T}{\partial t} = \alpha_s \frac{\partial^2 T}{\partial x^2} \qquad \text{(C-1)}$$

The finite difference formulation in explicit form is:

$$\frac{T_p^{k+1} - T_p^k}{\Delta t} = \alpha_s \frac{\left(T_{p+1}^k - T_p^k\right) - \left(T_p^k - T_{p-1}^k\right)}{(\Delta x)^2}$$

or

$$T_p^{k+1} = \alpha_s \frac{\Delta t}{\Delta x^2} \left(T_{p+1}^k + T_{p-1}^k - 2T_p^k\right) + T_p^k \qquad \text{(C-2)}$$

where k is the time index and p is the spatial index. Defining $M_s = \alpha_s \frac{\Delta t}{\Delta x^2}$, and normalizing to the initial temperature T_i, the equation becomes:

$$\frac{T_p^{k+1}}{T_i} = M_s \left(\frac{T_p^k}{T_i} + \frac{T_{p-1}^k}{T_i}\right) + (1-2M_s) \frac{T_p^k}{T_i} \qquad \text{(C-3)}$$

Stability considerations require that $M_s < 1/2$.

Stability considerations require that $M_s < 1/2$.

On the gas side the transformed energy equation results in a diffusion equation (Equation 2.2-20)

$$\frac{\partial \phi}{\partial \tau} = \alpha_i \frac{\partial^2 \phi}{\partial \psi^2} \tag{C-4}$$

This equation is first transformed back to the same time base as the equation for the solid side. Since

$$\frac{\partial}{\partial t} = \frac{P_\infty}{P_i} \frac{\partial}{\partial \tau}$$

the equation becomes:

$$\frac{P_i}{P_\infty} \frac{\partial \phi}{\partial t} = \alpha_i \frac{\partial^2 \phi}{\partial \psi^2} \tag{C-5}$$

In finite difference form :

$$\frac{\phi_s^{k+1} - \phi_s^k}{\Delta t} = \frac{P_\infty^k}{P_i} \alpha_i \frac{\left(\phi_{s+1}^k - \phi_s^k\right) - \left(\phi_s^k - \phi_{s-1}^k\right)}{(\Delta \psi)^2}$$

or

$$\phi_s^{k+1} = \left(\frac{P_\infty^k}{P_i} \alpha_i \frac{\Delta t}{(\Delta \psi)^2}\right)\left(\phi_{s+1}^k + \phi_{s-1}^k - 2\,\phi_s^k\right) + \phi_s^k \tag{C-6}$$

where s is the spatial index in the gas. Defining $M_g^k = \frac{P_\infty^k}{P_i} \alpha_i \frac{\Delta t}{(\Delta \psi)^2}$ gives

$$\phi_s^{k+1} = M_g^k \left(\phi_{s+1}^k + \phi_{s-1}^k\right) + \left(1-2\,M_g^k\right)\,\phi_s^k \qquad \text{(C-7)}$$

Stability requires that $M_g^k \leq 1/2$, but note that M_g^k varies with P_∞. Thus M_g^k reaches a maximum at P_∞^{max}. So,

$$M_g^{max} = \frac{P_\infty^{max}}{P_i}\,\alpha_i\,\frac{\Delta t}{\Delta\phi^2} = 1/2 \qquad \text{(C-8)}$$

Then, M_g^k for every time step is calculated as:

$$M_g^k = 1/2\;\frac{P_\infty^k/P_i}{P_\infty^{max}/P_i} \qquad \text{(C-9)}$$

The equation for the gas-solid interface is determined from the boundary conditions at the interface; i.e., equal heat flux and equal temperature. Denote the interface nodes as shown:

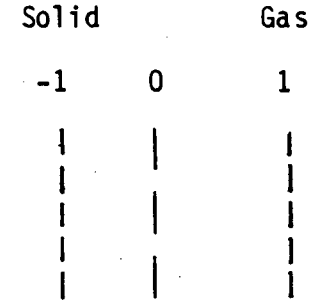

The heat flux to the solid in time step k is:

$$q_{solid}^k = -\,k_s\,\frac{\partial T}{\partial x}\Big|_{x=0} = -\,k_s\,\frac{T_{-1}^k - T_0^k}{\Delta x} \qquad \text{(C-10)}$$

The heat flux from the gas in time step k is:

$$q^k_{gas} = k_g \frac{\partial T}{\partial x}\Big|_{x=0}$$

$$= k_g \frac{\rho}{\rho_i} \frac{\partial T}{\partial \psi}\Big|_{\psi=0}$$

$$= k_{ig} \frac{T}{T_i} \frac{\rho}{\rho_i} \frac{\partial T}{\partial \psi}\Big|_{\psi=0}$$

$$= k_{ig} \frac{P_\infty}{P_i} \frac{\partial T}{\partial \psi}\Big|_{\psi=0}$$

$$= k_{ig} \frac{P^k_\infty}{P_i} \left(\frac{T^k_1 - T^k_0}{\Delta \psi} \right) \qquad \text{(C-11)}$$

The equal flux boundary condition, $q^k_{solid} = q^k_{gas}$, gives:

$$k_s \left(\frac{T^k_{-1} - T^k_0}{\Delta x} \right) = k_{ig} \frac{P^k_\infty}{P_i} \left(\frac{T^k_0 - T^k_1}{\Delta \psi} \right) \qquad \text{(C-12)}$$

or

$$T^k_o = \frac{T^k_{-1} + \frac{\Delta x}{\Delta \psi} \frac{k_{ig}}{k_s} \frac{P^k_\infty}{P_i} T^k_1}{1 + \frac{\Delta x}{\Delta \psi} \frac{k_{ig}}{k_s} \frac{P^k_\infty}{P_i}} \qquad \text{(C-13)}$$

Next an expression relating Δx and $\Delta \psi$ is needed. Recall

$$M_s = \frac{\alpha_s \Delta t}{\Delta x^2}$$

and $$M_g^k = \frac{\alpha_{ig} \frac{p_\infty^k}{P_i} \Delta t}{(\Delta\psi)^2}$$

so $$\frac{\Delta x}{\Delta\psi} = \left(\frac{\alpha_s M_g^k P_i}{\alpha_{ig} M_s P_\infty^k} \right)^{1/2} \qquad \text{(C-14)}$$

Substituting this expression into Equation (C-13) gives:

$$T_0^k = \frac{T_{-1}^k + \frac{k_{ig}}{k_s} \frac{p_\infty^k}{P_i} \sqrt{\frac{\alpha_s M_g^k P_i}{\alpha_{ig} M_s P_\infty^k}} \; T_1^k}{1 + \frac{k_{ig}}{k_s} \frac{p_\infty^k}{P_i} \sqrt{\frac{\alpha_s M_g^k P_i}{\alpha_{ig} M_s P_\infty^k}}} \qquad \text{(C-15)}$$

Define $$M_I = \frac{k_{ig}}{k_s} \sqrt{\frac{\alpha_s M_g p_\infty^k}{\alpha_{ig} M_s P_i}} \qquad \text{(C-16)}$$

so $$T_0^k = \frac{T_{-1}^k + M_I T_1^k}{1 + M_I} \qquad \text{(C-17)}$$

and finally normalizing to the initial temperature yields:

$$\frac{T_0^k}{T_i} = \frac{\left(T_{-1}^k / T_i\right) + M_I \left(T_1^k / T_i\right)}{1 + M_I} \qquad \text{(C-18)}$$

From these equations (C-3), (C-7), and (C-18) the temperature at each node in the gas and solid can be calculated. The wall heat transfer can then be calculated from the equation for either the solid side or the gas side. For the solid side:

$$q^k_{solid} = -k_s \frac{T^k_{-1} - T^k_0}{\Delta x} \qquad \text{(C-19)}$$

For the gas side, recall:

$$q^k_{gas} = k_{ig} \frac{p^k_\infty}{P_i} \frac{T^k_0 - T^k_1}{\Delta\psi} \qquad \text{(C-20)}$$

From Equation (C-14),

$$\Delta\psi = \frac{\Delta x}{\frac{\alpha_s}{\alpha_{ig}} \frac{M^k_g}{M_s} \frac{P_i}{p^k_\infty}} \qquad \text{(C-21)}$$

so

$$q^k_{gas} = k_{ig} \sqrt{\frac{p^k_\infty}{P_i}} \frac{T^k_0 - T^k_1}{\Delta x \sqrt{\frac{\alpha_{ig}}{\alpha_s} \frac{M_s}{M^k_g}}} \qquad \text{(C-22)}$$

To calculate the temperature profiles and heat flux (Equations C-3, C-7, C-9, C-17, C-18, and C-22), pressure data as a function of time is needed. This data is calculated from the engine geometry as discussed in Appendix D. The computer program written to calculate the temperature profiles and heat flux is shown in Figure C-1.

Figure C-1: Computer program for finite difference solution for wall heat flux and temperature profiles.

```
      PROGRAM COMPEXP(PRESS,OUTPUT,QFILE,TAPE2=PRESS,TAPE3=OUTPUT,
     1TAPE4=QFILE,TFILE,TAPE6=TFILE,TINFIL,TAPE7=TINFIL)
C     THIS PROGRAM CALCULATES  THE UNSTEADY WALL
C     HEAT FLUX FROM A GAS (AIR) UNDERGOING COMPRESSION AND
C     EXPANSION.
C     ON THE SOLID SIDE, A ONE DIMENSIONAL UNSTEADY DIFFUSION
C     EQUATION IN FINITE DIFFERENCE (EXPLICIT) FORM IS USED.
C     ON THE GAS SIDE, THE ENERGY EQUATION IS TRANSFORMED
C     (THUS SATISFYING CONTINUITY AND MOMENTUM EQUATIONS)
C     INTO A DIFFUSION TYPE EQUATION.  IT IS ASSUMED THAT:
C        SPATIAL PRESSURE GRADIENTS ARE NEGLIGIBLE;
C        CONDUCTIVITY IS LINEAR IN TEMPERATURE;
C        PERFECT GAS LAW APPLIES;
C        ISENTROPIC RELATIONS APPLY.
C     EXPLICIT FINITE DIFFERENCE FORM IS USED.
C
      DIMENSION TSOLID(101),TGAS(101),PRESS(360),QWALL(360)
      DIMENSION TINFIN(360),TSOLIDM(101),TGASM(101)
      DIMENSION T1(101),T2(101),T3(101),T4(101)
      REWIND 2
      REWIND 4
      REWIND 6
      REWIND 7
C
C     MATERIAL PROPERTY VALUES:
C     SOLID---CAST IRON
C     CONDUCTIVITY W/M-K
      CONDUS=44.99
C     DENSITY  KG/M**3
      DENSS=7208.3
C     SPECIFIC HEAT  J/KG-K
      SPECHS=460.55
C     THERMAL DIFFUSIVITY  M**2/S
      ALPHAS=CONDUS/(DENSS*SPECHS)
C**********************
C     GAS---AIR AT 240.78 K
C     CONDUCTIVITY  W/M-K
      CONDUG=0.0214
C     DENSITY  KG/M**3
      DENSG=1.4721
C     SPECIFIC HEAT  J/KG-K
      SPECHG=1005.25
C     THERMAL DIFFUSIVITY  M**2/S
      ALPHAG=CONDUG/(DENSG*SPECHG)
C     RATIO OF SPECIFIC HEATS---AIR
      GAMMA=1.38
C**********************
C
C     SET THE TIME STEP (CONVERTED TO SECONDS)
      DELTAT=40./(614.*360.)
C     SET INITIAL TEMPERATURE--KELVIN
      TINIT=240.78
C     SET VALUE OF COEFFICIENTS IN SOLID FINITE DIFFERENCE EQUATION
C     MUST BE < OR = TO 1/2 FOR STABILITY
      XMS=0.5
C     CALCULATE THE SPATIAL INCREMENT IN SOLID
      DELX=(ALPHAS*DELTAT/XMS)**0.5
C     CALCULATE THE SECONDARY COEFFICIENT FOR THE INTERFACE COEFFICIENT
      CI=(CONDUG/CONDUS)*((ALPHAS)/(ALPHAG*XMS))**0.5
C     SET THE NUMBER OF TIME AND SPACE INCREMENTS
      NTIME=360
      NSPACE=101
```

Figure C-1: continued

```
      TGASM(I)=1.0
   10 CONTINUE
C     READ IN THE PRESSURE DATA(NORMALIZED TO THE INITIAL PRESSURE)
      READ(2,20) (PRESS(I),I=1,NTIME)
   20 FORMAT(10(1X,F6.3))
      WRITE(3,25)
   25 FORMAT(1X,'INPUT--NORMALIZED PRESSURE ')
      WRITE(3,20) (PRESS(I),I=1,NTIME)
C      TO CALCULATE THE COEFFICIENT FOR GAS FINITE DIFFERENCE
C      EQUATION, NEED TO DETERMINE THE MAX PRESSURE
      PMAX=0.0
      DO 45 I=1,NTIME
      IF(PRESS(I).GT.PMAX) PMAX=PRESS(I)
   45 CONTINUE
C     CALCULATE FOR EACH TIME STEP, THE TEMPERATURE IN THE SOLID,
C     THE GAS, AND THE INTERFACE, AND THE HEAT FLUX.
      DO 30 I=2,NTIME
      IM=I-1
      TINFIN(I)=TINFIN(IM)*(PRESS(I)/PRESS(IM))**((GAMMA-1.)/
     1GAMMA)
C       CALCULATE TEMPERATURE IN SOLID
      NSP=NSPACE-1
      DO 40 J=2,NSP
      JP=J+1
      JM=J-1
      TSOLID(J)=XMS*(TSOLIDM(JP)+TSOLIDM(JM))+(1.0-2.0*XMS)*TSOLIDM
     1(J)
   40 CONTINUE
      TSOLID(NSPACE)=TSOLIDM(NSPACE)
C       CALCULATE TEMPERATURE IN GAS
      XMG=0.5*(PRESS(I)/PMAX)
      DO 50 K=2,NSP
      KP=K+1
      KM=K-1
      TGAS(K)=(PRESS(I)/PRESS(IM))**((GAMMA-1.0)/GAMMA)*(XMG*TGASM(KP
     1)+XMG*TGASM(KM)+(1.0-2.0*XMG)*TGASM(K))
   50 CONTINUE
      TGAS(NSPACE)=TGASM(NSPACE)*(PRESS(I)/PRESS(IM))**((GAMMA-1.0)/
     1GAMMA)
C       CALCULATE INTERFACE TEMPERATURE AND HEAT FLUX
      XMI=CI*(XMG**0.5)*(PRESS(I)**0.5)
      TSOLID(1)=(TSOLID(2)+XMI*TGAS(2))/(1.0+XMI)
      TGAS(1)=TSOLID(1)
      QWALL(I)=-1.0*CONDUG*(PRESS(I)**0.5)*(TGAS(1)-TGAS(2))/(DELX*
     1(((ALPHAG*XMS)/(ALPHAS*XMG))**0.5))
      QWALL(I)=QWALL(I)*TINIT
C       WRITE OUT TEMPERATURE PROFILES FOR PLOTTING PURPOSES
      IF(I.EQ.140) GO TO 8
      IF(I.EQ.190) GO TO 1
      IF(I.EQ.210)GO TO 2
      IF(I.EQ.240) GO TO 3
      GO TO 4
    1 CONTINUE
      DO 5 J=1,NSPACE
      T1(J)=TGAS(J)
    5 CONTINUE
      GO TO 4
    2 CONTINUE
      DO 6 J=1,NSPACE
      T2(J)=TGAS(J)
    6 CONTINUE
      GO TO 4
```

Figure C-1: continued

```
      GO TO 4
    8 CONTINUE
      DO 9 J=1,NSPACE
      T4(J)=TGAS(J)
    9 CONTINUE
    4 CONTINUE
C       UPDATE TSOLIDM AND TGASM FOR NEXT CALCULATION
      DO 70 J=1,NSPACE
      TSOLIDM(J)=TSOLID(J)
      TGASM(J)=TGAS(J)
   70 CONTINUE
   30 CONTINUE
C
C    PRINT THE TEMPERATURES IN GAS AND SOLID FOR LAST TIME STEP
C       TO CHECK THAT THE INFINITY BOUNDARY CONDITION IS MET
      WRITE (3,75)
   75 FORMAT(*1*,1X,*TIME STEP*,10X,*SOLID*,10X,*GAS*)
      I=NTIME
      DO 80 K=1,NSPACE
      WRITE(3,90) I,TSOLID(K),TGAS(K)
   90 FORMAT(1X,I8,5X,F15.10,5X,F15.10)
   80 CONTINUE
C    PRINT HEAT FLUX AT EACH TIME STEP
      WRITE(3,140)
  140 FORMAT(11X,*HEAT FLUX   W/SQ M  OUT OF GAS AND OUT OF SOLID*
     1,5X,*INFINITY  NORMALIZED*)
      DO 150 I=2,NTIME
      WRITE(3,160) I,QWALL(I),TINFIN(I)
  160 FORMAT(5X,I5,2X,F15.5,30X,F15.5)
      WRITE(4,161) QWALL(I)
      WRITE(7,164) TINFIN(I)
  164 FORMAT(1X,F15.5)
  161 FORMAT(1X,F12.3)
  150 CONTINUE
      DO 152 J=1,NSPACE
      WRITE(6,163) T1(J),T2(J),T3(J),T4(J)
  163 FORMAT(1X,4F12.3)
  152 CONTINUE
      STOP
      END
```

Appendix D

Calculation of Pressure from Engine Data

To calculate the pressure in a cylinder during compression and expansion, the displacement of the piston as a function of time must first be determined. A formulation for piston displacement for an engine can be obtained from the geometry of the design as follows. Figure D-1 shows the basic dimensions involved. Denoting the piston displacement as S, it is easy to see:

$$S = r + \ell - (oc + ac) \qquad \text{(D-1)}$$

and from basic trigonometry,

$$S = r + \ell - (r \cos\theta + \ell \cos\phi)$$

But $$\ell^2 = (cb)^2 + (ac)^2$$
$$= r^2 \sin^2\theta + \ell^2 \cos^2\phi$$

so $$\ell \cos\phi = \sqrt{\ell^2 - r^2 \sin^2\theta}$$

and $$S = r + \ell - r\cos\theta - \sqrt{\ell^2 - r^2 \sin^2\theta}$$

or $$S = r\left[\left(1-\cos\theta\right) + \frac{\ell}{r}\left(1 - \sqrt{1 - \frac{r^2}{\ell^2}\sin^2}\right)\right] \qquad \text{(D-2)}$$

An excellent approximation to the exact result is very often used and yields a much simpler form. The approximation is found by completing the square, adding $\frac{r^4}{4\ell^4}\sin^4\theta$ to obtain:

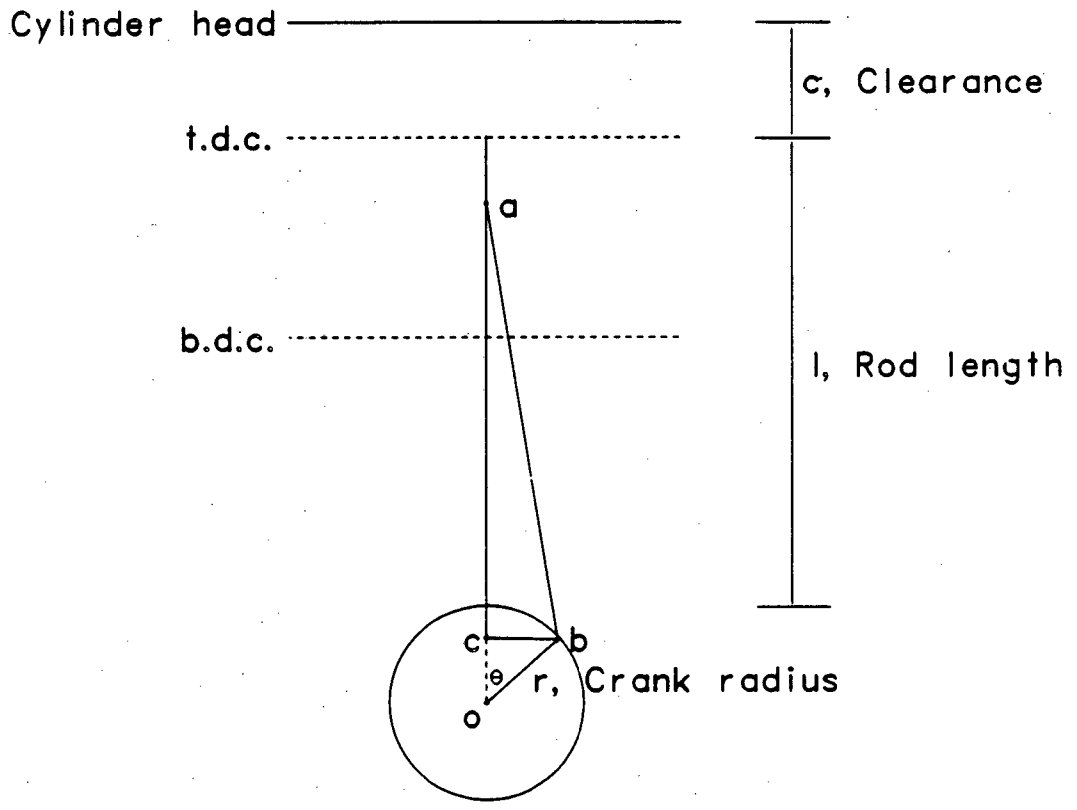

Figure D-1: Engine geometry.

$$S \simeq r \left[(1-\cos\theta) + \frac{r}{2\ell} \sin^2\theta\right]$$

or
$$S = r \left[(1-\cos\theta) + \frac{r}{4\ell} (1-\cos 2\theta)\right] \qquad \text{(D-3)}$$

With this result, the volume as a function of crank angle can be expressed as:

$$V = \left\{c + r \left[(1-\cos\theta) + \frac{r}{4\ell} (1-\cos 2\theta)\right]\right\} A \qquad \text{(D-4)}$$

where c is the clearance at TDC, and A is the piston area.

The pressure during compression and expansion is obtained from isentropic relation:

$$P_\infty = \frac{P_i V_i^\gamma}{V^\gamma} \qquad \text{(D-5)}$$

where P_i is the initial pressure and V_i is the initial volume, i.e. $V_i = c \cdot A$. A listing of the program written to perform this calculation is given in Figure D-2. A sample result is shown in Figure D-3.

Figure D-2: Computer program to calculate pressure from engine geometry.

```
      PROGRAM PRESCAL(PRESS,OUTPUT,TAPE2=PRESS,TAPE3=OUTPUT)
C      THIS ROUTINE CALCULATES PRESSURE VERSUS CRANK ANGLE OR
C      TIME DURING COMPRESSION AND EXPANSION OF A PISTON IN A CYLINDER;
C      THE PISTON DISPLACEMENT AND VELOCITY ARE CALCULATED AS
C      INTERMEDIATE RESULTS.
C      THE REQUIRED INPUTS INCLUDE:  CRANK RADIUS, ROD LENGTH, RPM,
C      PISTON AREA, CLEARANCE AT TDC, INITIAL PRESSURE, AND RATIO OF
C      SPECIFIC HEATS OR EQUIVALENT ISENTROPIC COEFFICIENT.
C      DIMENSIONS:  METERS AND KILOPASCALS
C      IT IS ASSUMED THAT THIS IS AN ISENTROPIC PROCESS.
C      IT IS ALSO ASSUMED THAT THE APPROXIMATION TO PISTON DISPLACEMENT
C      FOUND BY COMPLETING THE SQUARE IS ACCURATE FOR OUR PURPOSES.
C
      DIMENSION  S1(360),S2(360),V(360),P(360),TSTEP(360),PN(360)
      CRANK=0.05080
      ROD=0.1905
      RPM=614.
      PTAREA=0.004948
      CLEAR=0.007823
      PRESSI=130.250
      CPCV=1.38
C
C       THE CRANK ANGLE IS TAKEN TO BE ZERO AT BDC.
C
      PI=3.141593
      CON=PRESSI*((CLEAR+2.*CRANK)*PTAREA)**CPCV
      DO 10 I=1,360
      TSTEP(I)=FLOAT(I)
      THETA=(FLOAT(I)+180.)*PI/180.
      S1(I)=CRANK*((1.0-COS(THETA))+(ROD/CRANK)*(1.0-(1.0-(CRANK/ROD*
     1SIN(THETA))**2.0)**0.5))
      S2(I)=CRANK*((1.0-COS(THETA))+CRANK/(4.0*ROD)*(1.0-COS(2.0*THETA)
     1))
      V(I)=2.0*PI*RPM*CRANK/(60.)*(SIN(THETA)+CRANK/(2.0*ROD)*
     1SIN(2.*THETA))
      P(I)=CON/(((CLEAR+S2(I))*PTAREA)**CPCV)
      PN(I)=P(I)/PRESSI
   30 FORMAT(1X,F8.3,3X,F8.3,3X,F8.3,3X,F8.3)
   10 CONTINUE
      WRITE(2,40)(PN(I),I=1,360)
   40 FORMAT(10(1X,F6.3))
      CALL TEK14
      CALL TITLE('PRESSURES',-100,'CRANK ANGLE DEGREES$',100,'KILOPASCAL
     1S$',100,9.9,6.5)
      CALL GRAF(0.,20.,360.,0.,500.,4000.)
      CALL CURVE(TSTEP,P,360,0)
      CALL ENDPL(0)
      STOP
      END
```

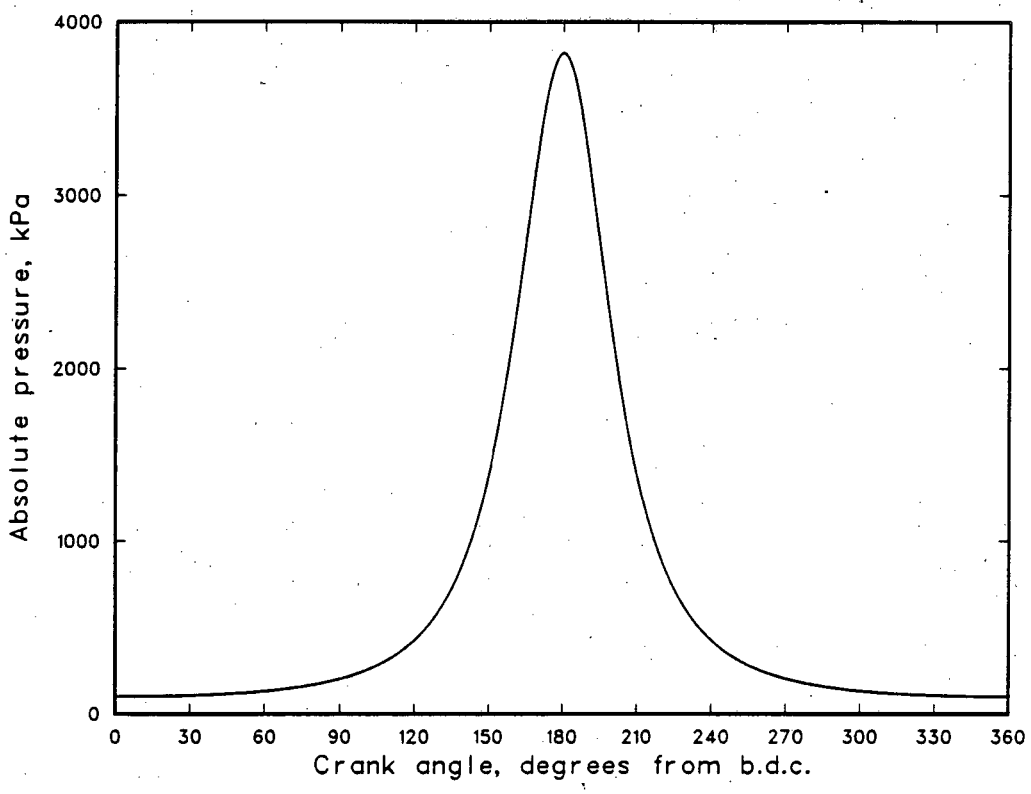

Figure D-3: Sample results.

Appendix E

Gas Chromatograph Analysis of the Premixed Fuel

To fill the test section with a premixed fuel/air mixture, a gas mixing apparatus involving flow rotometers was used. The calibration and assessment of repeatability of the mixing device were determined by performing a gas analysis using a Hewlett Packard Model 5750 Gas Chromatograph in conjunction with an Autolab System IV integrator. In this analysis, helium was used as a carrier gas, and a column of molecular sieve 5A was used for separation. Both the thermal conductivity detector (TCD) and the flame ionization detector (FID) were used.

Mixtures of unknown concentration of methane and air were analyzed. The oxygen and nitrogen concentrations were determined from the TCD while the methane concentration was taken from the FID results. The analysis of these gases includes one complication; that is, the peak produced by oxygen in the TCD also includes argon which is at a concentration level which would affect the results. Therefore the oxygen concentration measurement was corrected as follows. It has been shown by Mc Nair and Bonelli (1968) that the TCD peak area, A_x, of constituent x, is proportional to the concentration, C_x,

$$A_x \alpha (k_{He} - k_x) C_x$$

where k_{He} and k_x are the thermal conductivities of helium and the constituent gas. Thus for argon and the argon/oxygen combined gas we have:

$$\frac{A_{Ar}}{(k_{He} - k_{Ar})\, C_{Ar}} = \frac{A_{Ar + O_2}}{(k_{He} - k_{Ar + O_2})\, C_{Ar + O_2}}$$

Since the argon is a very small part of the argon/oxygen gas, a further simplification is made:

$$\frac{A_{Ar}}{(k_{He} - k_{Ar})\, C_{Ar}} = \frac{A_{Ar + O_2}}{(k_{He} - k_{O_2})\, C_{O_2}}$$

From this it is simple to calculate the argon area, A_{Ar}, which then can be subtracted from the combined are $A_{Ar + O_2}$, detected by the TCD.

To calibrate the mixing device, nine different concentrations ranging in equivalence ratio from .4 to 1.15 were analyzed. This analysis was repeated three time to assess repeatability and the error was found to be approximately one percent.

Appendix F

Data - Noise Filtering

The experimental measurements show a low level noise resulting from the use of an isolation transformer which was used to protect the minicomputer data acquisition system. This low level noise was removed before the data was analyzed. The data were processed by a data smoothing subroutine, PSMTH1 (Haskell and Vandevender, 1980). This subroutine smooths the data by making a piecewise fit to the measurements with a least squares polynomial. A comparison of experimental measurements and smoothed data is shown in Figure F-1. The results are very good with only a low level noise remaining in the tails of the data.

Figure F-1: Comparison of experimental measurements with smoothed data; pressure variation with time.

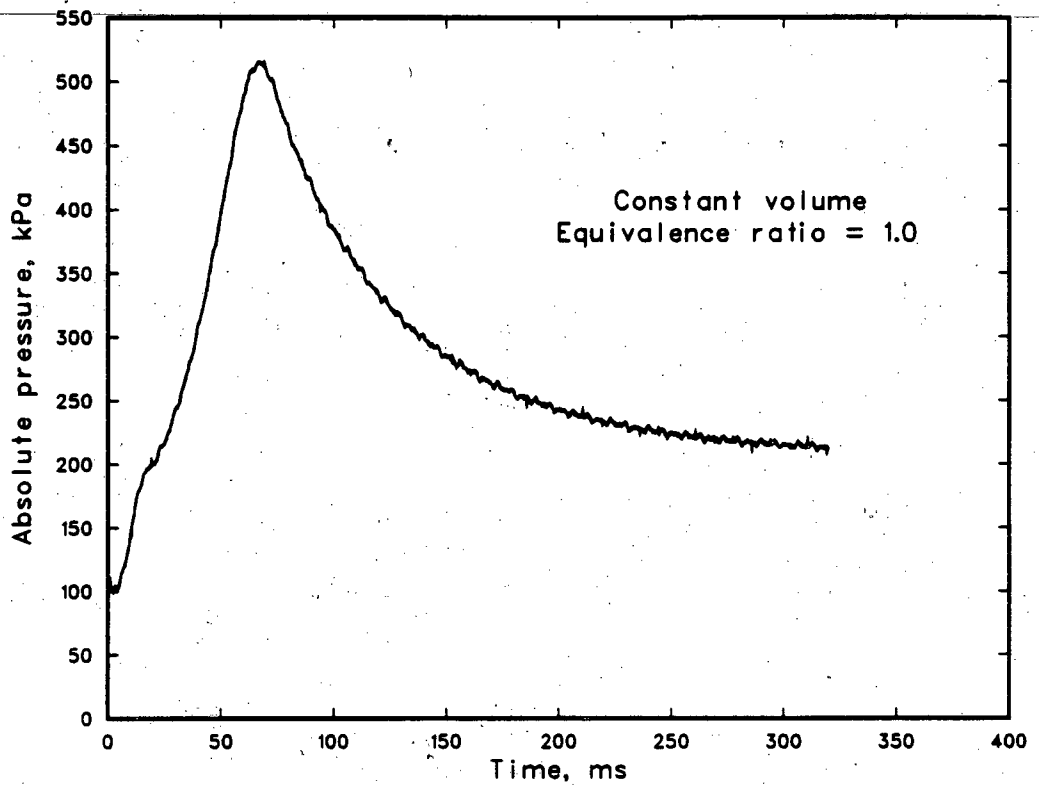

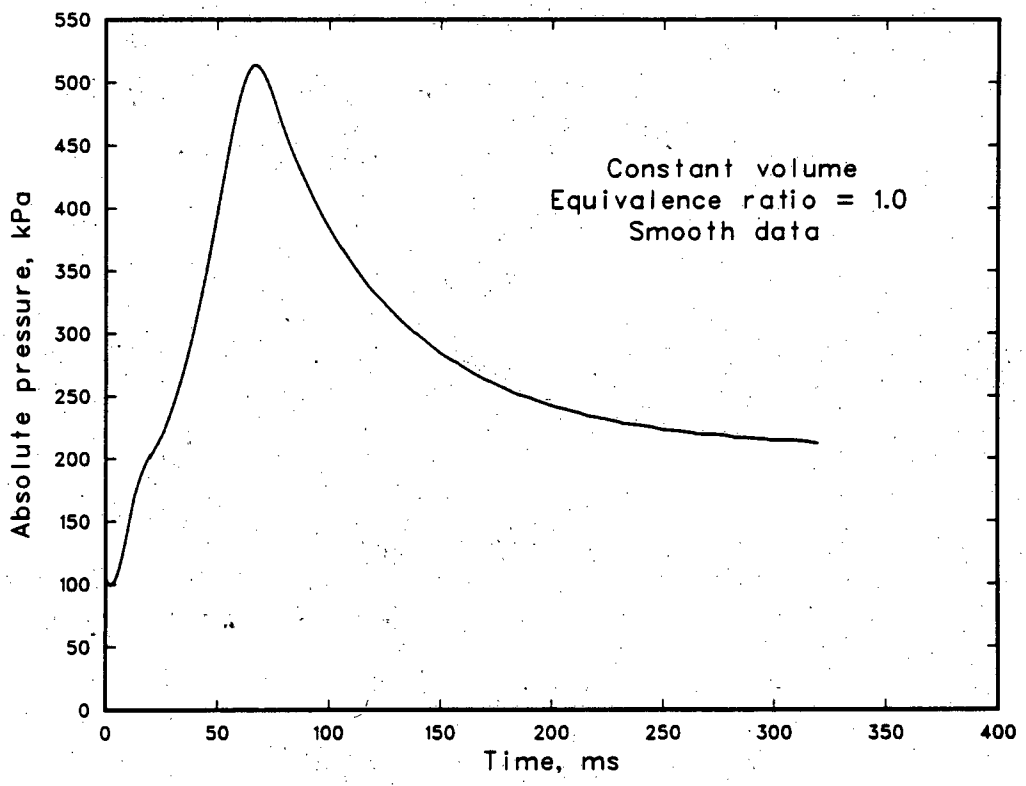

Appendix G

Determination of Heat Flux from Measured Wall Temperature

The solution for the heat flux in the solid takes the form:

$$q_w(0,t) = \sqrt{\frac{k\rho c}{\pi}} \left[\frac{T_w(t) - T_i}{\sqrt{t}} + \frac{1}{2} \int_0^t \frac{T_w(t) - T_w(\lambda)}{(t-\lambda)^{3/2}} d\lambda \right] \quad \text{(G-1)}$$

Thus, in order to calculate the heat flux from the wall temperature measurements, the integral in Equation (G-1) must be computed.

Defining $\tilde{T}(t) \equiv T_w(t) - T_i$ gives:

$$q_w = \sqrt{\frac{k\rho c}{\pi}} \left[\frac{\tilde{T}(t)}{\sqrt{t}} + \frac{1}{2} \int_0^t \frac{\tilde{T}(t) - \tilde{T}(\lambda)}{(t-\lambda)^{3/2}} d\lambda \right] \quad \text{(G-2)}$$

The measured change in wall temperature, $\tilde{T}(t)$ takes the form of discrete points $\tilde{T}_m$, m=1,...N where T_m is the wall temperature change corresponding to time t_m. The integral in Equation (G-2) can then be expressed as a sum of N-1 integrals:

$$q_w = \sqrt{\frac{k\rho c}{\pi}} \left[\frac{T_N(t)}{\sqrt{t_N}} + \frac{1}{2} \sum_{m=1}^{N-1} \left(\int_{t_m}^{t_{m+1}} \frac{\tilde{T}_N - \tilde{T}(\lambda)}{(t_N - \lambda)^{3/2}} d\lambda \right) \right] \quad \text{(G-3)}$$

Between any two successive data points $(t_m, \tilde{T}_m)$ and $(t_{m+1}, \tilde{T}_{m+1})$ a straight line variation for T is assumed as shown in Figure G-1. The temperature can then be expressed as:

Figure G-1: Representation of wall temperature data as a series of successive straight line segments

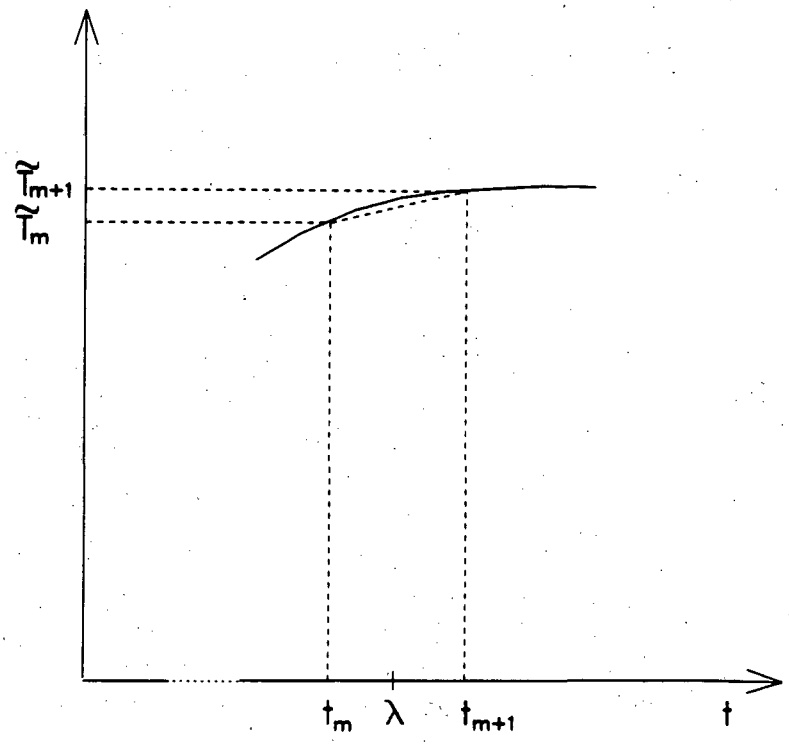

$$T_{m,m+1} + A_{m,m+1} + B_{m,m+1}\,\lambda$$

where $A_{m,m+1}$ and $B_{m,m+1}$ are derived from:

$$\frac{\tilde{T}_{m,m+1} - \tilde{T}_m}{\lambda - t_m} = \frac{\tilde{T}_{m+1} - \tilde{T}_m}{t_{m+1} - t_m}$$

or

$$\tilde{T}_{m,m+1} - \tilde{T}_m - t_m\left(\frac{\tilde{T}_{m+1} - \tilde{T}_m}{t_{m+1} - t_m}\right) + \left(\frac{\tilde{T}_{m+1} - \tilde{T}_m}{t_{m+1} - t_m}\right)\lambda \qquad \text{(G-4)}$$

$$\underbrace{\qquad\qquad}_{A_{m,m+1} \equiv A_{m+1}} \qquad \underbrace{\qquad\qquad}_{B_{m,m+1} \equiv B_{m+1}}$$

For all but the last in the sum of integrals, the integration is straight forward:

$$\int_{t_m}^{t_{m+1}} \frac{\tilde{T}_N - A_{m+1} - B_{m+1}\,\lambda}{(t_N - \lambda)^{3/2}}\, d\lambda$$

$$= -(\tilde{T}_N - A_{m+1}) \int_{t_m}^{t_{m+1}} \frac{d\lambda}{(t_N - \lambda)^{3/2}} - B_{m+1} \int_{t_m}^{t_{m+1}} \frac{\lambda\, d\lambda}{(t_N - \lambda)^{3/2}} \qquad \text{(G-5)}$$

Employing the following integrals:

$$\int \frac{d\lambda}{(a + b\,\lambda)^{3/2}} = \frac{-2}{b\sqrt{a + b\lambda}}$$

$$\int \frac{\lambda\, d\lambda}{(a + b\lambda)^{3/2}} = (2a + b\lambda)\,\frac{2}{b^2\sqrt{a + b\lambda}}$$

Equation (G-5) simplifies to:

$$(\tilde{T}_N - A_{m+1}) \left[\frac{2}{\sqrt{t_N - \lambda}}\right]_{\lambda=t_m}^{t_{m+1}} - B_{m+1} \left[\frac{2(2t_N - \lambda)}{\sqrt{t_N - \lambda}}\right]_{\lambda=t_m}^{t_{m+1}}$$

$$= 2\left[\frac{\tilde{T}_N - A_{m+1} - B_{m+1}(2t_N - t_{m+1})}{\sqrt{t_N - t_{m+1}}} - \frac{\tilde{T}_N - A_{m+1} - B_{m+1}(2t_N - t_m)}{\sqrt{t_N - t_m}}\right] \qquad \text{(G-6)}$$

For the last integral in the sum:

$$\int_{t_{N-1}}^{t_N} \frac{\tilde{T}_N - \tilde{T}(\lambda)}{(t_N - \lambda)^{3/2}}\, d\lambda = \int_{t_{N-1}}^{t_N} \frac{A_N + B_N t_N - A_N - B_N \lambda}{(t_N - \lambda)^{3/2}}\, d\lambda$$

$$= B_N \int_{t_{N-1}}^{t_N} \frac{d\lambda}{(t_N - \lambda)^{1/2}}$$

$$= 2 B_N \sqrt{t_N - t_{N-1}} \qquad \text{(G-7)}$$

Substituting Equations (G-6) and (G-7) into (G-3) yields:

$$q_w(t_N) = \sqrt{\frac{k\rho c}{\pi}} \left\{ \frac{\tilde{T}(t_N)}{\sqrt{t_N}} + \sum_{m=1}^{N-2} \left[\frac{\tilde{T}_N - A_{m+1} - B_{m+1}(2t_N - t_{m+1})}{\sqrt{t_N - t_{m+1}}} - \frac{\tilde{T}_N - A_{m+1} - B_{m+1}(2t_N - t_m)}{\sqrt{t_N - t_m}}\right] + B_N \sqrt{t_N - t_{N-1}} \right\} \qquad \text{(G-8)}$$

The computer program to calculate the wall heat flux using Equation (G-8) is shown in Figure G-2.

To verify this procedure and test the computer program the special case of a linear variation in wall temperature was analyzed. Assuming variation $T(\tilde{t}) = Kt$, Equation (G-3) simplifies to:

$$q_w(t) = \sqrt{\frac{k\rho c}{\pi}} \; (2 \; K \sqrt{t}) \qquad \text{(G-9)}$$

This result is in excellent agreement with the results of the computer program.

Figure G-2: Computer program for the determination of wall heat flux from wall temperature measurements.

```
      PROGRAM QSOLID(INPUT,OUTPUT,TAPE2=INPUT,TAPE3=OUTPUT,
     1QDATA,TAPE4=QDATA,TDATA,TAPE5=TDATA,PDATA,TAPE6=PDATA)
      DIMENSION TIME(2000),WTEMP(2000),WTEMPN(2000),A(2000),B(2000),
     1Q(2000),P(2000),QS(2000)
C*****************************************************************
C  ROUTINE TO CALCULATE THE WALL HEAT FLUX IN THE SOLID,GIVEN WALL
C  TEMPERATURE DATA.
C  WTEMP-EXPERIMENTALLY MEASURED WALL TEMPERATURE (K)
C  WTEMPN-WALL TEMPERATURE MINUS INITIAL TEMPERATURE
C  A AND B - PARAMETERS IN LINEAR INTERPOLATION BETWEEN POINTS
C  AUGUST 12,1981  J.B.WOODARD
C*****************************************************************
C
C  PROPERTIES OF THE WALL - MACOR AT 298 K
C  CONDUCTIVITY  (W/M*K)
      COND=1.676
C  DENSITY  (KG/M**3)
      DENS=2520.024
C  SPECIFIC HEAT  (J/KG*K)
      CP=460.55
C  THERMAL DIFFUSIVITY  (M**2/SEC)
      ALPHA=COND/(DENS*CP)
      REWIND 4
      REWIND 5
      REWIND 6
C  CALCULATE CONSTANTS NEEDED:
      PI=4.0*ATAN(1.0)
C  CALCULATE TIME AT EACH DATA POINT IN SECONDS
      DO 10 I=1,2000
      TIME(I)=(FLOAT(I)-1.0)*0.0002
   10 CONTINUE
C  CALCULATE CONSTANT FOR HEAT FLUX
      CONS=((DENS*CP*COND)/PI)**0.5
C
C  READ IN TOTAL NUMBER OF DATA POINTS AND RUN ID
    1 CONTINUE
      READ(5,5) NMAX,RUNID
    5 FORMAT(1X,I4,A9)
      IF(EOF(5)) 110,15
   15 CONTINUE
C
C  READ IN TEMPERATURE DATA AND NORMALIZE
      READ(5,30) (K,WTEMP(I),X,I=1,NMAX)
   30 FORMAT(3(1X,I4,2F9.3))
      DO 40 I=1,NMAX
      WTEMPN(I)=WTEMP(I)-WTEMP(1)
   40 CONTINUE
C
C  CALCULATE A AND B FOR ALL TIME STEPS
      DO 50 I=2,NMAX
      IM=I-1
      A(I)=WTEMPN(IM)-TIME(IM)*(WTEMPN(I)-WTEMPN(IM))
     1/(TIME(I)-TIME(IM))
      B(I)=(WTEMPN(I)-WTEMPN(IM))/(TIME(I)-TIME(IM))
   50 CONTINUE
C
C  CALCULATE HEAT FLUX FOR FIRST TIME STEPS
      Q(1)=0.0
      Q(2)=CONS*(WTEMPN(2)/(TIME(2)**0.5)+B(2)*(TIME(2)-
     1TIME(1))**0.5)
C
C  CALCULATE HEAT FLUX FOR REMAINING TIME STEPS
```

Figure G-2: Continued

```
      SUM=0.0
      DO 70 M=1,NN
      MP=M+1
      SUM=SUM+(WTEMPN(N)-A(MP)-B(MP)*(2.*TIME(N)-TIME(MP)))/
     1((TIME(N)-TIME(MP))**0.5)-(WTEMPN(N)-A(MP)-B(MP)
     2*(2.*TIME(N)-TIME(M)))/((TIME(N)-TIME(M))**0.5)
   70 CONTINUE
      NM=N-1
      SUM=SUM+WTEMPN(N)/(TIME(N)**0.5)+B(N)*(TIME(N)-TIME(NM))**0.5
      Q(N)=SUM*CONS
   60 CONTINUE
      READ(6,33)(K,P(I),X,I=1,NMAX)
C
C  SMOOTH THE CALCULATED HEAT FLUX
C
      DO 130 I=1,NMAX
      QS(I)=Q(I)
  130 CONTINUE
      CALL QSMOOT(TIME,QS,NMAX)
C
C  PRINT AND WRITE RESULTS ON FILE
      WRITE(3,120) RUNID
  120 FORMAT(#1#,#RUN ID#,5X,A9)
      WRITE(3,100)
  100 FORMAT(//5X,#TIME  STEP#,8X,#TIME  MSEC#,8X,#WALL TEMP  K#,
     15X,#PRESSURE  KPA#,5X,#RAW HEAT FLUX  KW/SQM#,5X,
     1#SMOOTHED HEAT FLUX  KW/SQM#//)
      DO 80 I=1,NMAX
      D1=TIME(I)*1000.0
      D2=Q(I)/1000.0
      D3=QS(I)/1000.0
      WRITE(3,90) I,D1,WTEMP(I),P(I),D2,D3
   90 FORMAT(8X,I4,14X,F8.2,12X,F9.3,10X,F9.3,10X,F9.3,8X,F9.3)
      WRITE(4,90)I,D1,D2,D3
   80 CONTINUE
      GO TO 1
  110 CONTINUE
      STOP
      END
      SUBROUTINE QSMOOT(X,Y,NTOTAL)
      DIMENSION X(2000),Y(2000),LPARAM(4),WORK(520)
      NDERIV=0
      WEIGHT=1.0
      DO 10 I=1,4
      LPARAM(I)=0
   10 CONTINUE
      LPARAM(1)=99
      CALL PSMTH1(X,Y,NTOTAL,NDERIV,WEIGHT,LPARAM,WORK,YP)
      RETURN
      END
```

Appendix H

Comparison of Heat Flux for Macor and Metal Walls

The temperature gauges used in this experimental study (see Chapter 3 for a detailed description) are made from a glass ceramic known as Macor. Thus the heat flux calculation from the measured wall temperature is actually the heat flux into a Macor wall. It would be useful then to know how the heat flux into a metal wall would compare to that into a Macor wall. To make this comparison, the finite difference formulation for the wall heat transfer problem as described in Appendix C was used. With that computer program, the heat flux between air and a cast iron wall was calculated (See Figure 2.3-2). With the same program, the heat flux between air and a Macor wall was also determined. These two are shown in Figure H-1. The comparison is found to be very good. The peak heat flux shows a difference of approximately 2%.

This good comparison is primarily explained by the thermal and physical properties of air compared to Macor or cast iron. More specifically, consider a simplified problem consisting of two thermally semi-infinite bodies in contact. One body is a solid, either Macor or cast iron, and the other is air for which only conduction heat transfer will be considered. Initially, the temperature of the Macor or cast iron is a constant taken as reference, and the temperature of the air above the reference is T_h. To solve this problem the temperature at the boundary is assumed to be a constant, call it T_m, with this assumption to be verified after a solution has been obtained.

Figure H-1: Comparison of wall heat flux into a cast iron wall and into a Macor wall.

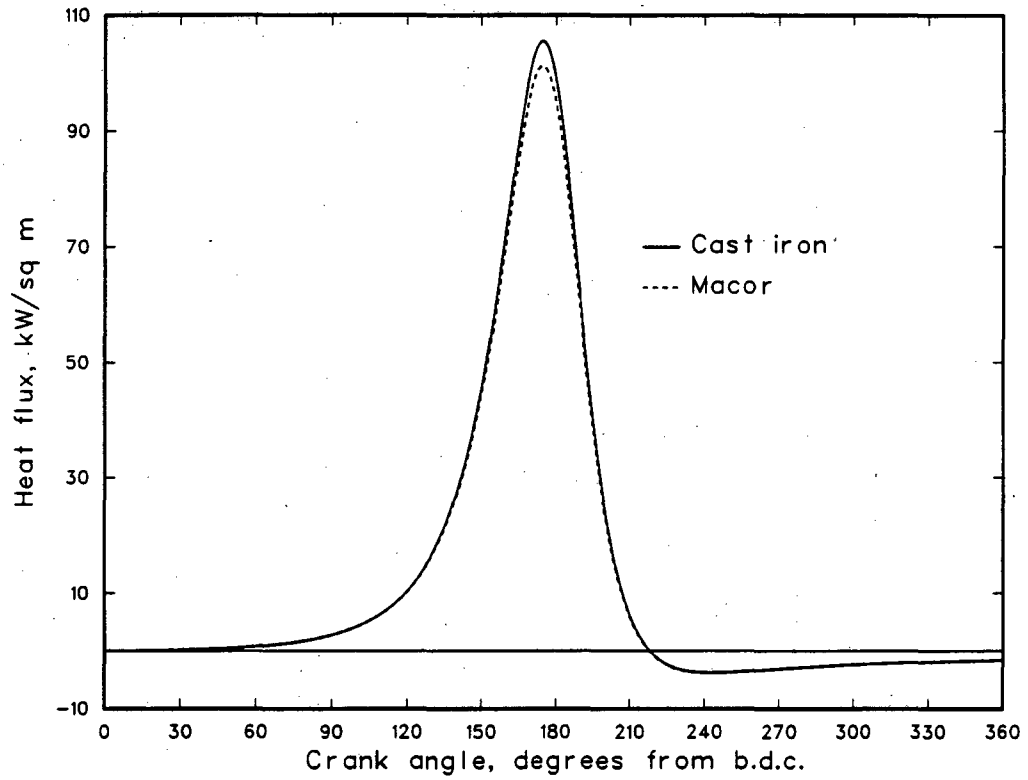

The problem to solve for the air is:

$$\frac{\partial T_a}{\partial t} = \alpha_a \frac{\partial^2 T_a}{\partial x_a^2} \qquad \text{(H-1)}$$

$$T_a\ (t = 0) = T_h$$

$$T_a\ (x_a = 0) = T_m$$

The initial temperature here is taken as reference, giving a solution:

$$T_a = T_h + (T_m - T_h)\ \text{erfc}\ \frac{x_a}{2\sqrt{\alpha_a t}} \qquad \text{(H-2)}$$

For the solid side, we have

$$\frac{\partial T_s}{\partial t} = \alpha_s \frac{\partial^2 T_s}{\partial x_s^2} \qquad \text{(H-3)}$$

$$T_s\ (t = 0) = 0$$

$$T_s\ (x = 0) = T_m$$

The solution is:

$$T_s = T_m\ \text{erfc}\ \frac{x_s}{2\sqrt{\alpha_s t}} \qquad \text{(H-4)}$$

From these solutions it is easy to verify that the temperatures at the boundary are equal. From the condition of equal heat flux at the boundary, the boundary temperature can be obtained:

$$T_m = \frac{\sqrt{k_a \rho_a c_a}\ T_h}{\sqrt{k_s\ \rho_s c_s} - \sqrt{k_a \rho_a c_a}} \qquad \text{(H-5)}$$

The properties of air, Macor, and cast iron give the following values for the constant $\sqrt{k\rho c}$:

Air	5.6 $J/m^2\ K\ \sqrt{s}$
Macor	1394.7 $J/m^2\ K\ \sqrt{s}$
Cast Iron	12222.4 $J/m^2\ K\ \sqrt{s}$

Thus it is appropriate for both Macor and cast iron to make the following simplification.

$$T_m \simeq \frac{\sqrt{k_a \rho_a c_a}}{\sqrt{k_s \rho_s c_s}}\ T_h \qquad \text{(H-6)}$$

The heat flux at the boundary from each of these solutions is:

$$q_a = \frac{\sqrt{k_a \rho_a c_a}}{\sqrt{\pi t}}\ (T_m - T_h) \qquad \text{(H-7)}$$

$$q_s = \frac{\sqrt{k_s \rho_s c_s}}{\sqrt{\pi t}} T_m \qquad \text{(H-8)}$$

Equation (H-6) is now substituted into the heat flux equations and a further simplification is made in noting that $T_m << T_h$:

$$q_a = \frac{-\sqrt{k_a \rho_a c_a}}{\sqrt{\pi t}} T_h \qquad \text{(H-9)}$$

$$q_s = \frac{\sqrt{k_a \rho_a c_a}}{\sqrt{\pi t}} T_h \qquad \text{(H-10)}$$

Thus since the value for the constant $\sqrt{k\rho c}$ is much smaller for air than for either solid, the heat flux is essentially independent of the properties of the solid. The experimental wall heat flux results in this study are therefore essentially the same as would be measured on a metal wall.

Appendix I

Experimental Results

In Chapters 5 and 6, representative measurements and results were presented. The remaining results are presented in this appendix to provide a complete record of the data from this study.

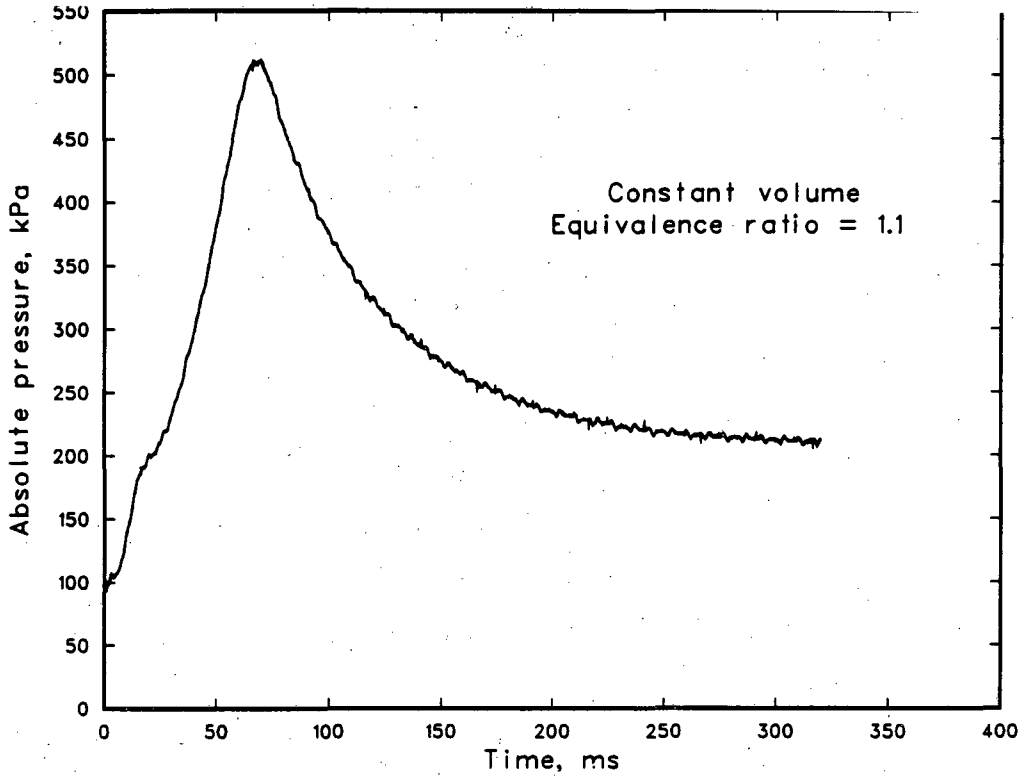

Figure I-1: Absolute pressure variation with time; constant volume combustion; equivalence ratio 1.1.

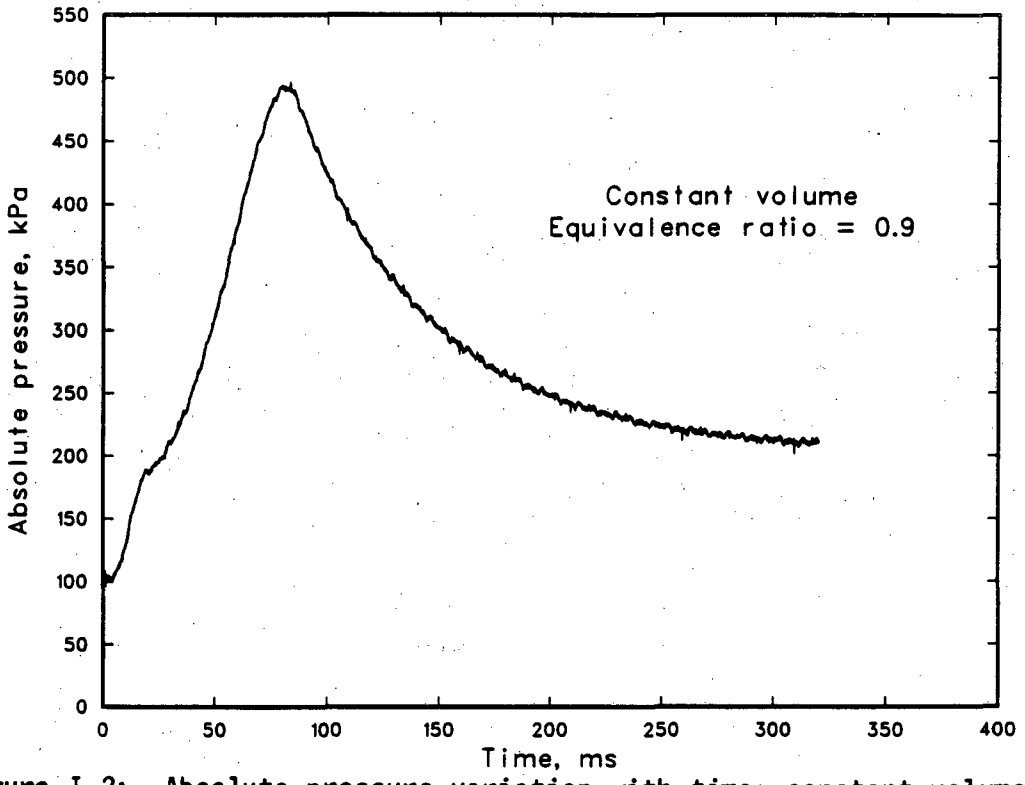

Figure I-2: Absolute pressure variation with time; constant volume combustion; equivalence ratio 0.9.

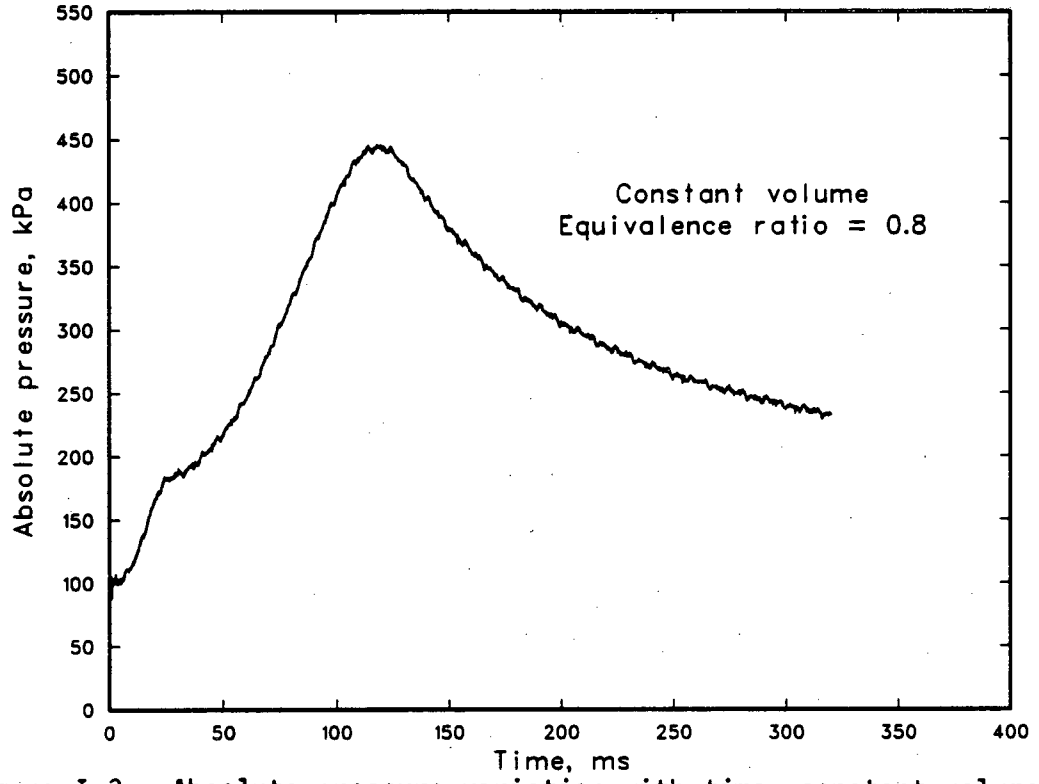

Figure I-3: Absolute pressure variation with time; constant volume combustion; equivalence ratio 0.8.

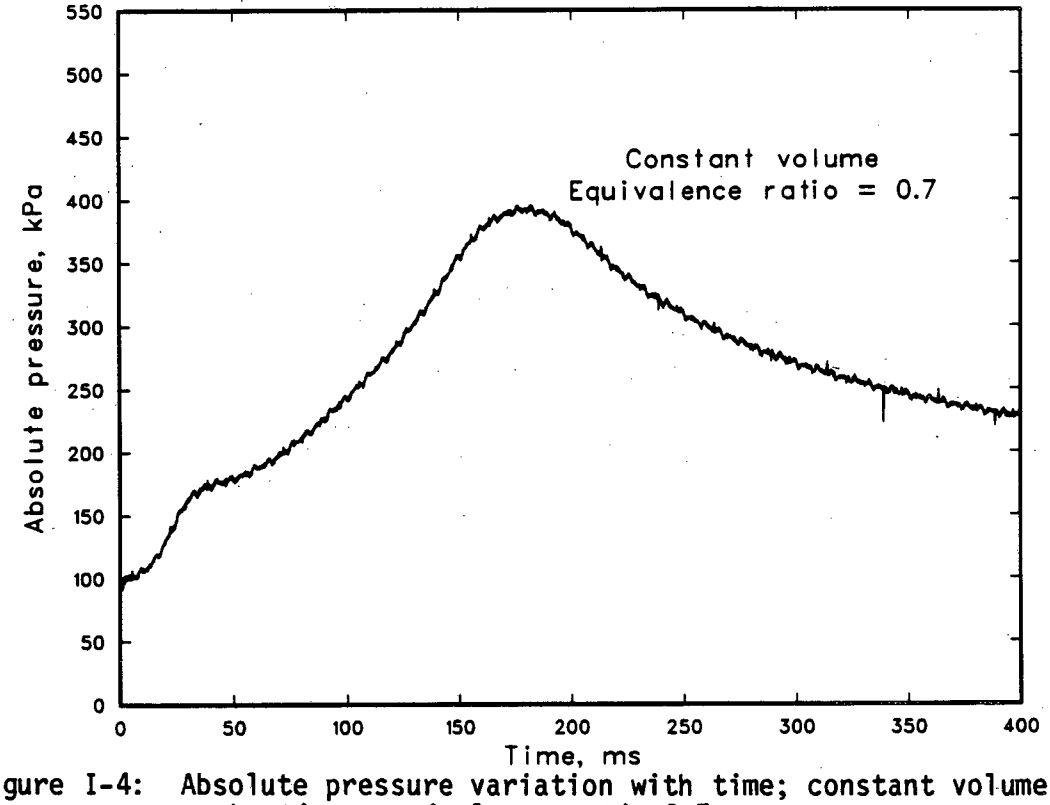

Figure I-4: Absolute pressure variation with time; constant volume combustion; equivalence ratio 0.7.

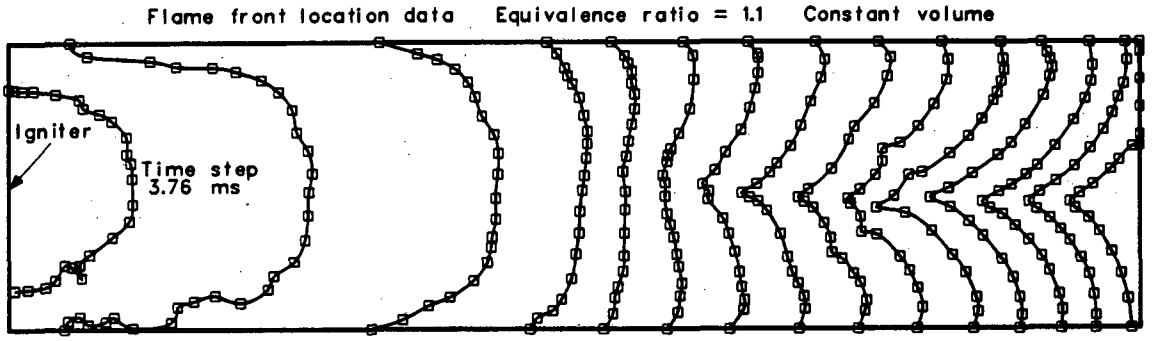

Figure I-5: Flame front location from schlieren movies for time steps of 3.76 ms starting at ignition; total elapsed time to last location shown is 56.4 ms; constant volume combustion; equivalence ratio 1.1.

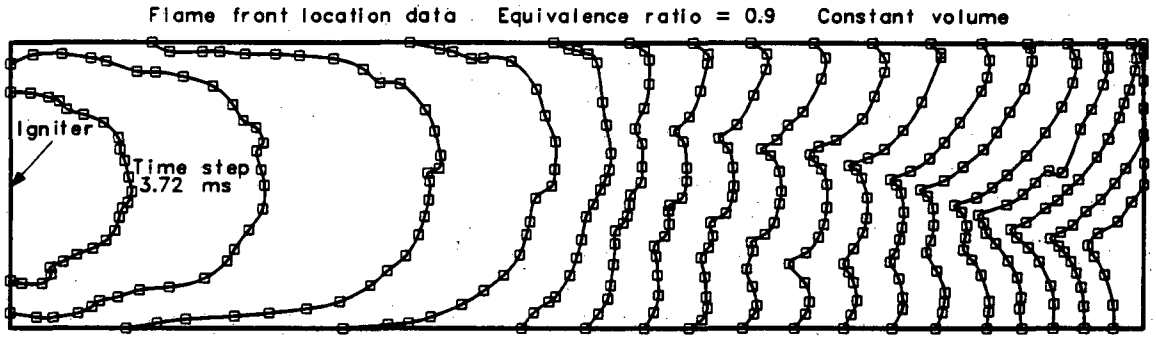

Figure I-6: Flame front location from schlieren movies for time steps of 3.72 ms starting at ignition; total elapsed time to last location shown is 66.9 ms; constant volume combustion; equivalence ratio 0.9.

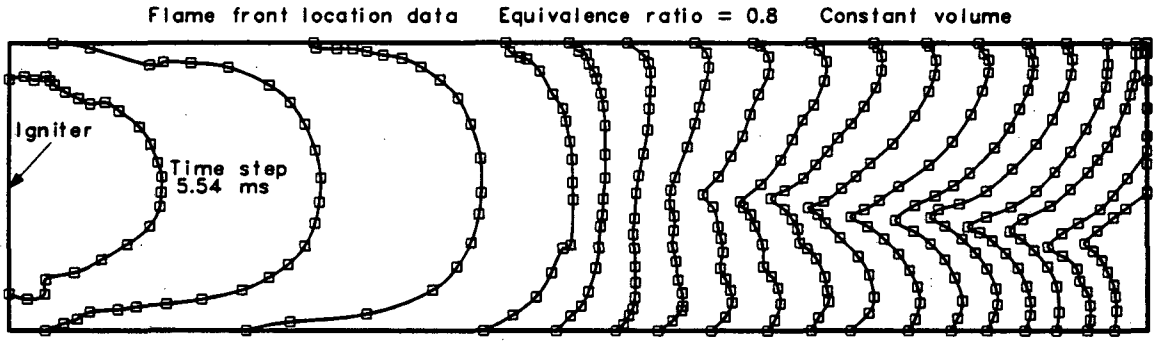

Figure I-7: Flame front location from schlieren movies for time steps of 5.54 ms starting at ignition; total elapsed time to last location shown is 99.7 ms; constant volume combustion; equivalence ratio 0.8.

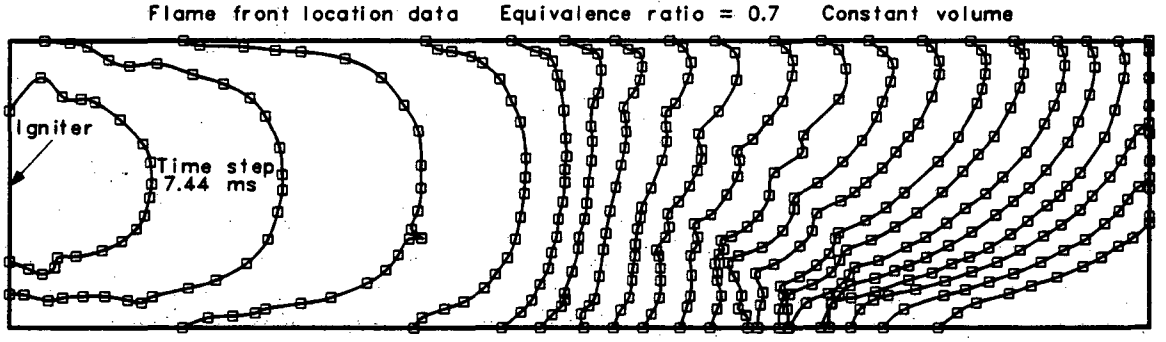

Figure I-8: Flame front location from schlieren movies for time steps of 7.44 ms starting at ignition; total elapsed time to last location shown is 156.2 ms; constant volume combustion; equivalence ratio 0.7.

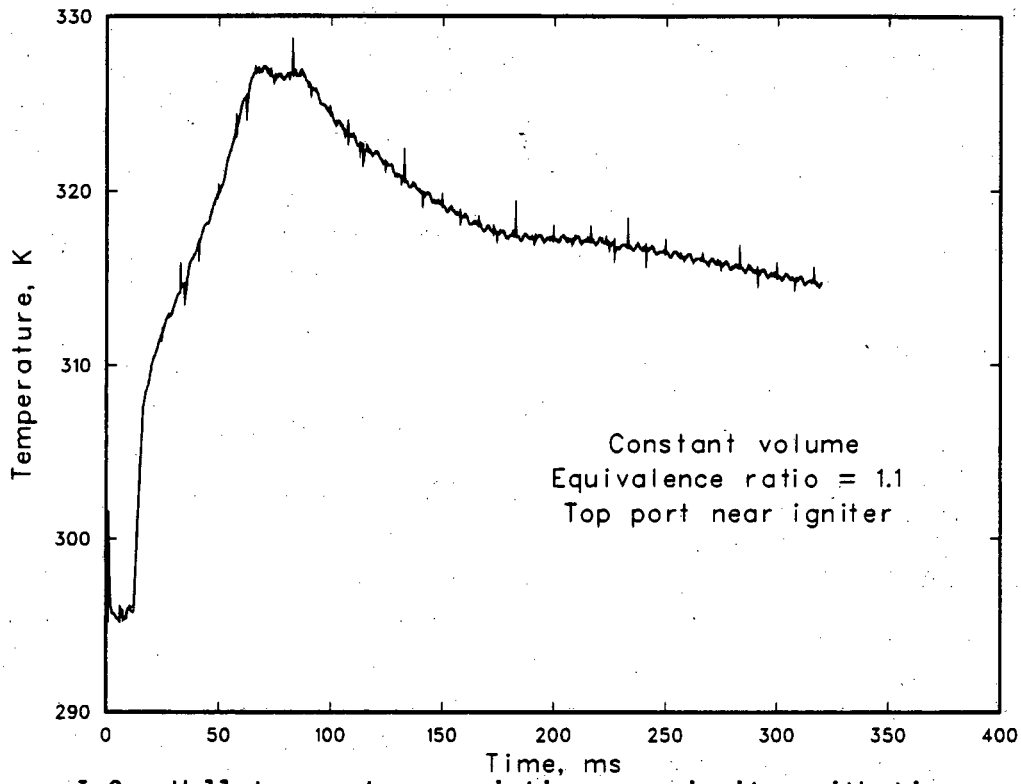

Figure I-9: Wall temperature variation near igniter with time; constant volume combustion; equivalence ratio 1.1; without voltage follower.

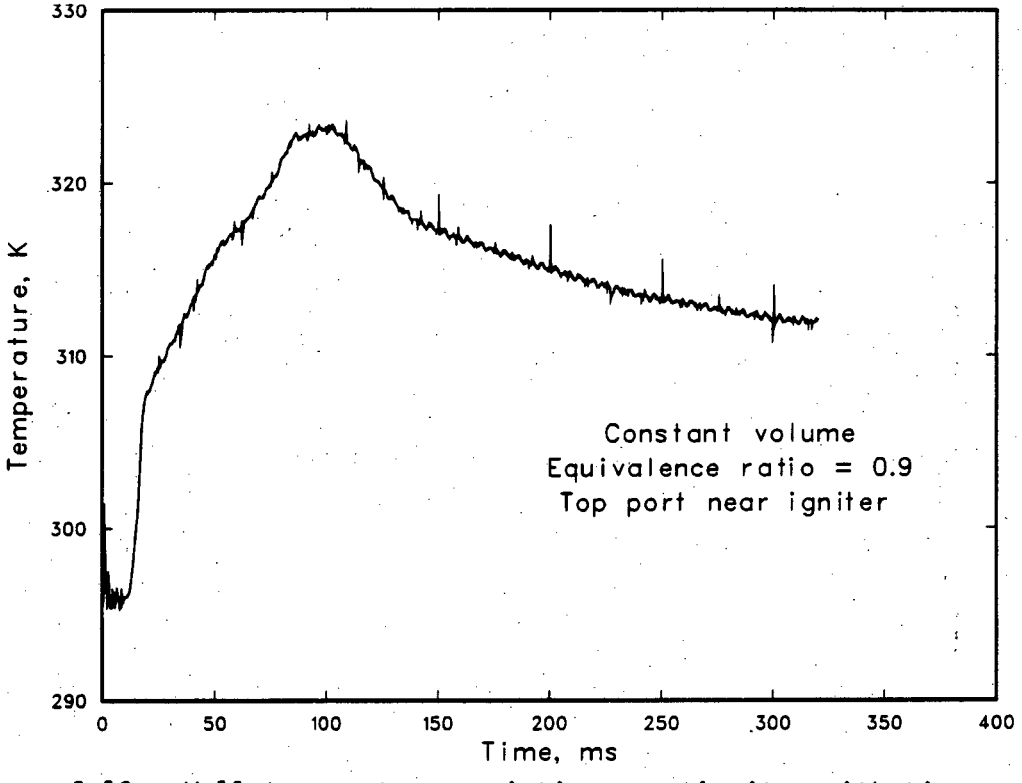

Figure I-10: Wall temperature variation near igniter with time; constant volume combustion; equivalence ratio 0.9; without voltage follower.

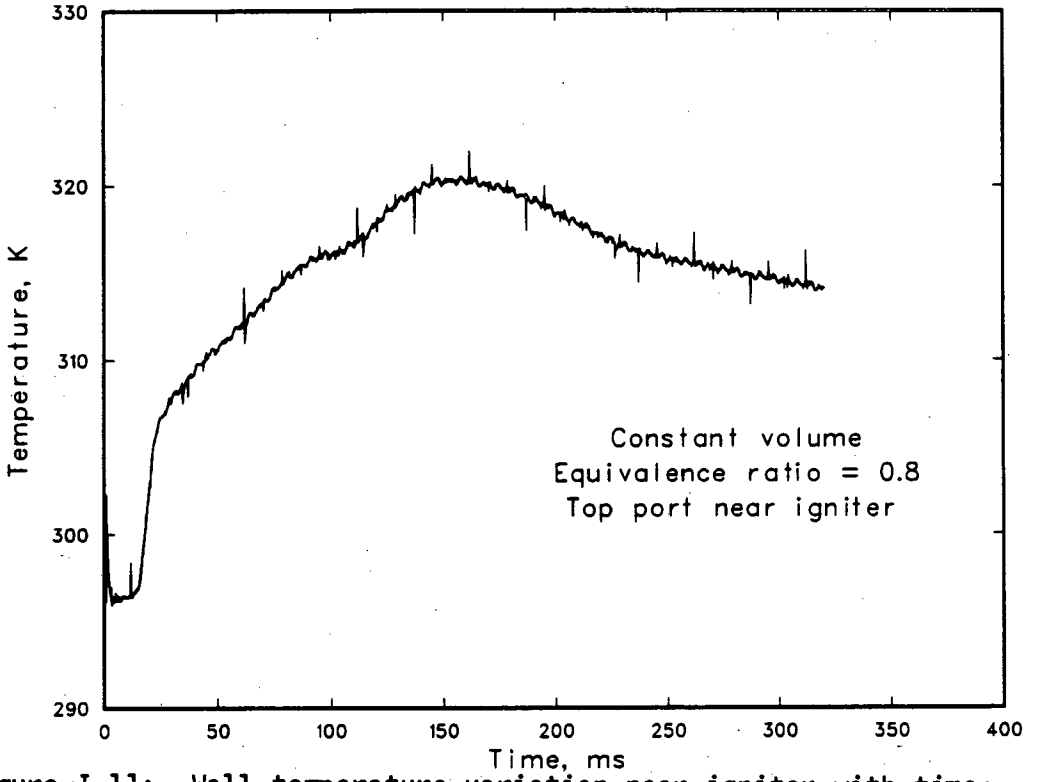

Figure I-11: Wall temperature variation near igniter with time; constant volume combustion; equivalence ratio 0.8; without voltage follower.

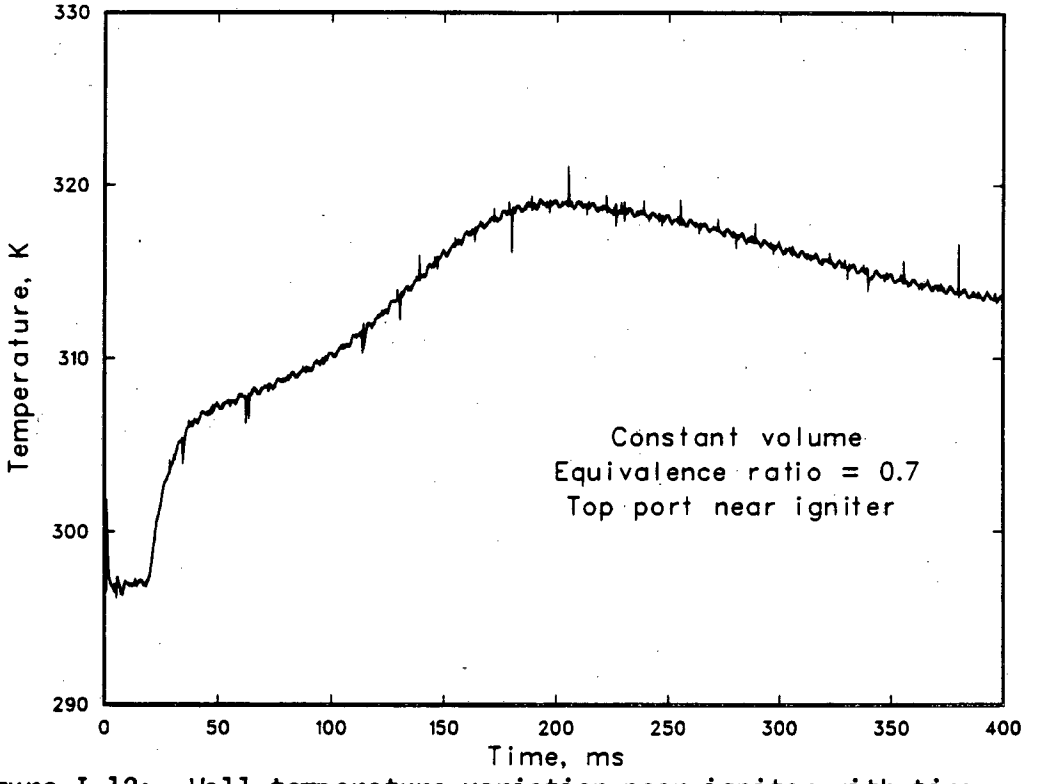

Figure I-12: Wall temperature variation near igniter with time; constant volume combustion; equivalence ratio 0.7; without voltage follower.

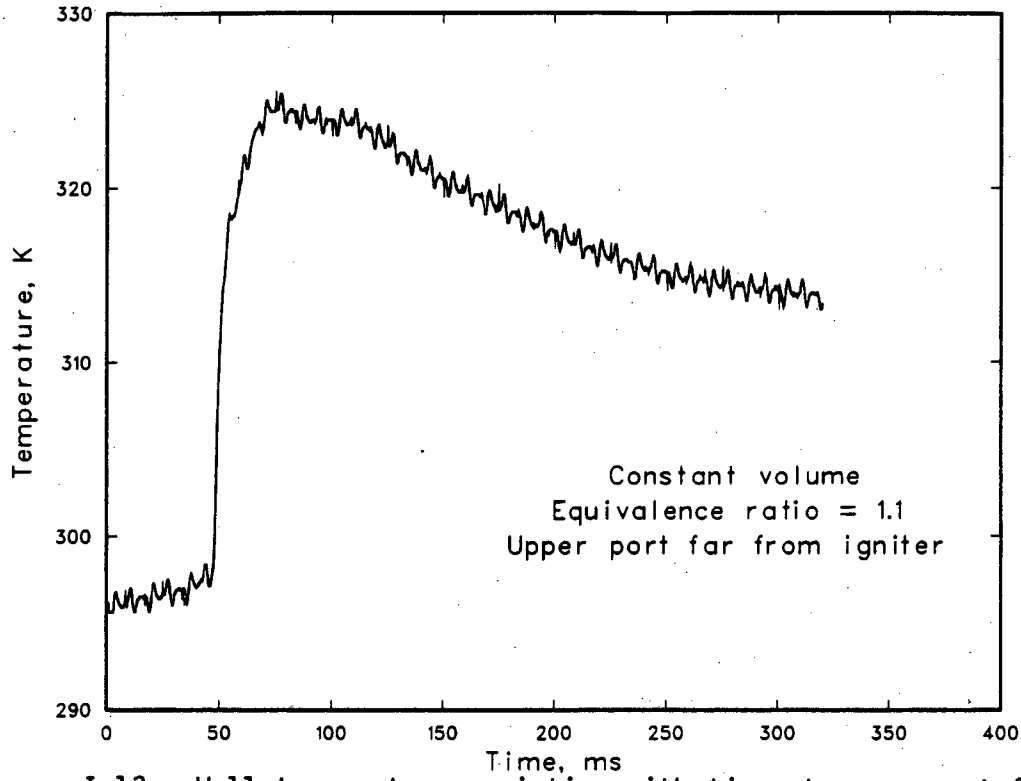

Figure I-13: Wall temperature variation with time at upper part far from igniter; constant volume combustion; equivalence ratio 1.1.

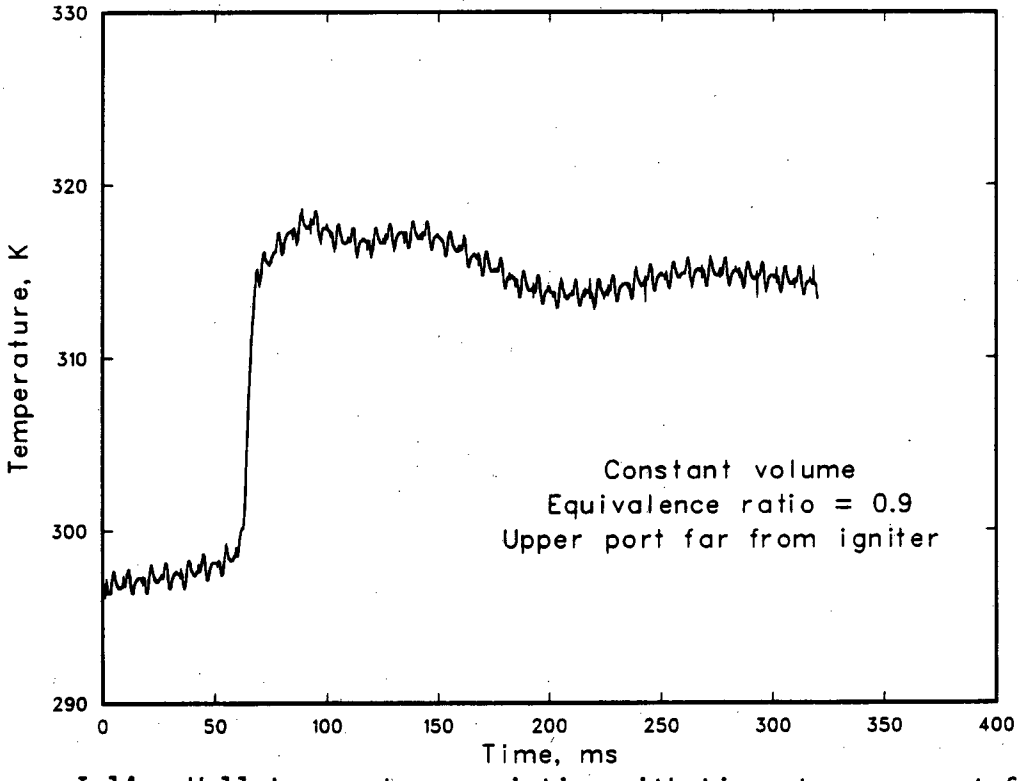

Figure I-14: Wall temperature variation with time at upper port far from igniter; constant volume combustion; equivalence ratio 0.9.

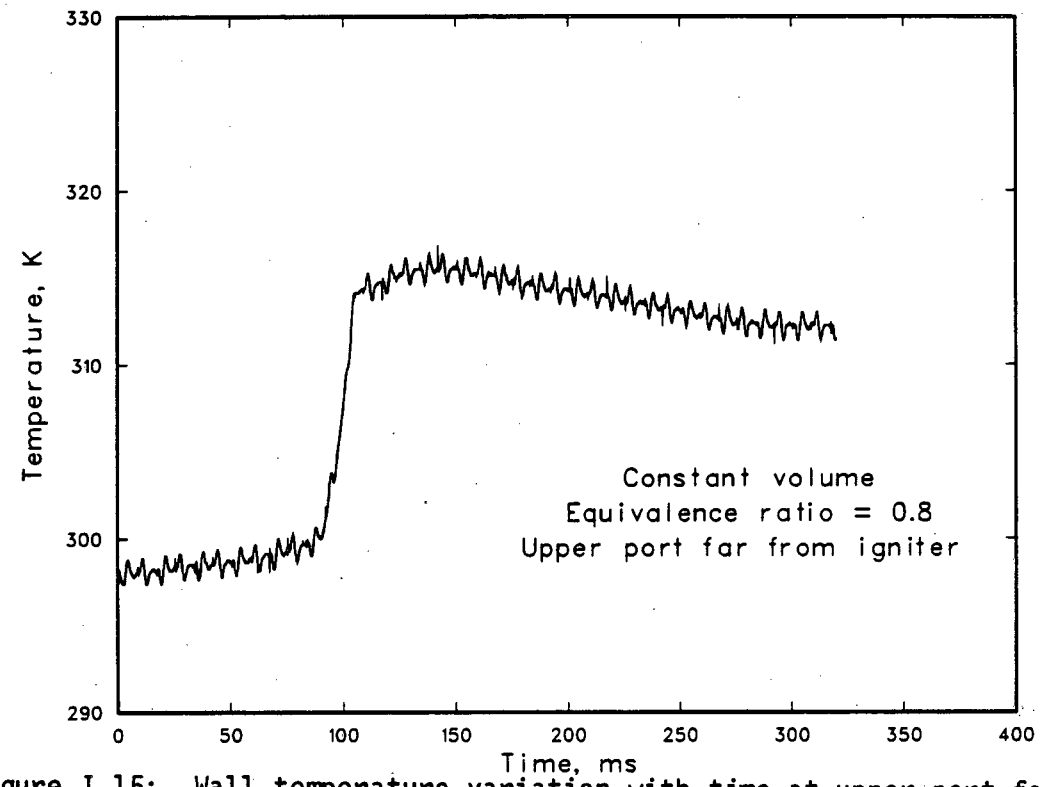

Figure I-15: Wall temperature variation with time at upper port far from igniter; constant volume combustion; equivalence ratio 0.8.

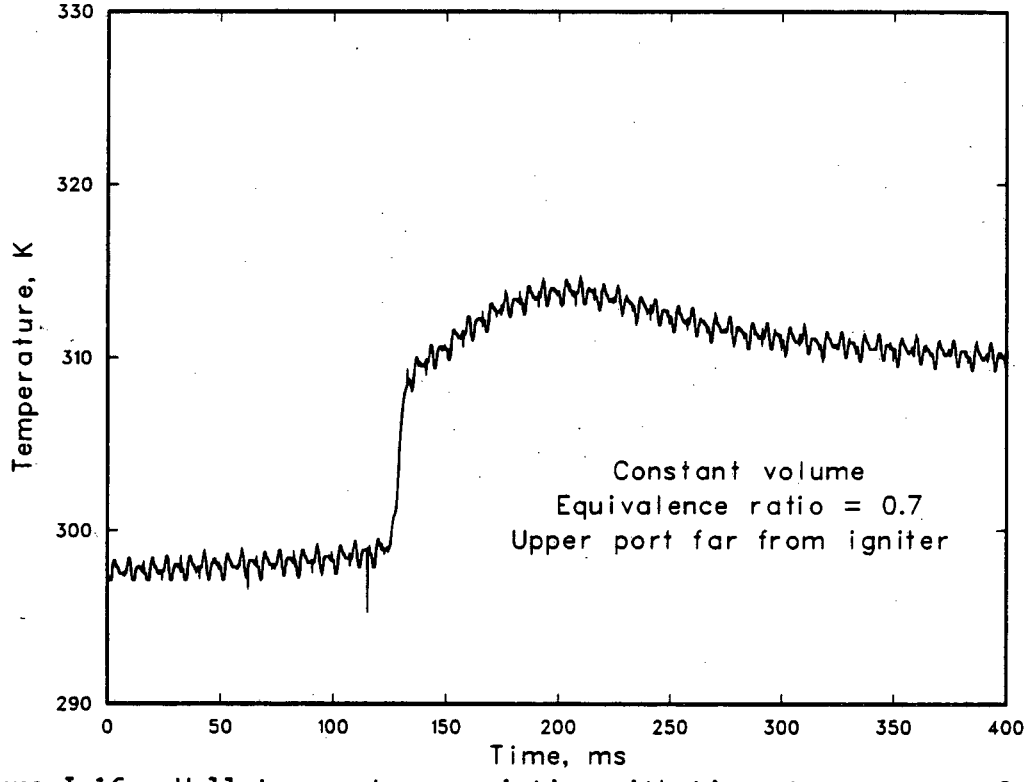

Figure I-16: Wall temperature variation with time at upper port far from igniter; constant volume combustion; equivalence ratio 0.7.

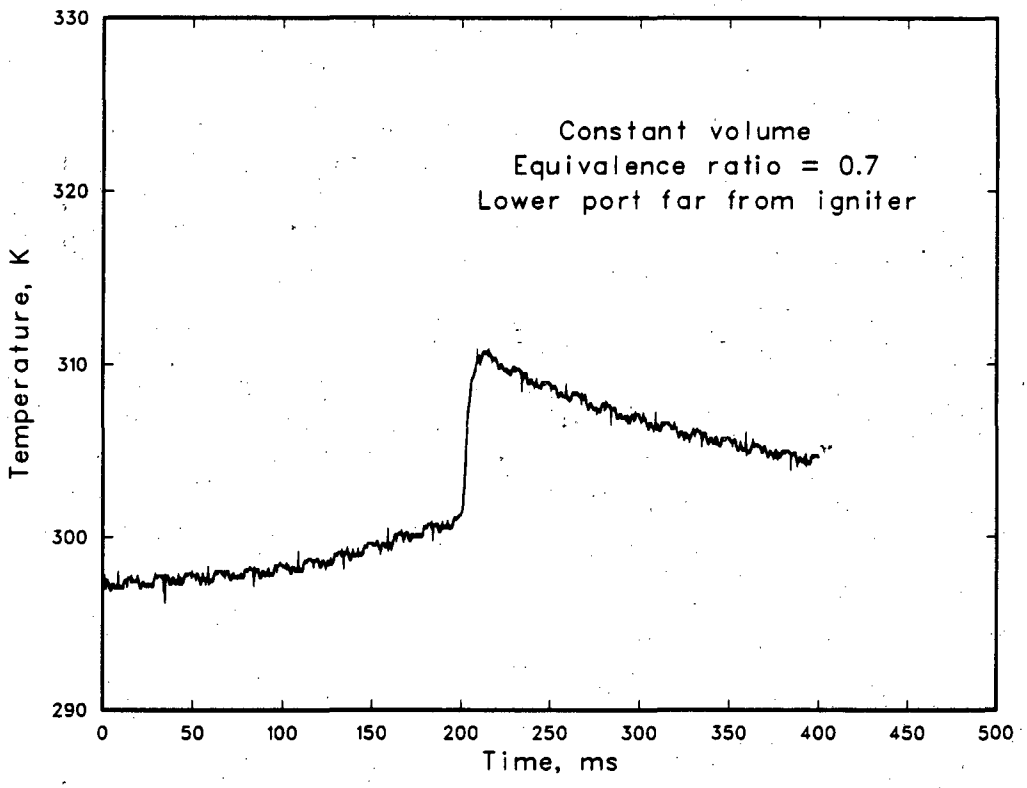

Figure I-17: Wall temperature variation with time at lower port far from igniter; constant volume combustion; equivalence ratio 0.7.

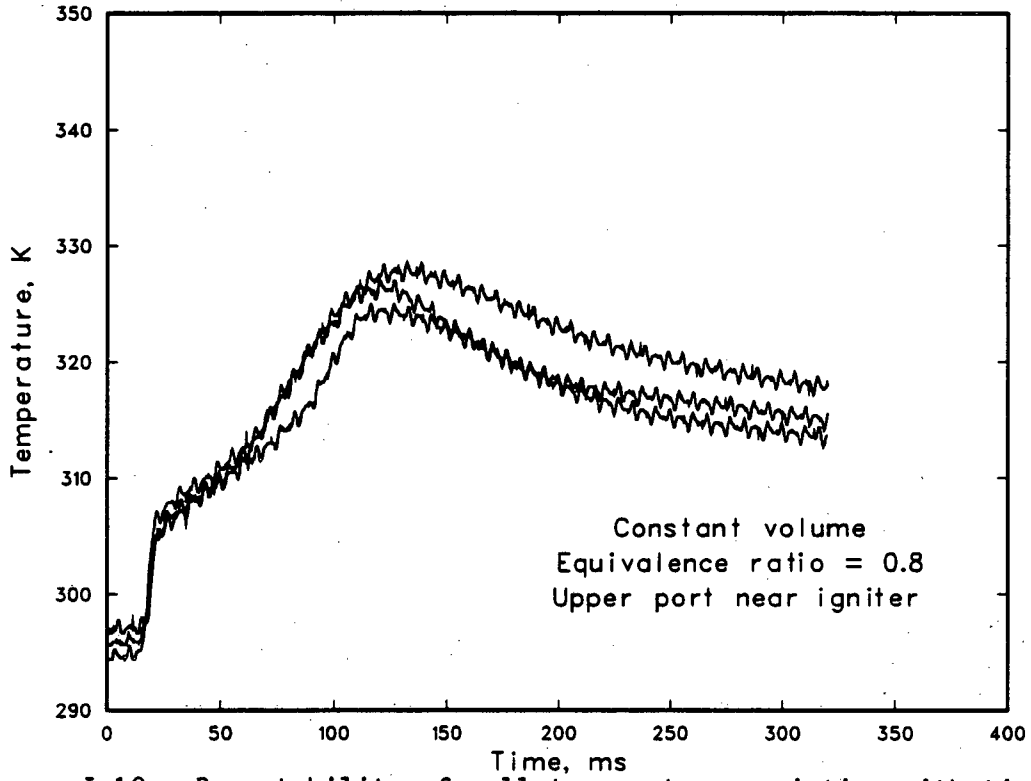

Figure I-18: Repeatability of wall temperature variation with time; three measurements for identical conditions.

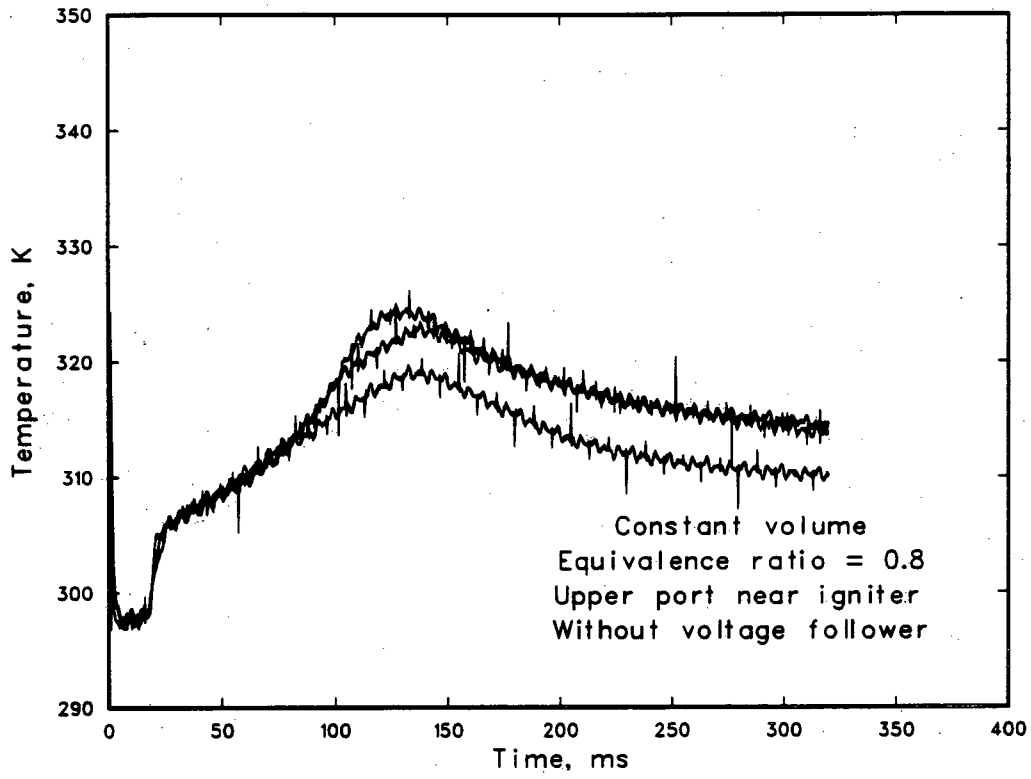

Figure I-19: Repeatability of wall temperature variation with time without voltage follower; three measurements for identical conditions.

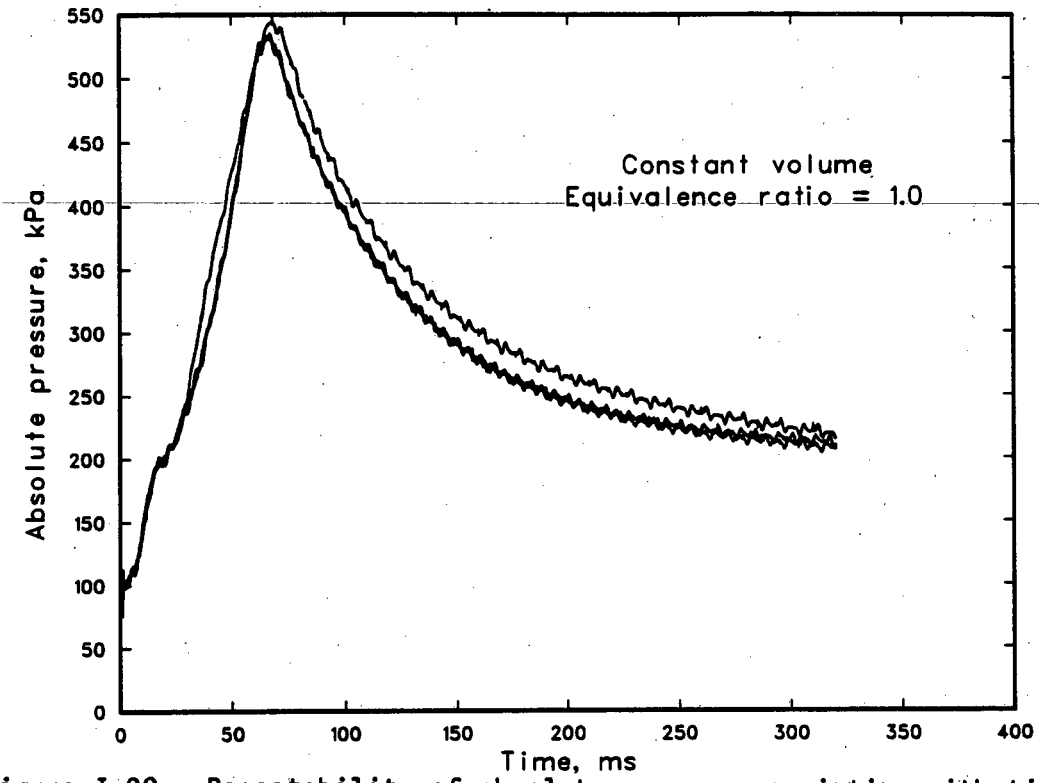

Figure I-20: Repeatability of absolute pressure variation with time; three measurements for identical conditions; equivalence ratio 1.0

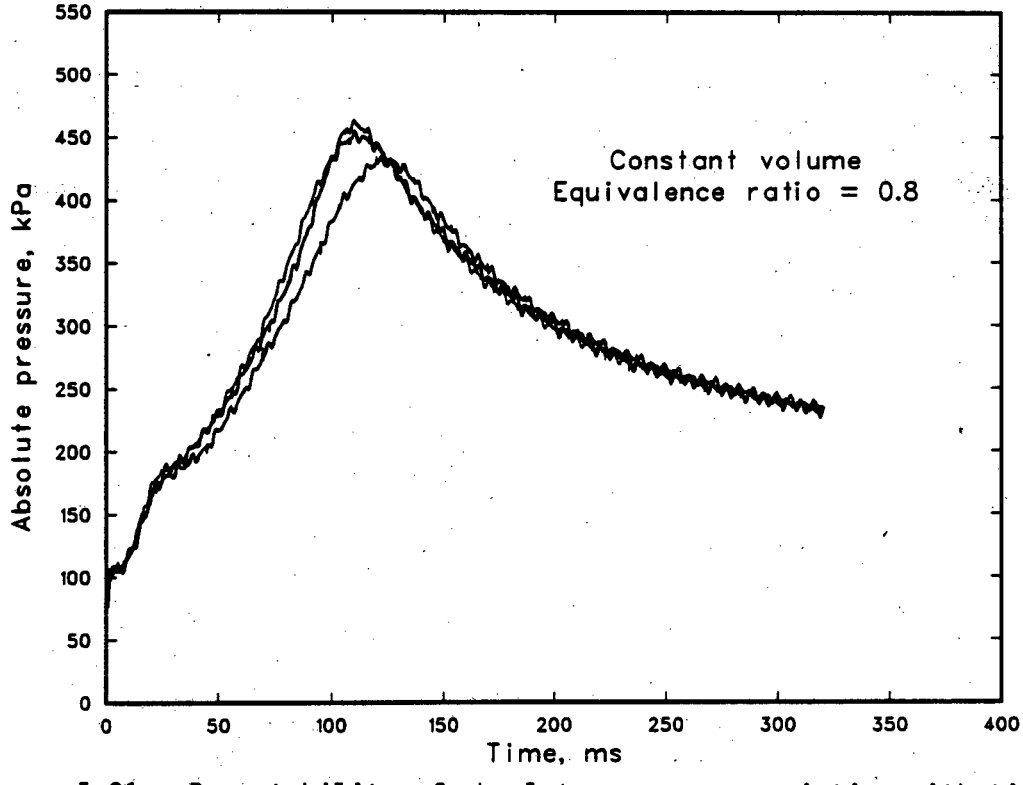

Figure I-21: Repeatability of absolute pressure variation with time; three measurements for identical conditions; equivalence ratio 0.8.

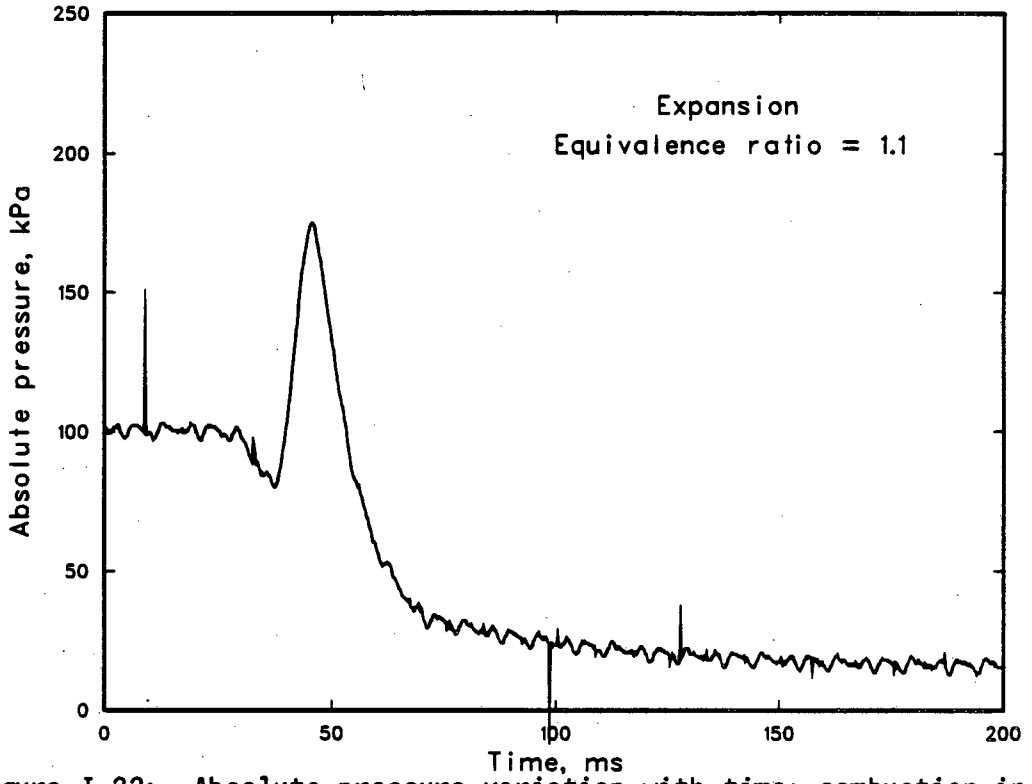

Figure I-22: Absolute pressure variation with time; combustion in an expanding volume; equivalence ratio 1.1.

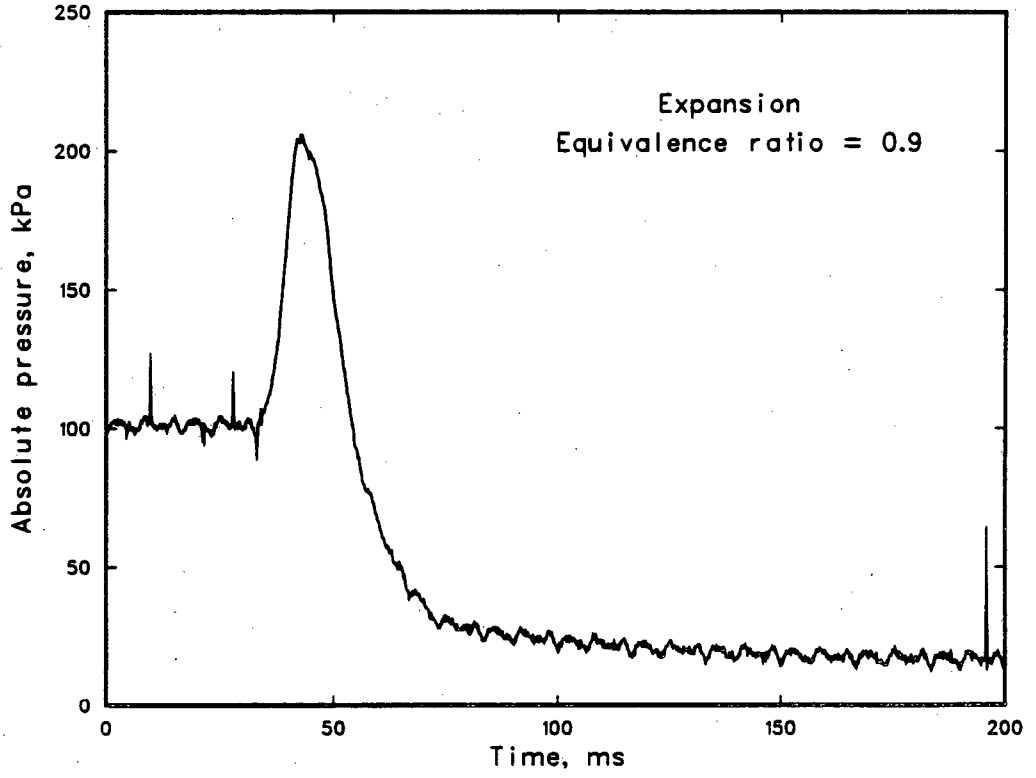

Figure I-23: Absolute pressure variation with time; combustion in an expanding volume; equivalence ratio 0.9.

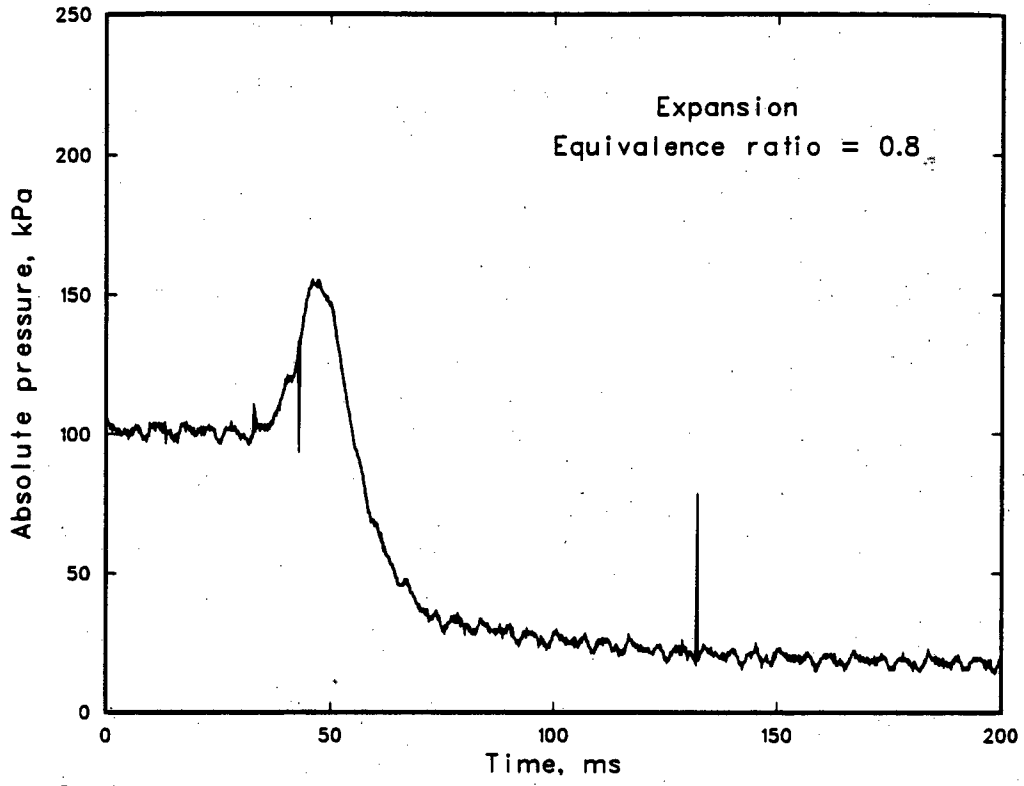

Figure I-24: Absolute pressure variation with time; combustion in an expanding volume; equivalence ratio 0.8.

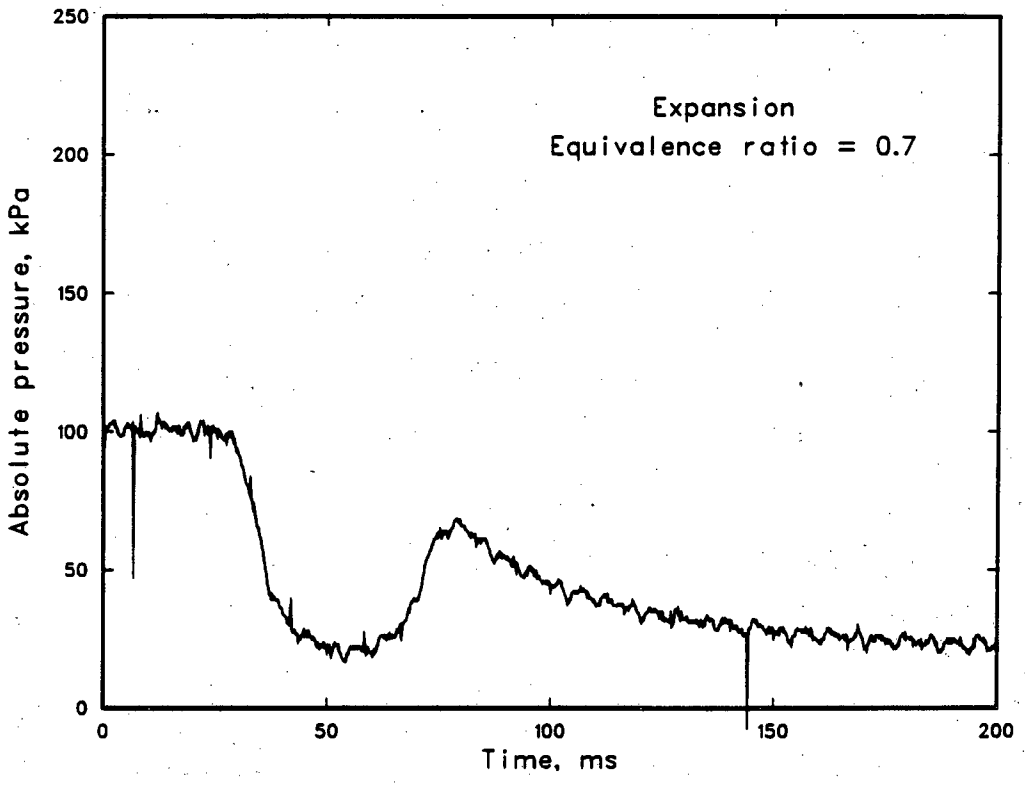

Figure I-25: Absolute pressure variation with time; combustion in an expanding volume; equivalence ratio 0.7.

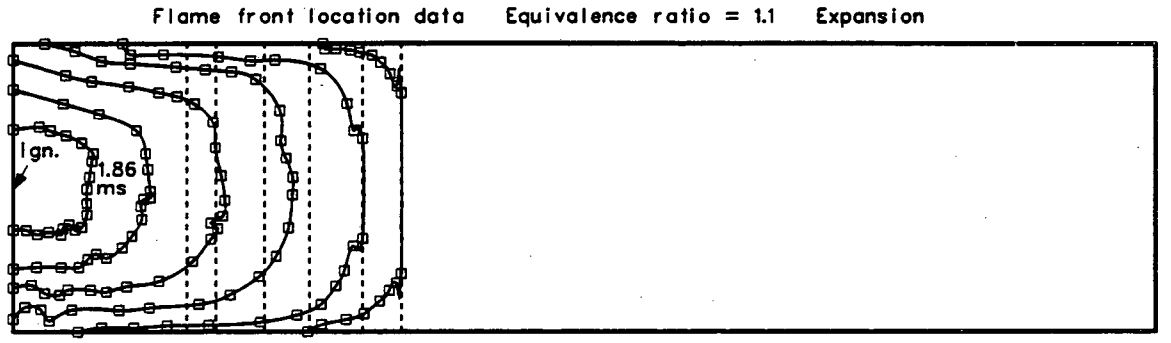

Figure I-26: Flame front location and piston face location from schlieren movies for time teps of 1.86 ms starting at ignition; combustion in an expanding volume; equivalence ratio 1.1.

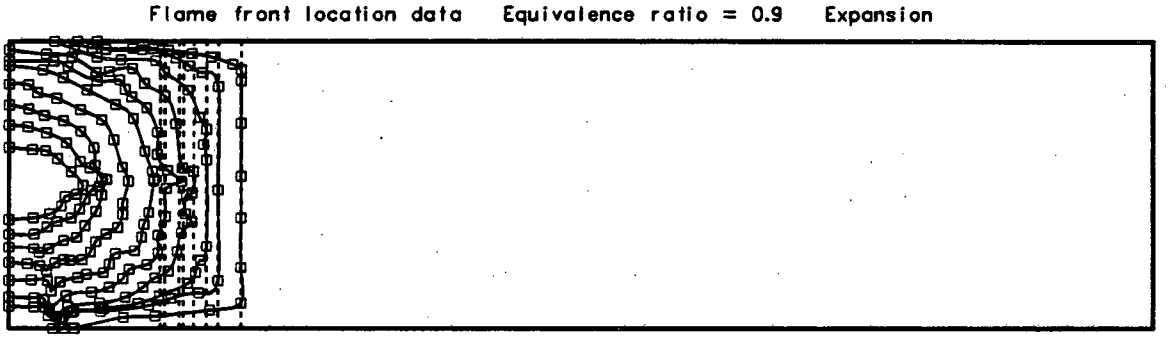

Figure I-27: Flame front location and piston face loation from schlieren movies for time steps of 1.86 ms starting at ignition; combustion in an expanding volume; equivalence ratio 0.9

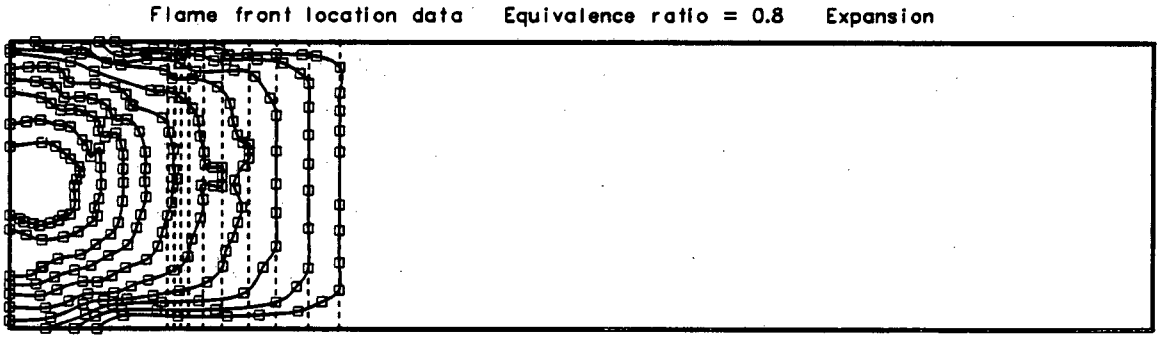

Figure I-28: Flame front location and piston face location from schlieren movies for time steps of 1.1 ms starting at igniton; combustion in an expanding volume; equivalence ratio 0.8

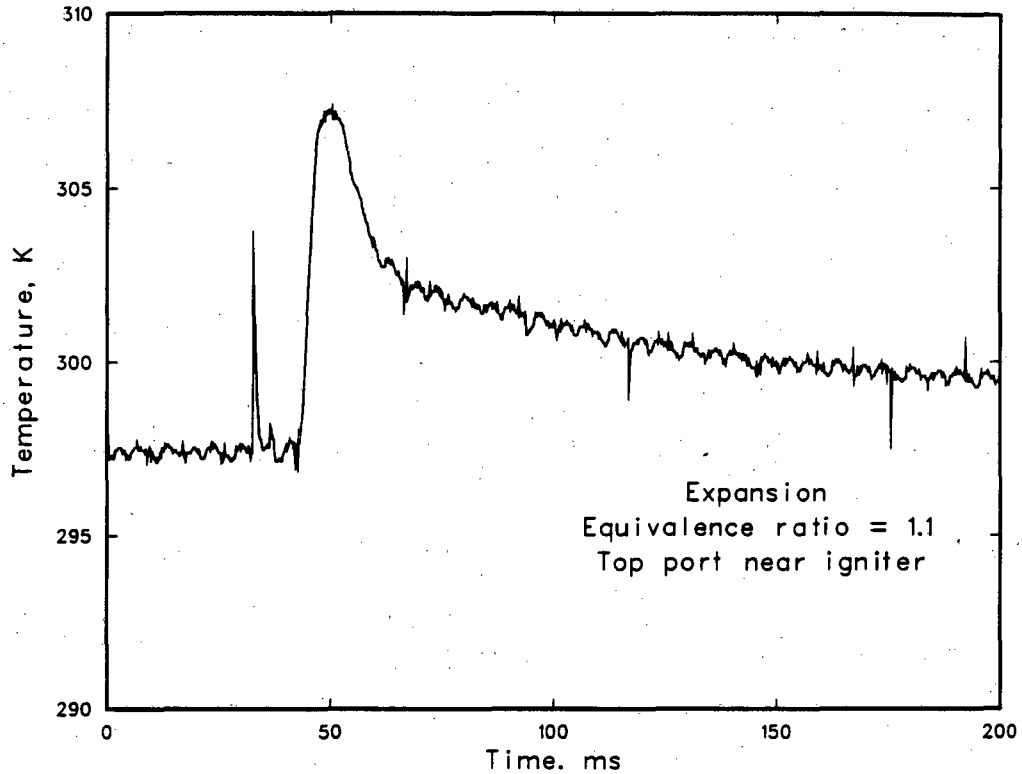

Figure I-29: Wall temperature variation with time; combustion in an expanding volume; equivalence ratio 1.1; without voltage follower.

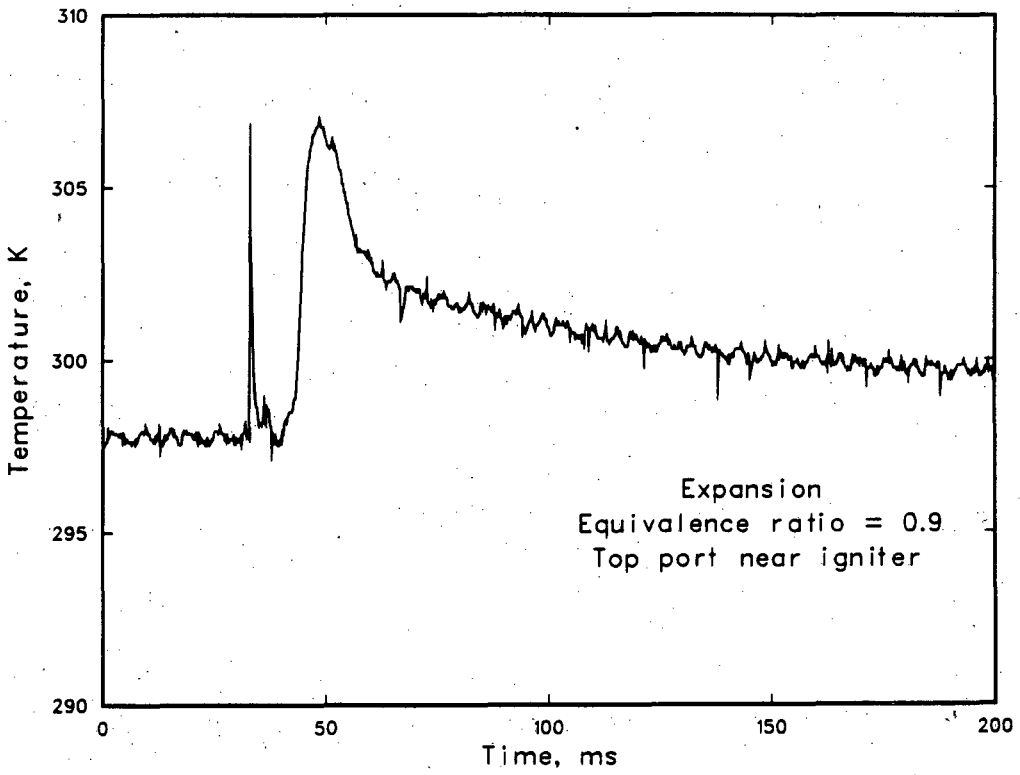

Figure I-30: Wall temperature variation with time; combustion in an expanding volume; equivalence ratio 0.9; without voltage follower.

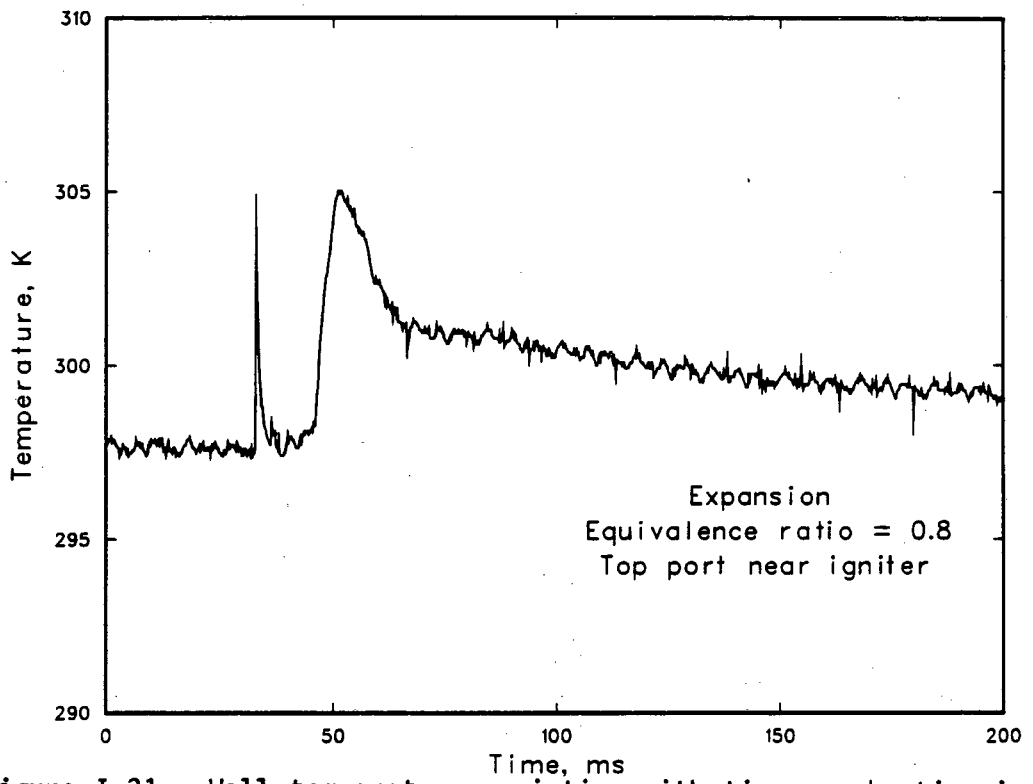

Figure I-31: Wall temperature variation with time; combustion in an expanding volume; equivalence ratio 0.8; without voltage follower.

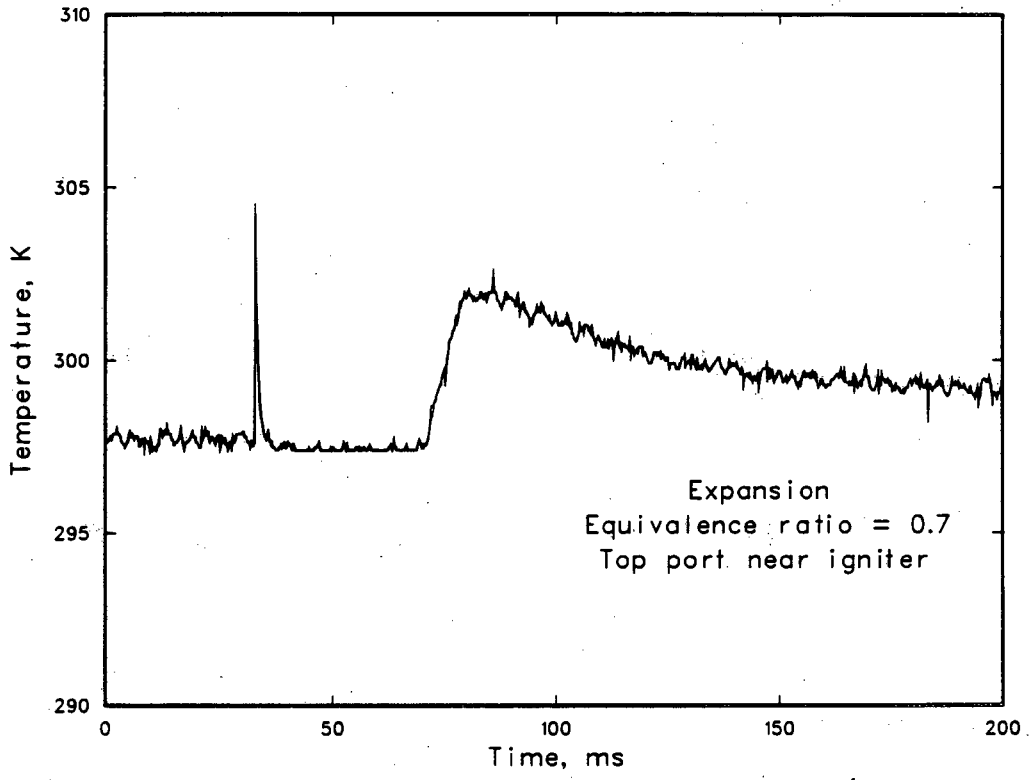

Figure I-32: Wall temperature variation with time; combustion in an expanding volume; equivalence ratio 0.7; without voltage follower.

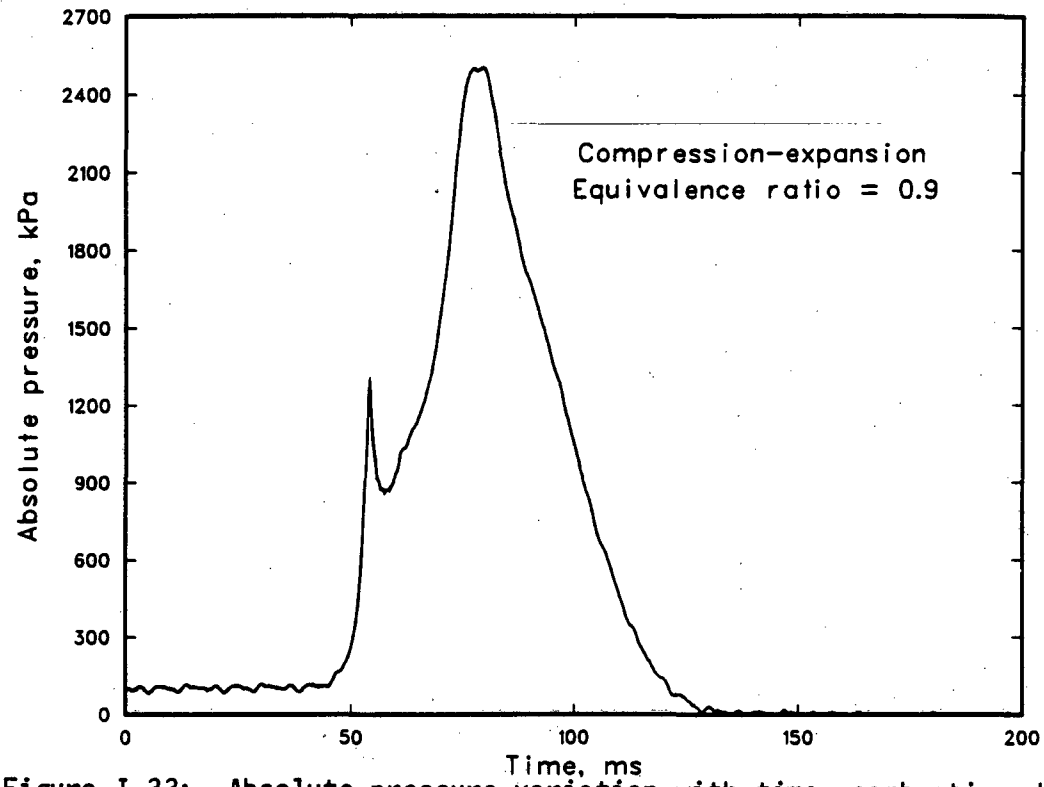

Figure I-33: Absolute pressure variation with time; combustion during compression-expansion equivalence ratio 0.9.

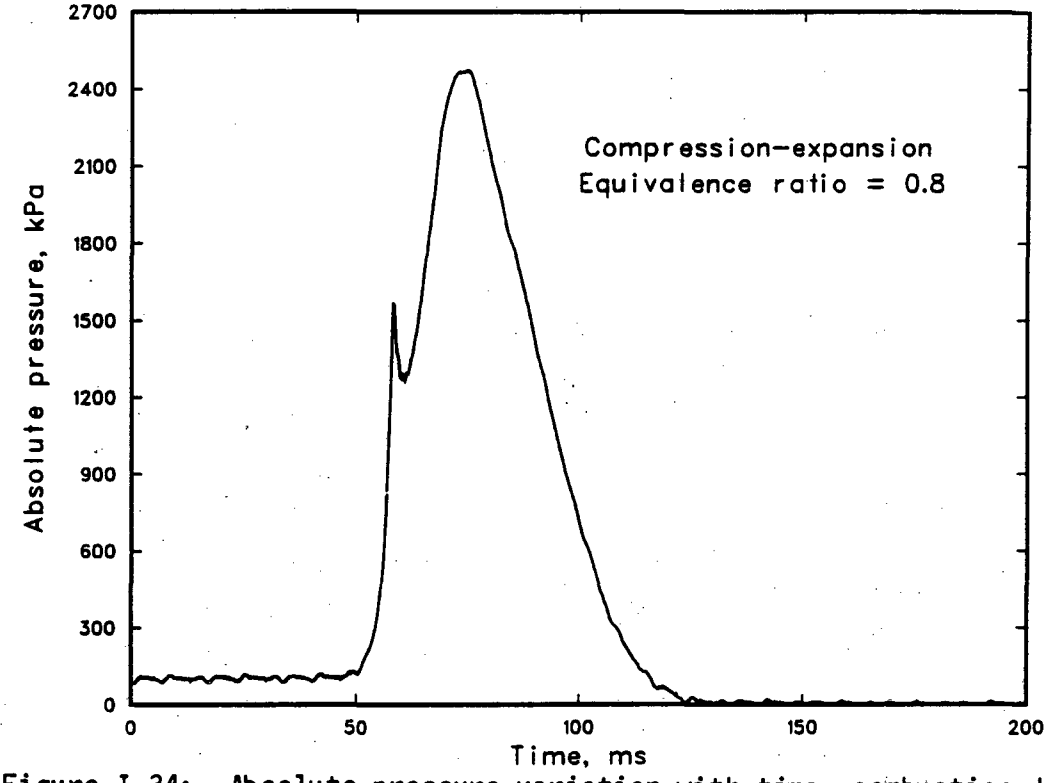

Figure I-34: Absolute pressure variation with time; combustion during compression-expansion; equivalence ratio 0.8.

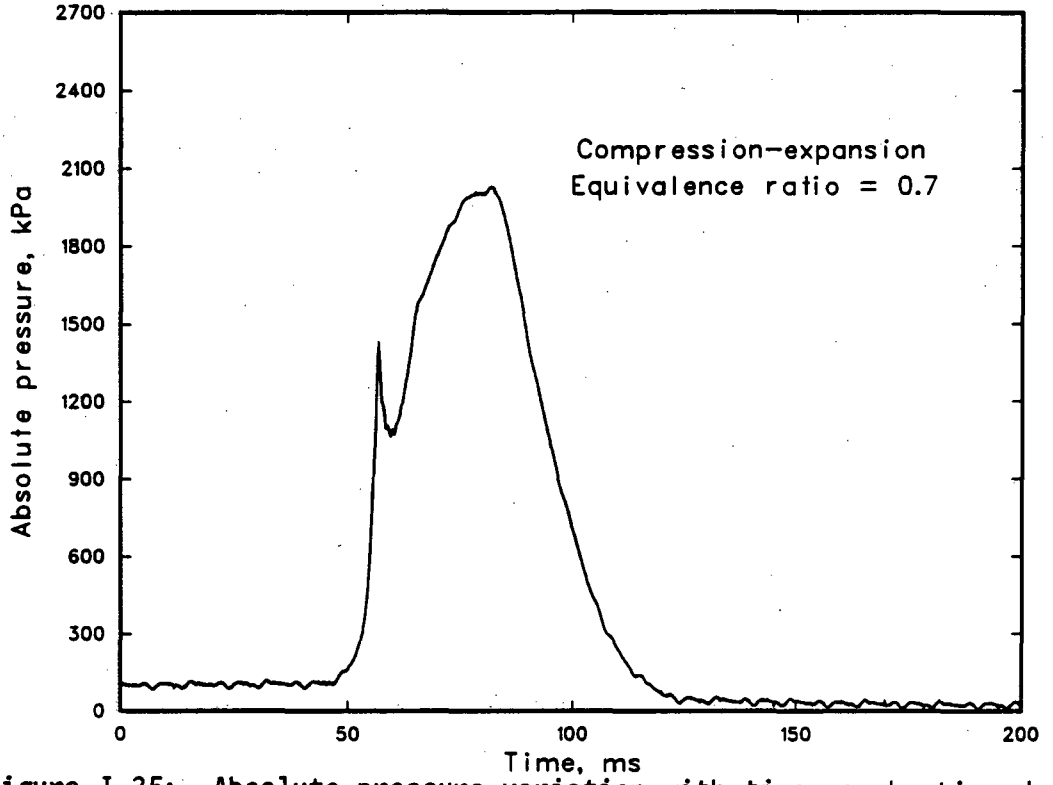

Figure I-35: Absolute pressure variation with time; combustion during compression-expansion equivalence ratio 0.7.

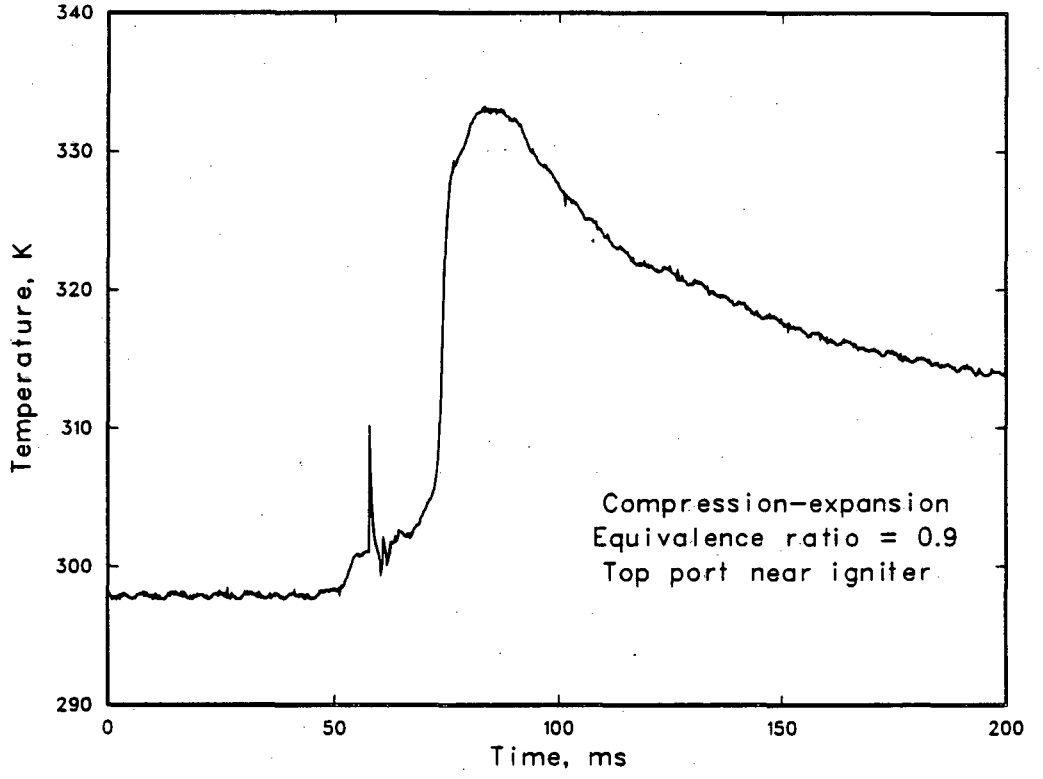

Figure I-36: Wall temperature variation with time; combustion during compression-expansion; equivalence ratio 0.9; without voltage follower.

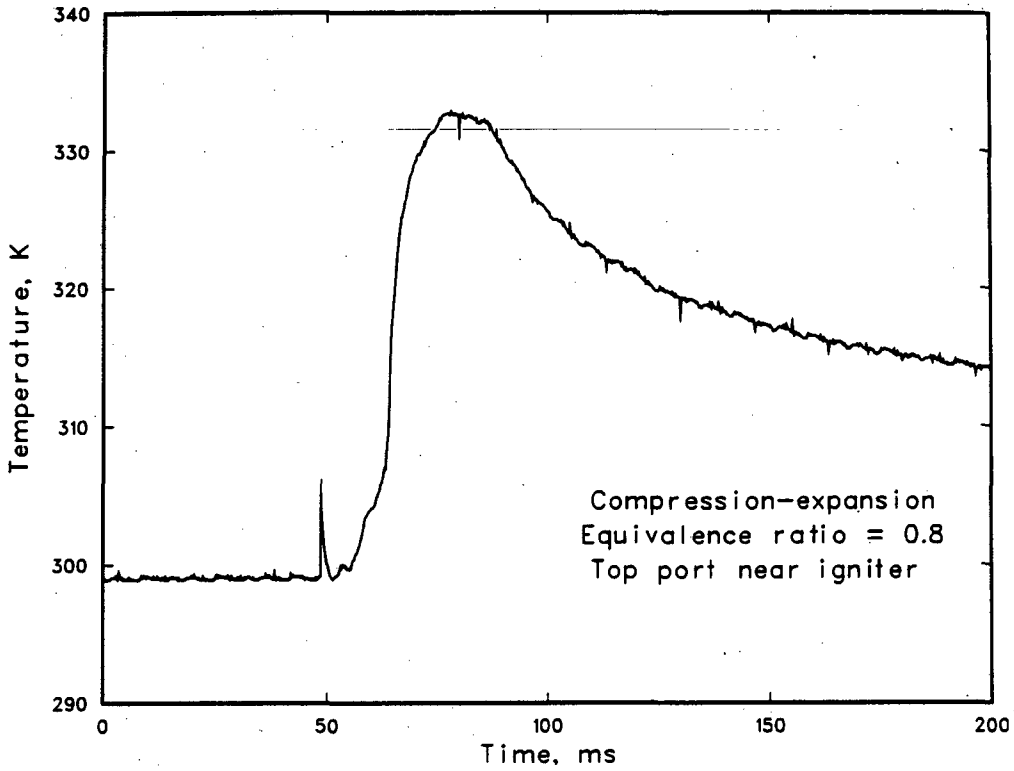

Figure I-37: Wall temperature variation with time; combustion during compression-expansion; equivalence ratio 0.8; without voltage follower.

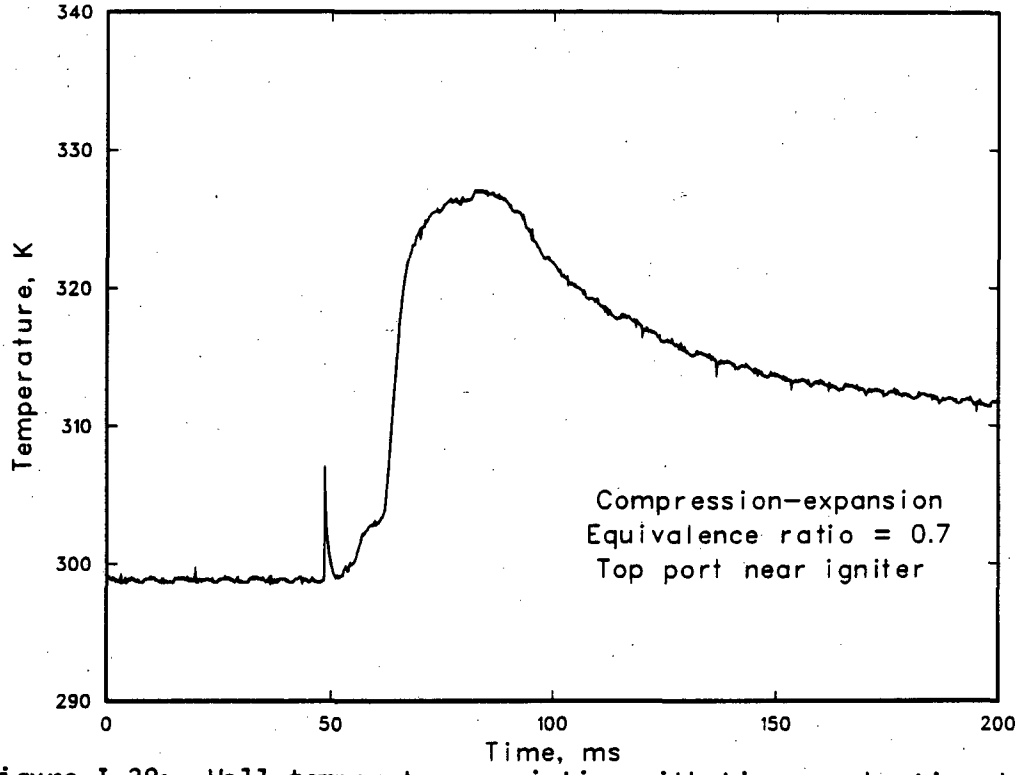

Figure I-38: Wall temperature variation with time; combustion during compression-expansion; equivalence ratio 0.7; without voltage follower.

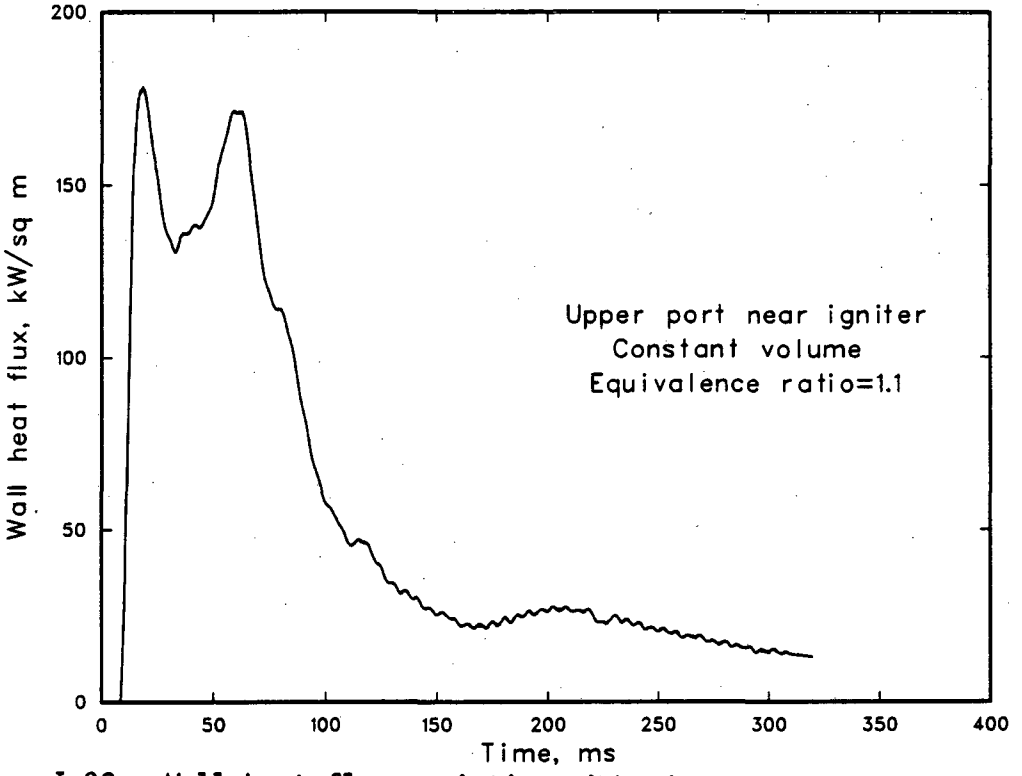

Figure I-39: Wall heat flux variation with time near igniter; constant volume combustion; equivalence ratio 1.1; without voltage follower.

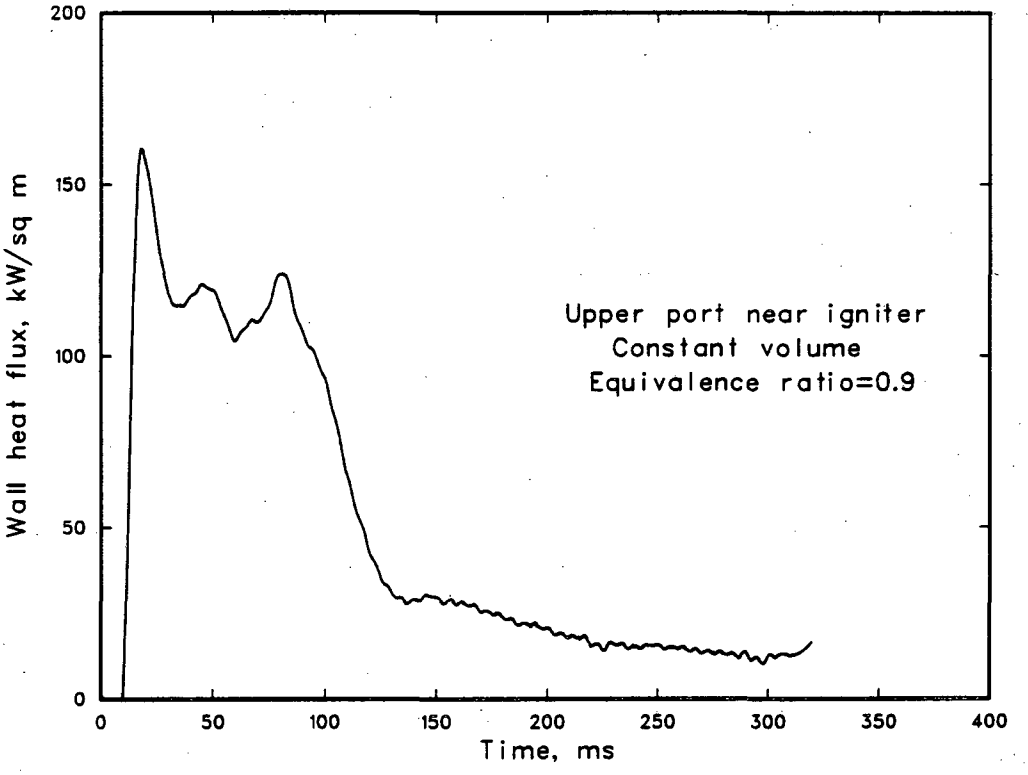

Figure I-40: Wall heat flux variation with time near igniter; constant volume combustion; equivalence ratio 0.9; without voltage follower.

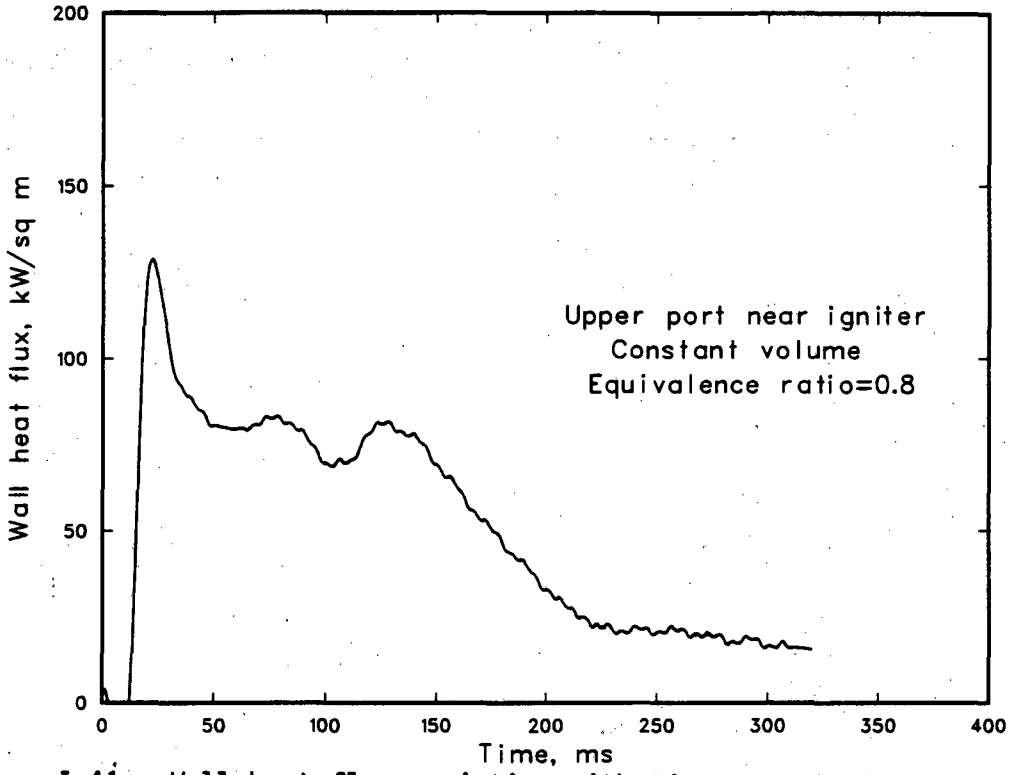

Figure I-41: Wall heat flux variation with time near igniter; constant volume combustion; equivalence ratio 0.8; without voltage follower.

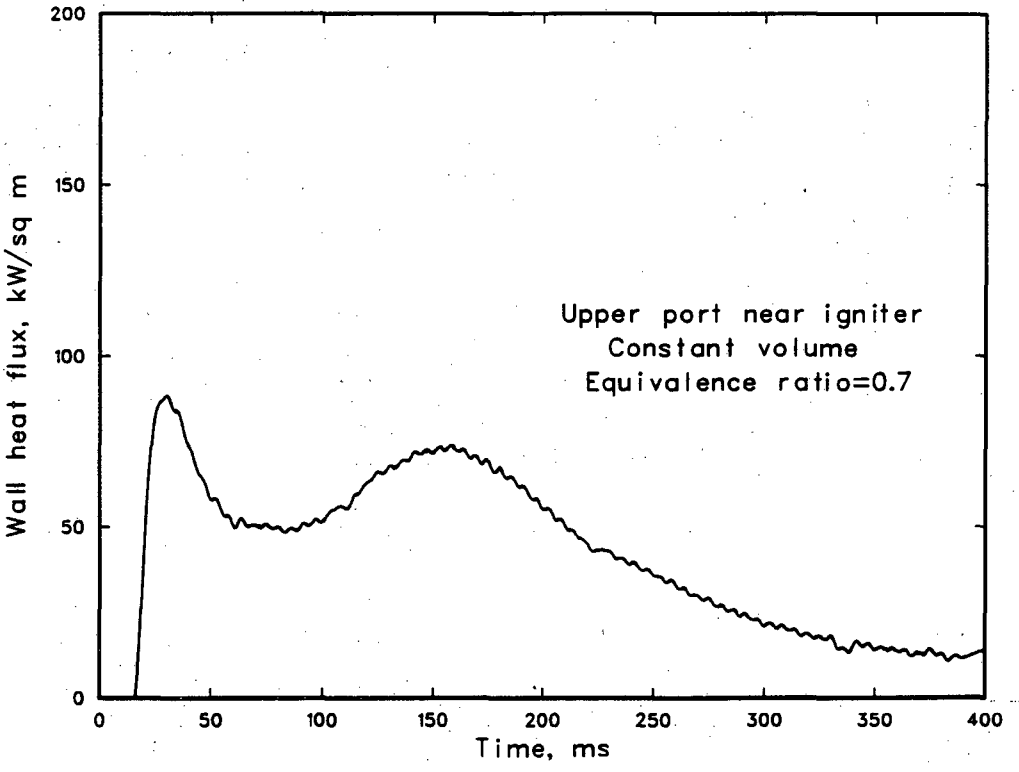

Figure I-42: Wall heat flux variation with time near igniter; constant volume combustion; equivalence ratio 0.7; without voltage follower.

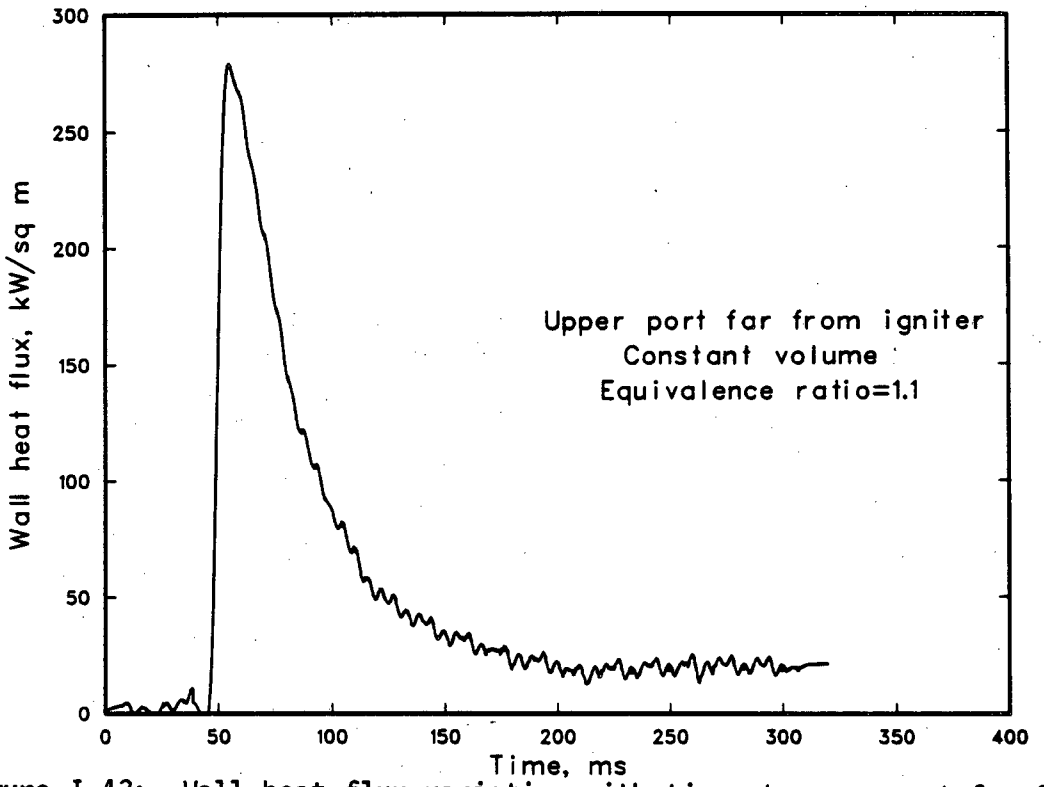

Figure I-43: Wall heat flux variation with time at upper port far from igniter; constant volume combustion; equivalence ratio 1.1.

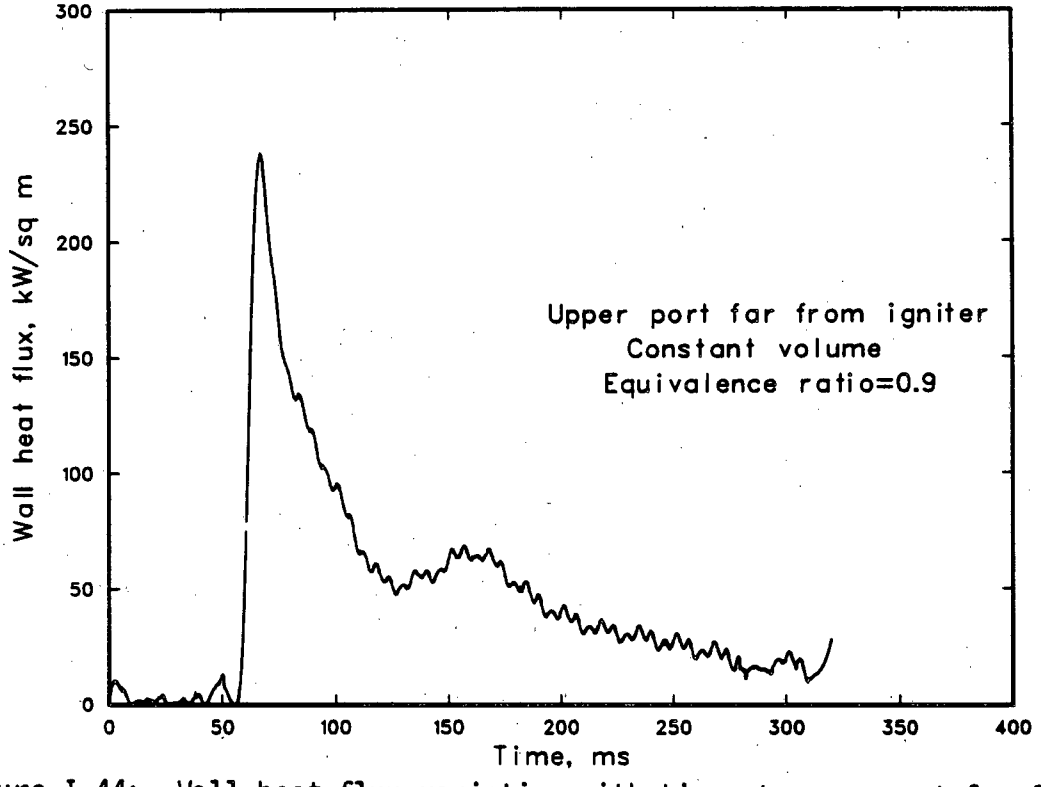

Figure I-44: Wall heat flux variation with time at upper port far from igniter; constant volume combustion; equivalence ratio 0.9.

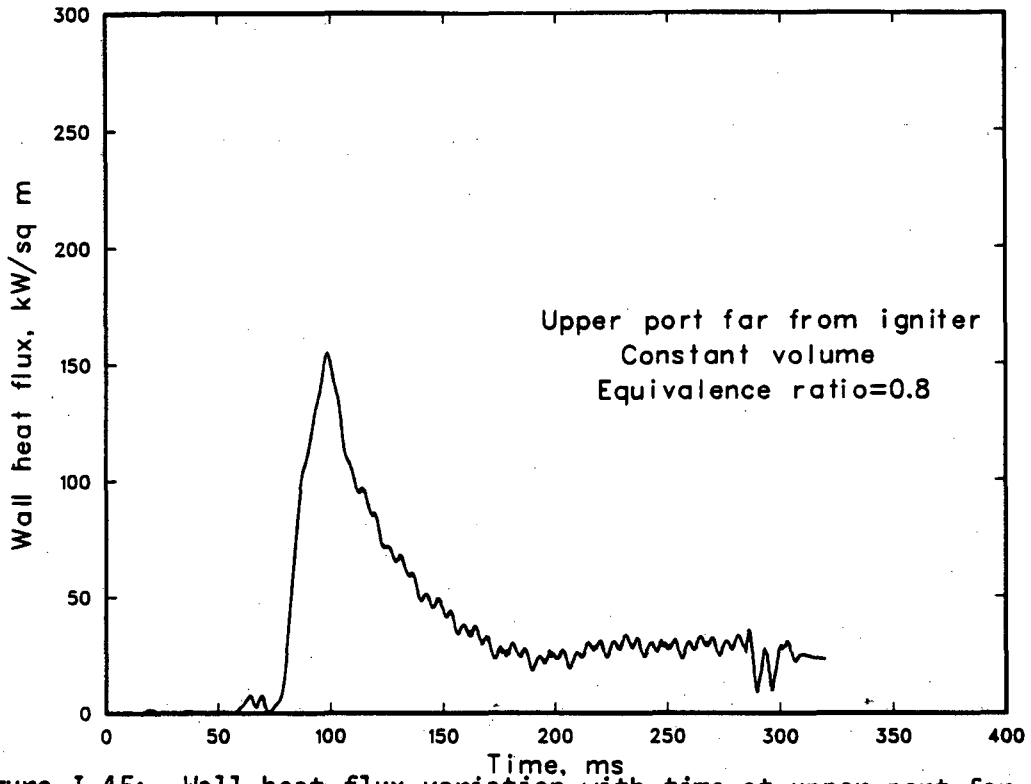

Figure I-45: Wall heat flux variation with time at upper port far from igniter; constant volume combustion; equivalence ratio 0.8.

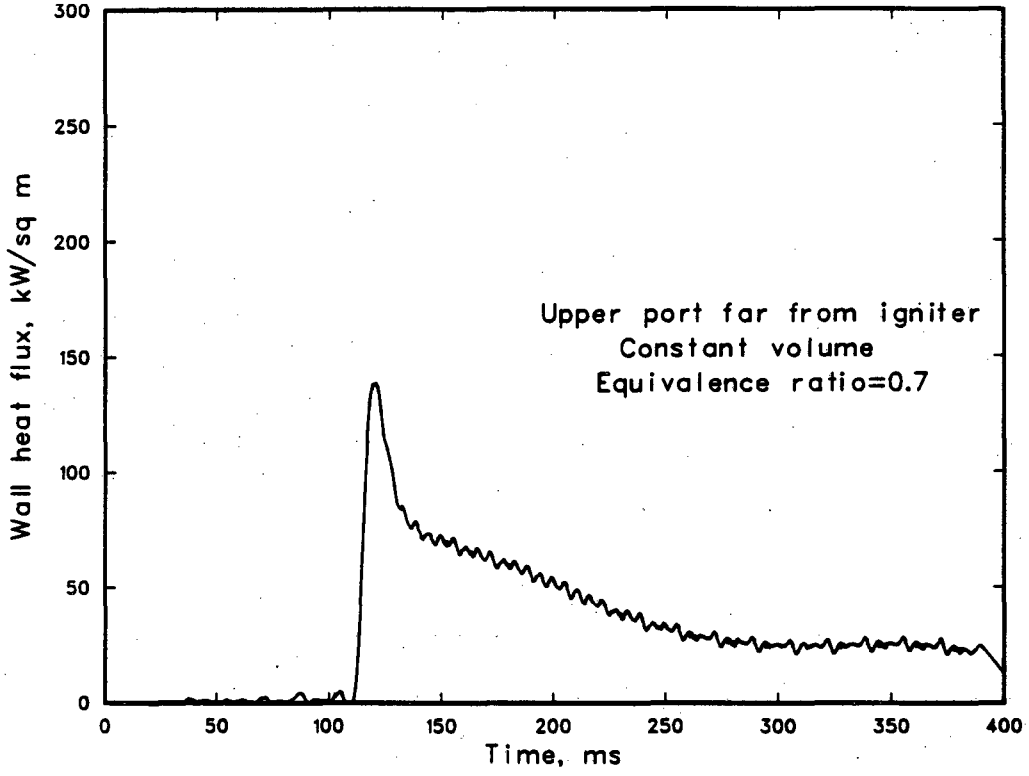

Figure I-46: Wall heat flux variation with time at upper port far from igniter; constant volume combustion; equivalence ratio 0.7.

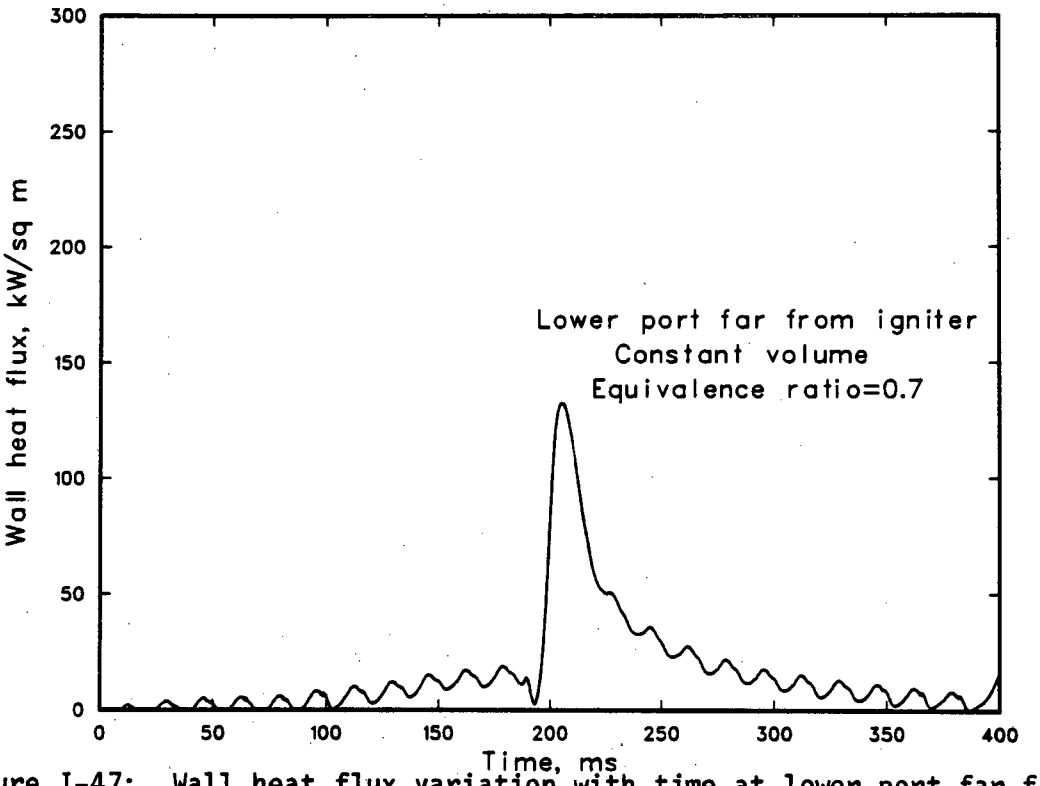

Figure I-47: Wall heat flux variation with time at lower port far from igniter; constant volume combustion; equivalence ratio 0.7.

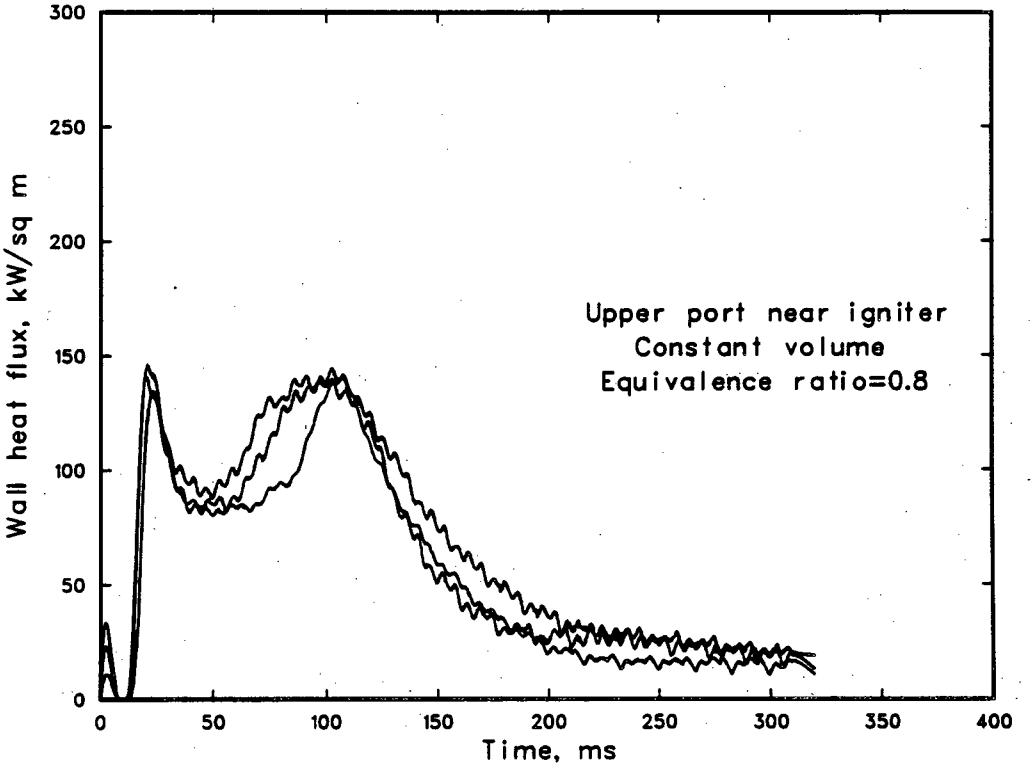

Figure I-48: Repeatability of wall heat flux variation with time; three measurements for identical conditions.

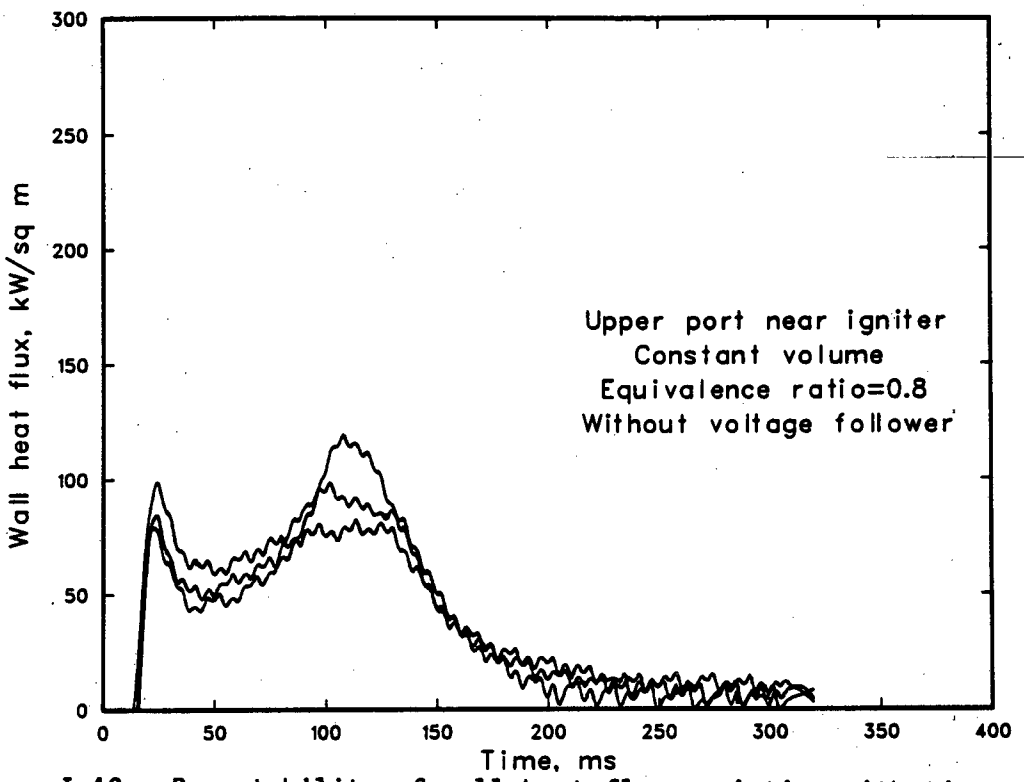

Figure I-49: Repeatability of wall heat flux variation with time, without voltage follower; three measurements for identical conditions.

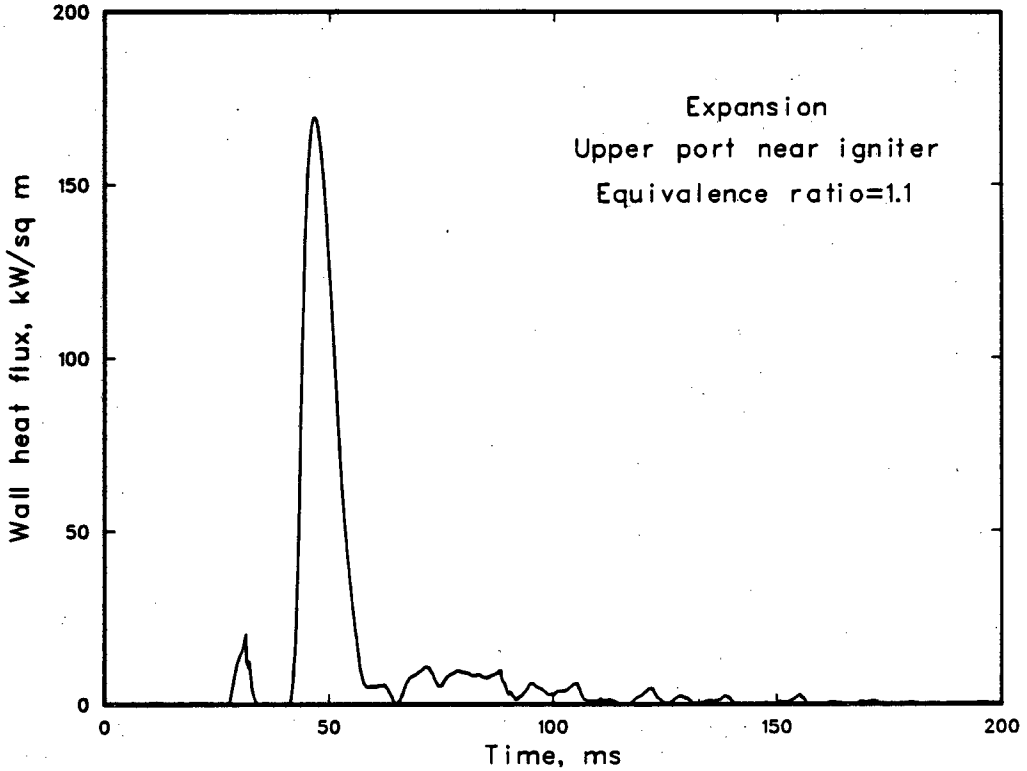

Figure I-50: Wall heat flux variation with time; combustion in an expanding volume; equivalence ratio 1.1; without voltage follower.

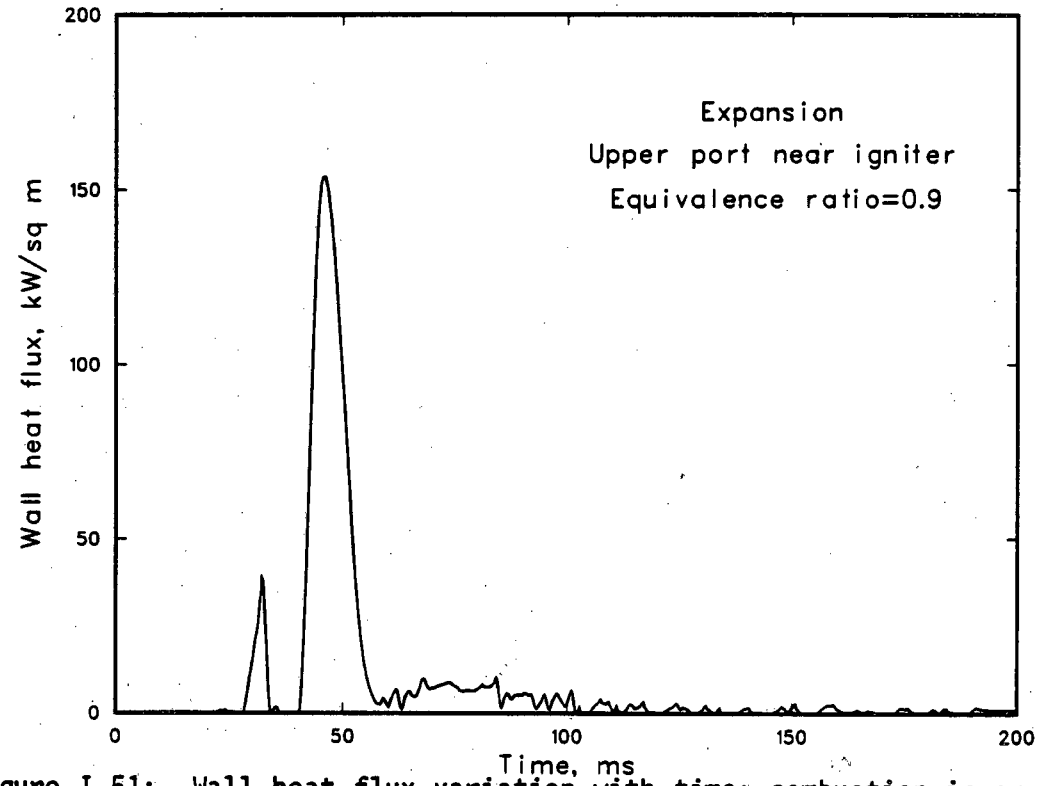

Figure I-51: Wall heat flux variation with time; combustion in an expanding volume; equivalence ratio 0.9; without voltage follower.

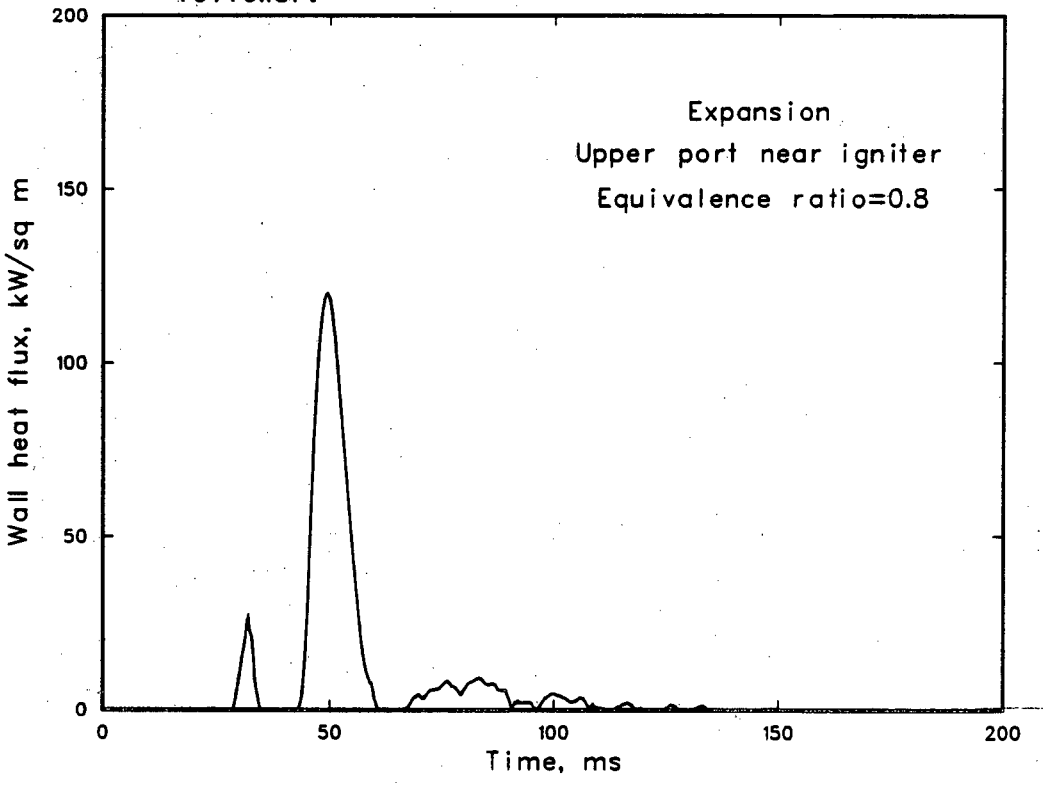

Figure I-52: Wall heat flux variation with time; combustion in an expanding volume; equivalence ratio 0.8; without voltage follower.

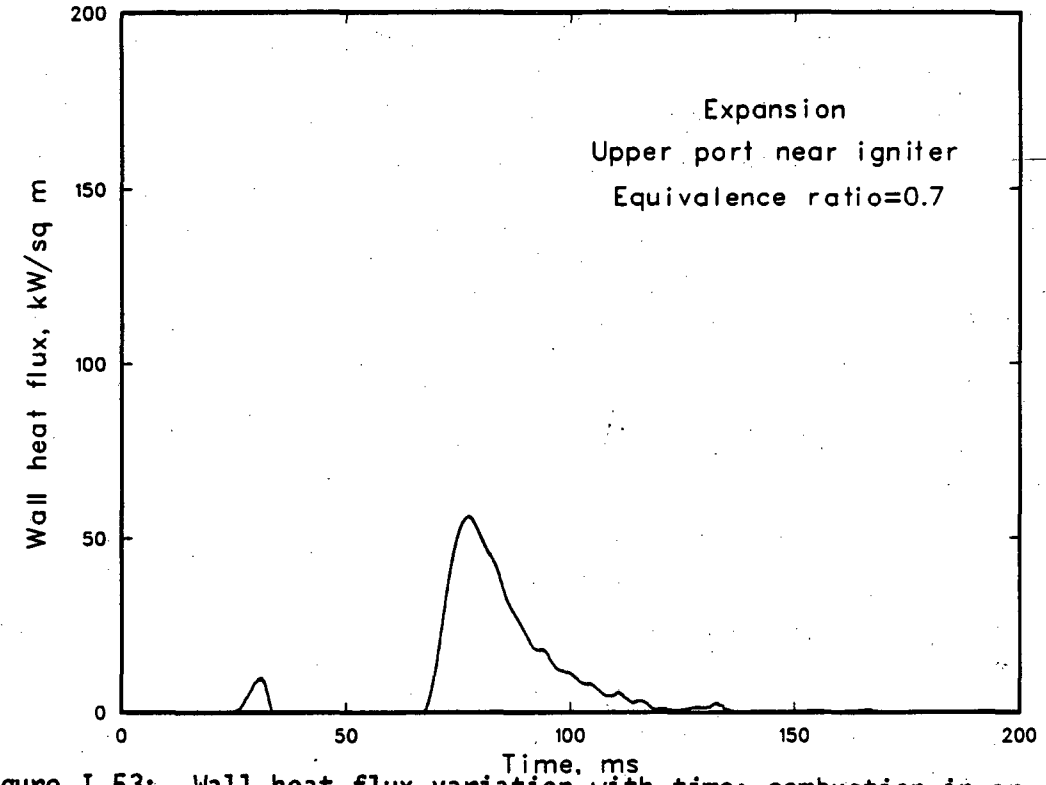

Figure I-53: Wall heat flux variation with time; combustion in an expanding volume; equivalence ratio 0.7; without voltage follower.

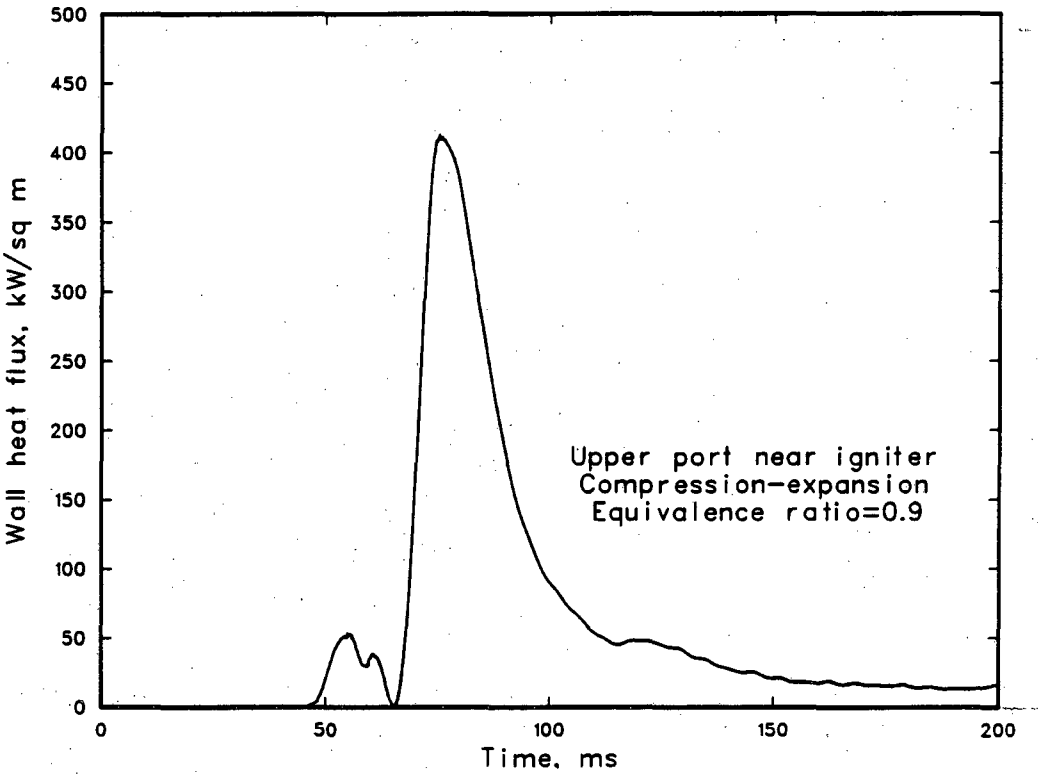

Figure I-54: Wall heat flux variation with time; combustion during compression-expansion; equivalence ratio 0.9; without voltage follower.

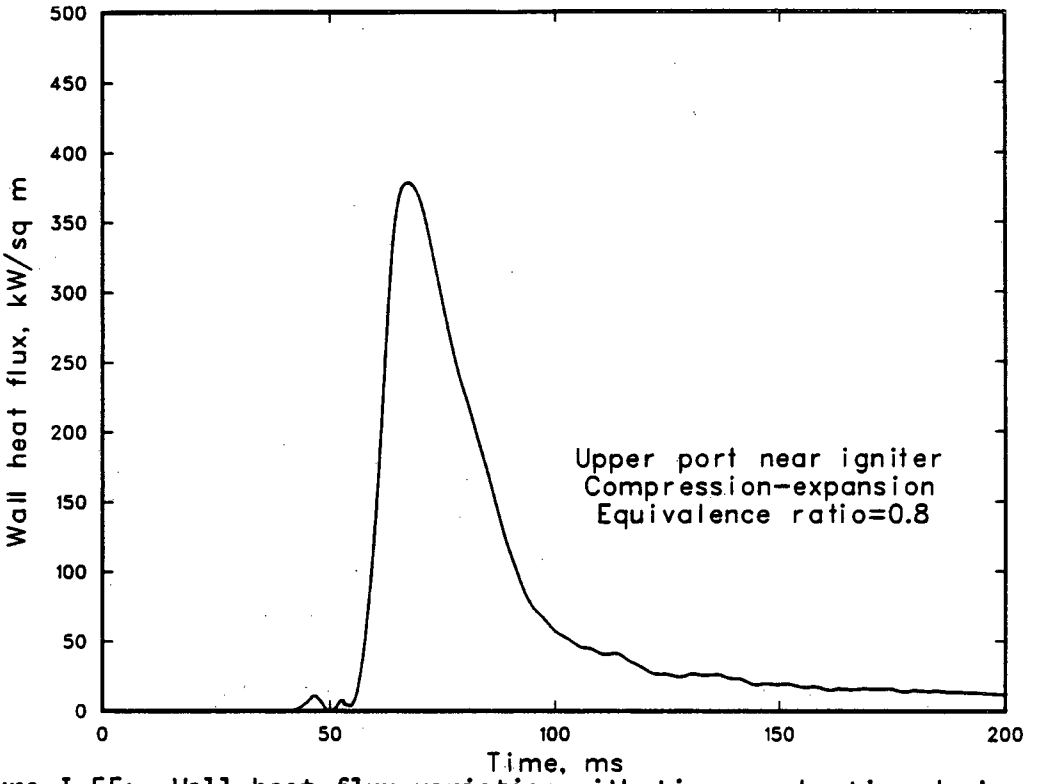

Figure I-55: Wall heat flux variation with time; combustion during compression-expansion; equivalence ratio 0.8; without voltage follower.

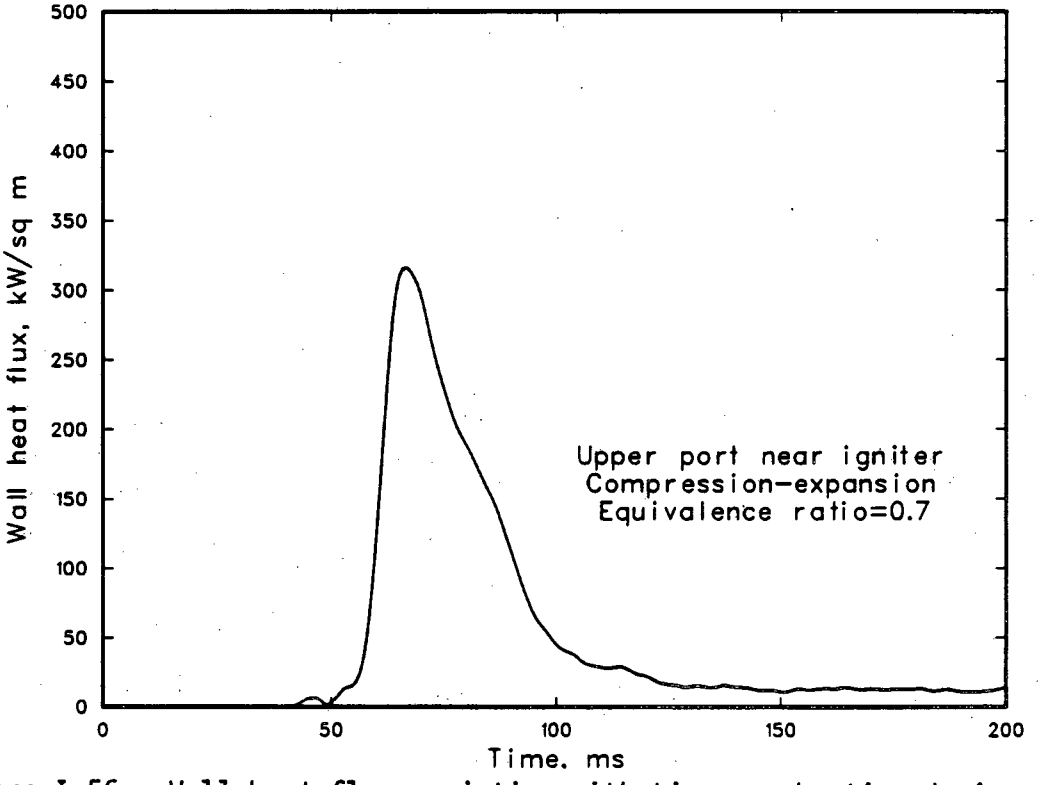

Figure I-56: Wall heat flux variation with time; combustion during compression-expansion; equivalence ratio 0.7; without voltage follower.

TECHNICAL INFORMATION DEPARTMENT
LAWRENCE BERKELEY LABORATORY
UNIVERSITY OF CALIFORNIA
BERKELEY, CALIFORNIA 94720